Conceptual design of a sustainable aviation fuel production route from biomethane

Juhani Rahikka

School of Chemical Engineering

Thesis submitted for examination for the degree of Master of Science in Technology.
Helsinki 30.6.2022

Thesis supervisor:

Prof. Ville Alopaeus

Thesis advisors:

D.Sc. (Tech.) Ilkka Malinen

D.Sc. (Tech.) Kaj Jakobsson

Aalto University
School of Chemical Engineering

AALTO UNIVERSITY
SCHOOL OF CHEMICAL ENGINEERING

ABSTRACT OF THE
MASTER'S THESIS

Author: Juhani Rahikka

Title: Conceptual design of a sustainable aviation fuel production route from biomethane

Date: 30.6.2022 Language: English Number of pages: 127+12

Degree programme: Chemical, Biochemical and Materials Engineering

Major: Chemical and Process Engineering

Supervisor: Prof. Ville Alopaeus

Advisors: D.Sc. (Tech.) Ilkka Malinen, D.Sc. (Tech.) Kaj Jakobsson

This work aims to provide a conceptual design and preliminary economic evaluation for a process where biomethane is converted to sustainable aviation fuel via a synthesis gas production route using Ficher-Tropsch synthesis to produce renewable liquid fuel products.

The motivation behind the work is to find an economically viable route to utilize biogas to produce liquid fuels, mainly sustainable aviation fuel. This can be done by first producing synthesis gas from the biomethane in the biogas and using that as a feedstock for Fischer-Tropsch synthesis. The Fischer-Tropsch product is then distilled and processed further using a hydrocracker to obtain liquid products from the heavy wax fraction.

The theoretical section of the work explores the fundamental theories behind the different production processes. Basic reaction equations, chemistries and thermodynamics are presented and different process configurations are evaluated. Based on these evaluations, the most suitable process options are chosen.

The experimental part of the work is done in Aspen Plus simulation environment, where a simulation of the process is done to obtain mass and heat balances for the process. This is done by using the Peng-Robinson Boston-Mathias property method and components and operation blocks that are readily available in Aspen Plus.

Based on these balances, the capital and operational expenditures for the process are calculated. Based on these calculations, the work finds that the process is narrowly economically viable in its current state with current feedstock and product prices but could very well be even more economically viable in the future depending on the development of the respective markets.

Keywords: Biogas, biomethane, sustainable aviation fuel, biojet, synthesis gas, Fischer-Tropsch, hydrocracking

AALTO-YLIOPISTO
KEMIAN TEKNIIKAN KORKEAKOULU

DIPLOMITYÖN
TIIVISTELMÄ

Tekijä: Juhani Rahikka

Työn nimi: Konseptisuunnittelu uusiutuvan lentopolttoaineen tuotannolle biometaanista

Päivämäärä: 30.6.2022 Kieli: Englanti Sivumäärä: 127+12

Koulutusohjelma: Kemian, Biokemian ja Materiaalitekniikan Maisteriohjelma

Pääaine: Chemical and Process Engineering

Työn valvoja: Prof. Ville Alopaeus

Työn ohjaaja: TkT Ilkka Malinen, TkT Kaj Jakobsson

Tämän työn tarkoituksena on luoda konsepti- sekä kannattavuusarvio uusiutuvan lentopolttoaineen tuotannolle biometaanista, käyttäen synteesikaasureittiä sekä Fischer-Tropsch synteesiä nestemäisten polttoaineiden tuottamiseen. Työn motivaationa on löytää taloudellisesti kannattava reitti biokaasun hyödyntämiseen nestemäisten polttoaineiden, erityisesti nestemäisen lentopolttoaineen tuotannossa. Tämä voidaan toteuttaa tuottamalla ensin snyteesikaasua biokaasun sisältämästä metaanista ja käyttäen sitä raaka-aineena Fischer-Tropsch synteesissä. Fischer-Tropsch synteesin tuote tislataan ja prosessoidaan edelleen käyttäen vetykrakkeria nestemäisten tuotteiden saamiseksi raskaasta vahajakeesta.
Työn teoreettinen osuus tutkii työn kannalta keskeisiä teorioita tuotantoprosessien takana. Prosessien reaktioyhtälöt, kemiat sekä termodynamiikat esitellään ja erilaisia prosessivaihtoehtoja arvioidaan. Näiden arvioiden pohjalta valitaan prosessiin sopivimmat vaihtoehdot.
Työn kokeellinen osuus on toteutettu Aspen Plus -simulaatio-ohjelmistolla, jossa simulaatio prosessista on toteutettu massa ja lämpötaseiden laskemiseksi. Tämä on toteutettu käyttäen Peng-Robinson Boston-Mathias tilanyhtälöä sekä komponentteja ja yksikköoperaatioita jotka ovat valmiiksi saatavilla Aspen Plus -ohjelmistossa. Näiden taseiden perusteella prosessin investointi- sekä käyttökustannukset on laskettu. Näiden laskelmien perusteella prosessi on niukasti taloudellisesti kannattava nykytilassaan nykyisillä raaka-aine- sekä tuotehinnoilla, mutta voi hyvin olla vielä huomattavasti kannattavampi tulevaisuudessa riippuen markkinoiden kehityksestä.

Avainsanat: Biokaasu, biometaani, uusiutuva lentopolttoaine, synteesikaasu, Fischer-Tropsch, hydrokrakkaus

Preface

The topic for this thesis was conceived at St1 offices during December 2021. I want to thank St1 and Marko Maukonen for providing me the opportunity to work on a thesis topic that was very close to my own interests and enabled me to apply the topics I have learned during my studies. I want to thank my advisors Ilkka Malinen and Kaj Jakobsson for helping me during the thesis and helping me iron out some of the kinks we came across during the beginning of the thesis. I also want to thank my supervisor Ville Alopaues for help and support with the thesis and especially for picking up the thesis topic and helping me arrange everything during January 2022. I also want to thank my friend Jere Eilavaara for keeping me company at Maarintalo, all my other friends for their support during the thesis and my girlfriend for support and being able to bounce concepts and ideas off of her at home.

Helsinki, 30.6.2022

Juhani Rahikka

Contents

Symbols and abbreviations

Symbols

W_n	product weight percentage
n	number of carbon atoms
C_i	plant CAPEX
V_i	plant capacity
X	scale-up factor
COP_{HP}	coefficient of performance
T_L	temperature of incoming heat
T_H	temperature of outgoing heat
W_{net}	net amount of work required
Q_h	heat delivered

Abbreviations

APEA	Aspen Process Economic Analyzer
APR	aqueous phase reforming
ASF	Anderson-Schultz-Flory
ASTM	American Society for Testing and Materials
ASU	air-separation unit
ATJ	alcohol-to-jet
ATR	autothermal reforming
BTL	biomass-to-liquid
CAPEX	capital expenditure
CO	carbon monoxide
COP	coefficient of performance
CPOX	catalytic partial oxidation
DCF	discounted cash flow
DMR	dry methane reforming
DSHC	direct sugars to hydrocarbons
EBITDA	earnings before interest, taxes, depreciation and amortization
FEHE	feed-effluent heat exchanger
FRL	fuel readiness level
FT	Fischer-Tropsch
FTP	Fischer-Tropsch product
FTS	Fischer-Tropsch synthesis
GHG	greenhouse gas
GHSV	gas hourly space velocity
GTJ	gas-to-jet
GTL	gas-to-liquid
HCP	hydrocracking product
HDCJ	hydrotreated depolymerized cellulosic jet
HEFA	hydroprocessed esters and fatty acids
HHV	high heating value
HTFT	high-temperature Fischer-Tropsch
HTL	hydrothermal liquefaction

Abbreviations

IATA	International Air Transport Association
ICAO	International Civil Aviation Organization
IRR	internal rate of return
ISBL	inside battery limits
LCA	life-cycle assessment
LHV	lower heating value
LTFT	low-temperature Fischer-Tropsch
MFSP	minimum fuel selling price
NPV	net present value
OPEX	operational expenditure
OSBL	outside battery limits
OTJ	oil-to-jet
POX	partial oxidation
PR-BM	Peng-Robinson Boston-Mathias
RPK	revenue passenger-kilometers
RWGS	reverse water-gas shift
SAF	sustainable aviation fuel
SMR	steam methane reforming
SPK	synthetic paraffinic kerosene
SR	steam reforming
STJ	sugar-to-jet
TAC	total annual cost
TCI	total capital investment
UCO	used cooking oil
WGS	water-gas shift

Introduction

The aviation sector accounted for 2.4% of the global anthropogenic CO_2 emissions in the year 2018, with the entire sector's total emissions being 918 MMT of CO_2. [1] Prior to the COVID-19 pandemic, these emissions were projected to increase threefold between 2020 and 2050. [2] To account for this increase in emissions, decarbonization of the industry is required if the current trend of increasing demand for aviation remains. Decarbonization means reducing or eliminating carbon dioxide emissions by replacing fossil-based fuels with sustainable energy carriers. While the use of electricity and hydrogen as energy carriers for aviation has been researched, these solutions remain novel for the current time being. In the near future, liquid fuels remain as the most likely solution to the decarbonization of the aviation industry.

This thesis topic is commissioned by the company St1. St1 is a Finnish energy company operating mainly in the Nordic region and operates a service station chain in Finland, Sweden, Norway and Poland. The company aims towards carbon neutral solutions for transportation with their own refinery and plant operations. In the year 2021 St1 launched its own biogas division, increasing the company's internal production of renewable natural gases. This thesis aims to provide the St1 company with a techno-economic assessment for the production of sustainable aviation fuel (SAF) via Fischer-Tropsch synthesis (FTS) using biomethane as a feedstock. The process is evaluated step-by-step, starting from the generation of syngas from biomethane, followed by the FT synthesis.

Literature Review

In this part, the justifications for producing SAFs are reviewed, as well as the contributing factors such as mandates, incentives, markets and process maturity. First, the current landscape in aviation and its current and future emission reduction requirements are examined, after which the different options for decarbonization are briefly explained. The review goes into depth only on renewable liquid fuels and covers the essential prerequisites SAFs have to become a marketable fuel product. The markets are briefly covered to justify the process, which is lastly covered. The process options and steps are explained, but the deeper technical information on the processes are presented in their corresponding chapters in the experimental section.

1 Emissions in the Aviation Industry

The aviation industry has been on a steady rise since 1990. The growth and increased demand have increased the overall fuel consumption of the aviation industry, which is seen as a rise in the greenhouse gas (GHG) emissions from the aviation sector. According to Chiaramonti [3], the transport sector is the only one within the energy sector that has failed to reduce its carbon emissions since the year 1990 within the EU. The figure of the evolution of the carbon emissions is presented in Figure 1.

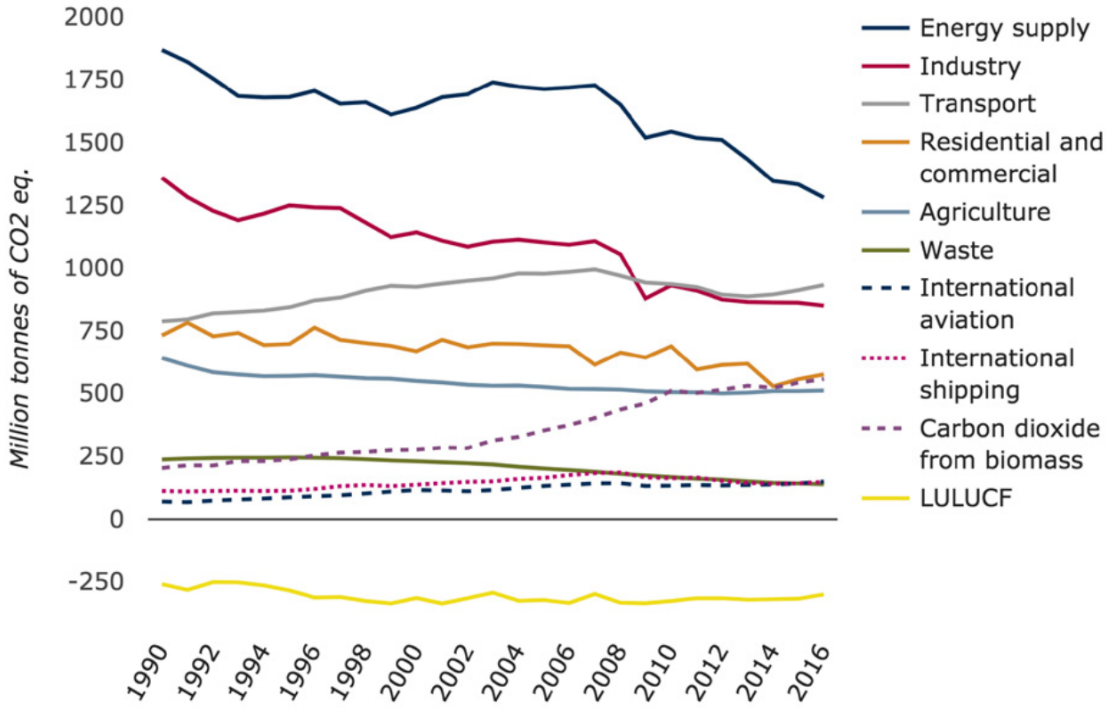

Figure 1: The CO_2 emission trends within different energy sectors in the EU since 1990 [3].

While CO_2 emissions are the most commonly considered emissions when discussing anthropogenic GHG emissions, there are also other contributing factors to the overall emissions from aviation, such as water vapour, nitrogen oxides, sulfur dioxides and aerosols. Alongside CO_2, these contribute to the total radiative effect aviation emissions have, which is a major contributing factor to the concept of global warming. While these species of emissions are a contributing factor to the overall emissions, they are not easily quantifiable by their short-lived nature in the atmosphere. Boucher et

al. [4] describe a method of quantifying the effect of these emissions but generally only the CO_2 emissions are considered when evaluating the emissions from the aviation industry. [4]

Prior to the decreased air traffic activity caused by the COVID-19 pandemic, the aviation sector accounted for 2.4% of the global anthropogenic CO_2 emissions, a total of 918 MMT of CO_2. 81% of these emissions stem from passenger transportation. These passenger transportation emissions are quantified by emissions per revenue passenger-kilometers (RPK), averaging between 75 and 95 grams of CO_2 per RPK.[1] There is limited information available on how the total emissions are divided between subsections of the industry, for example, how freight transport compares to passenger flights. There are several sectors such as private and military flights that are unaccounted for in the official International Civil Aviation Organization (ICAO) emission data. [2]

Despite the pandemic, passenger aviation has been on a steady recovery during 2021, with an expected return to 98% of the 2019 pre-pandemic RPK level according to International Air Transport Association (IATA) passenger reports [5]. The current global RPK levels compared to pre-pandemic figures are presented in Figure 2.

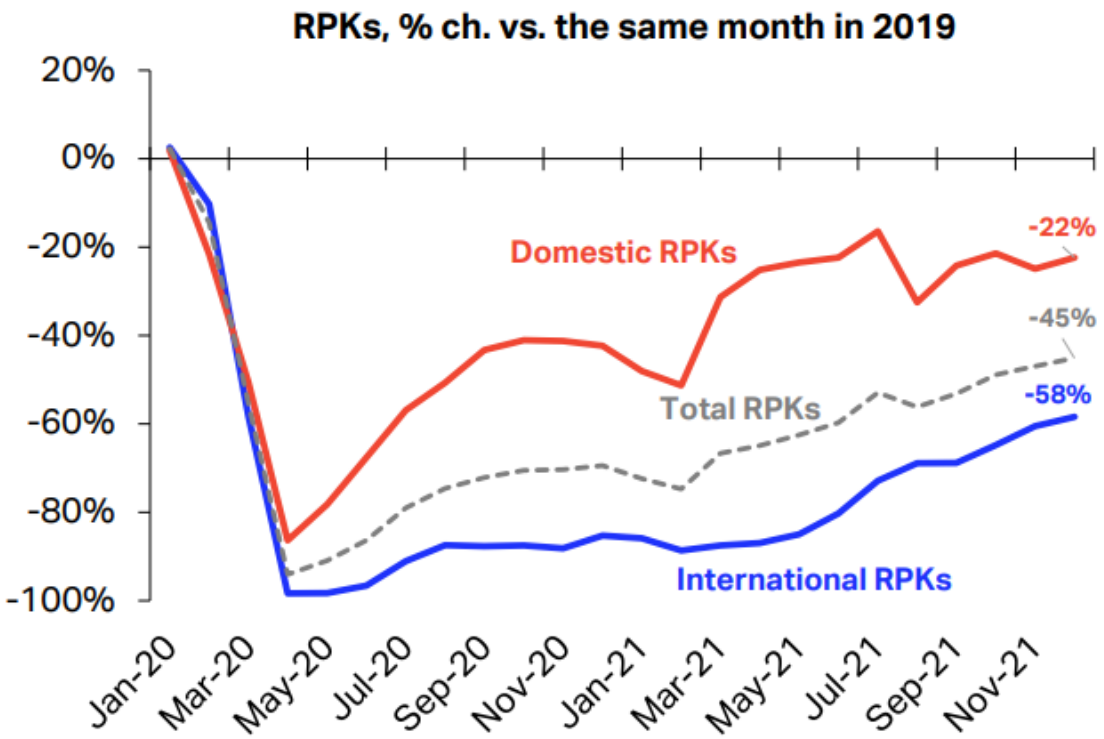

Figure 2: The revenue passenger-kilometer values for passenger flights between 2020 and November 2021 compared to the pre-pandemic 2019 values compiled by IATA. [5]

According to IATA reports, aviation activity can be expected to grow despite the pandemic. [6] Between the years 1980 and 2015, the aviation industry had seen an annual growth of 5.4% in demand leading to a 2.2% annual growth in emissions during the same 35-year period. Despite aircraft requiring less fuel, with an annual decrease of 2-3% in fuel consumption, this rise in demand more than makes up for any possible reduction in overall emissions. [7] According to a study conducted by the European Parliament, even with technological improvements, emissions from the aviation industry are projected to reach 1 750 MMT CO_2 annually by the year 2050. The projected emissions are presented in Figure 3. The study considers the scenario where technological advancements are made the baseline scenario, where a 33% reduction in CO_2 emissions is achieved compared to the scenario where the current baseline technology sees no improvements. [8]

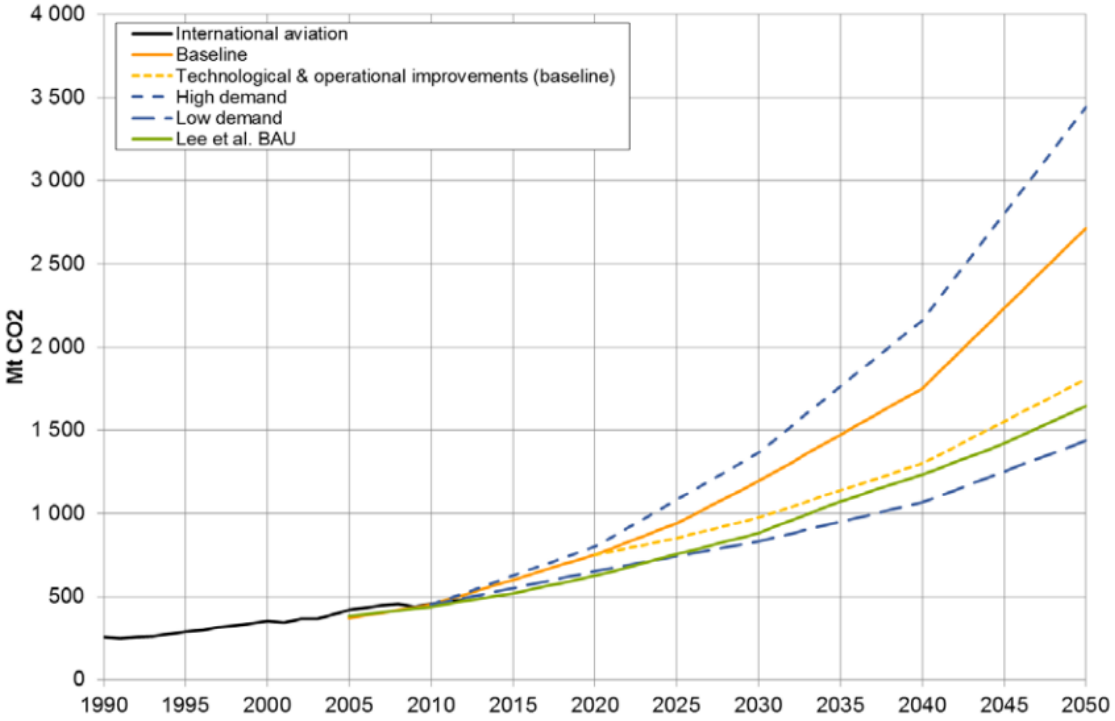

Figure 3: Projected CO_2 emissions from international aviation [8].

The Paris Agreement set in 2015 sets a goal of limiting global warming to below 2 °C above the pre-industrial level. [9]. To achieve this goal, the 2030 CO_2 emissions should not exceed 39% of the 2005 level, and by the year 2050 they should already be 41% less than what they were in 2005. As can be seen from Figure 3, with the current development of aviation emissions, these goals will not be met. To meet these goals, decarbonization of the aviation industry must become a reality in the near future. [8]

According to the IATA Aircraft Technology Roadmap to 2050, the aviation industry has committed to climate action goals, including improving fuel efficiency, achieving net carbon neutral growth from 2020, and reducing the global net carbon emissions from aviation by 50% by the year 2050. These goals are to be achieved by implementing improvements to the technology of the aircraft, efficient flight operations, improved infrastructure, positive economic measures and SAFs. [10]

While the technological improvements to the aircraft themselves are important for achieving long-term industry goals for CO_2 emissions, they have a limited potential

for reducing the emissions. According to the IATA Roadmap most of the CO_2 reduction would have to come from adopting SAFs in the aviation industry. The wide-scale deployment of SAFs is less of a technological issue and more of a financial one, as the production of SAF is not yet competitive when compared to conventional jet fuel (CJF). [10]

2 Sustainable aviation fuels

In life-cycle assessments (LCA), the GHG emissions for different SAF production pathways range from 15–50 $kgCO_2/GJ$. Compared to the baseline GHG emissions for CJF of 83 $kgCO_2/GJ$, these equate to GHG reductions of 40–82%. The LCAs conducted by Wang et al. [11] include alcohol-to-jet (ATJ), oil-to-jet (OTJ), gas-to-jet (GTJ) and sugar-to-jet (STJ) pathways. The life-cycle GHG emissions for different production pathways are presented in Figure 4. [11]

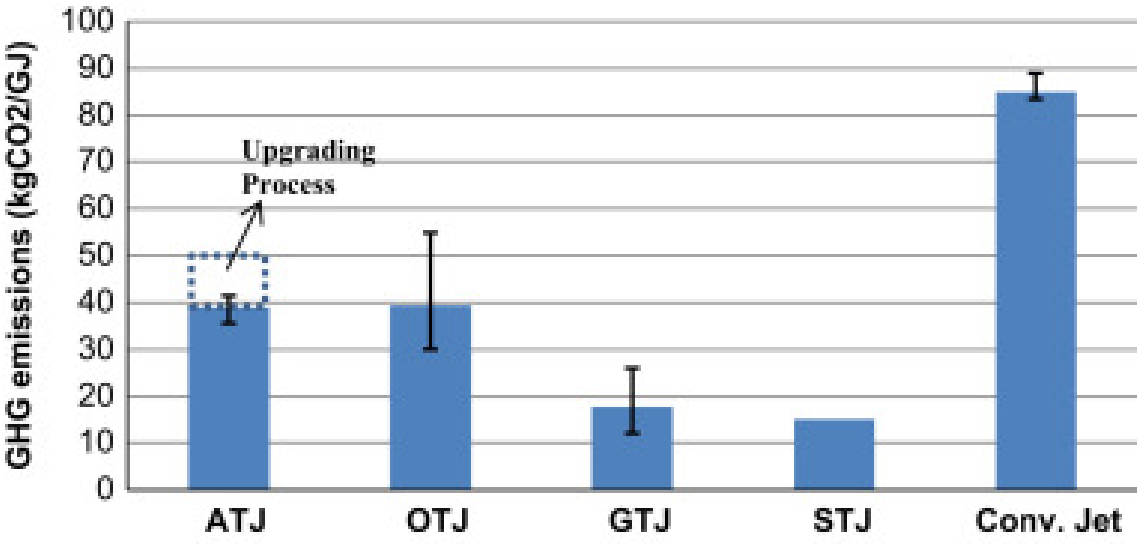

Figure 4: GHG emissions for different SAF production pathways. ATJ = alcohol-to-jet, OTJ = oil-to-jet, GTJ = gas-to-jet, STJ = sugar-to-jet. [11]

For SAFs to be usable in place of CJFs, jet fuel must meet several different specifications in order to be allowed for use. SAFs have target compositions and fuel specifications, including acceptable minimum energy density by mass, maximum allowable freeze point temperature, maximum allowable deposits in standard heating tests, maximum allowable viscosity, maximum allowable sulfur and aromatics content, maximum allowable amount of wear in standardized test, maximum acidity and mercaptan concentration, minimum aromatics content, minimum fuel electrical conductivity and minimum allowable flash point. The required specifications for the most common commercially used jet fuel type, Jet A-1, are presented in Table 1.

The three standards for jet fuels are the American Society for Testing and Materials' (ASTM), IATA and the United Kingdom Ministry of Defence's Standards. The ASTM D7566 standard is specfically set for synthetic fuels, targeting alternative jet fuels such as SAFs. [11]

Table 1: Jet A-1 fuel specifications (modified from source: [11]).

Jet A-1

	ASTM D1655-04a	IATA	Def Stan 91–91	ASTM D7566
Composition				
Acidity, total (mg KOH/g)	0.1, max	0.015, max	0.012, max	0.1, max
Aromatics (vol %)	25, max	25, max	25, max	25, max (8, min)
Sulfur, total (wt %)	0.3, max	0.3, max	0.3, max	0.3, max
Volatility				
Distillation temperature:				
10% Recovery (°C)	205, max	205, max	205, max	205, max
20% Recovery (°C)	–	–	–	–
50% Recovery (°C)	–	–	–	(15, min)
90% Recovery (°C)	–	–	–	(40, min)
Final BP (°C)	300, max	300, max	300, max	300, max
Flash point (°C)	38, min	38, min	38, min	38, min
Density @ 15 °C (kg/m3)	775–840	775–840	775–840	775–840
Fluidity				
Freezing point (°C), max	−47	−47	−47	−40 Jet A ; −47 Jet A−1
Viscosity @ −20 °C (cSt)	8, max	8, max	8, max	8, max
Combustion				
Net heat of comb. (MJ/kg)	42.8, min	42.8, min	42.8, min	42.8, min
Smoke point (mm)	25, min	25, min	25, min	25, min
Smoke point (mm) and naphthalenes (vol%)	19 (min), 3 (max)	19 (min), 3 (max)	19 (min), 3 (max)	18 (min), 3 (max)
Thermal stability				
JFTOT Delta P @ 260 °C (mm Hg)	25, max	25, max	25, max	25, max
Tube deposit Rating (Visual)	< 3	< 3	< 3	< 3
Conductivity				
Conductivity (pS/m)	50–450	50–450	50–600	–
Lubricity				
BOCLE wear scar diameter (mm)	–	0.85, max	0.85, max	0.85, max

In terms of the chemistry of the fuel, Jet A-1 type fuels correspond to kerosene-type fuels, with a carbon number in the range of C8–C16. [12] While this carbon range falls within the lighter fractions of distillates, which may not provide a great yield, the availability of heavier fractions allows for them to be hydrotreated to obtain hydrocarbons within this range.

2.1 Fuel readiness level

According to Mawhood et al. [13], the fuel readiness levels (FRL) for different pathways vary significantly. The definitions for each FRL are presented in Table 2.

The most advanced pathway currently is the hydroprocessed esters and fatty acids pathway, with a FRL of 9, with ASTM classifications and three commercial-scale facilities globally. The Fischer-Tropsch (FT) pathway has the second highest FRL ranging from 7 to 8 depending on the feedstocks used. The FT pathway is moving towards the start-up of commercial facilities. However, Mawhood cites current market conditions as a limiting factor for the widescale spread of industrial FT plants. Direct sugars-to-alcohols processes have been developed, with a FRL of 5–7. Other pathways have been developed and demonstrated but not scaled. These pathways currently have a FRL of 4–6. [13]

Table 2: Fuel readiness level definitions (modified from source: [13]).

	Level	FRL Description	FRL 'Toll Gate'
Technological R&D	1	Basic principles	• Feedstock & process basic principles identified
	2	Technology concept formulated	• Feedstock & complete process identified
	3	Proof of concept	• Lab-scale fuel sample produced from realistic feedstock • Energy balance analysis conducted for initial environmental assessment • Basic fuel properties validated
	4	Preliminary technical evaluation	• System performance and integration studies • Specification properties evaluated
	5	Process validation	• Scaling from laboratory to pilot plant
Certification processes	6	Full-scale technical evaluation	• ASTM certification tests conducted: fit-for-purpose properties evaluated, turbine hot section testing, components and testing
	7	Certification / fuel approval	• Fuel listed in international standards
Commercial deployment	8	Commercialization	• Business model validated for production • Airline purchase agreements secured • Plant-specific independent greenhouse gas assessment conducted in line with internationally-accepted methodology
	9	Production capability established	• Full-scale plant operational

2.2 SAF production pathways

This section covers the most commercially interesting processing methods for SAFs. Although Fischer-Tropsch is the process of interest in this thesis, other production pathways are briefly discussed to give justification for the selection of FT as the production method for SAF.

2.2.1 Hydroprocessed esters and fatty acids

An OTJ pathway, hydroprocessed esters and fatty acids (HEFA) technologies combine hydrotreatment and isomerization processes to produce hydrocarbons from triglycerides. Companies with commercial HEFA production include ARA & Blue Sun Energy, Honeywell and Neste. [13] A simplified diagram of HEFA production is presented in Figure 5.

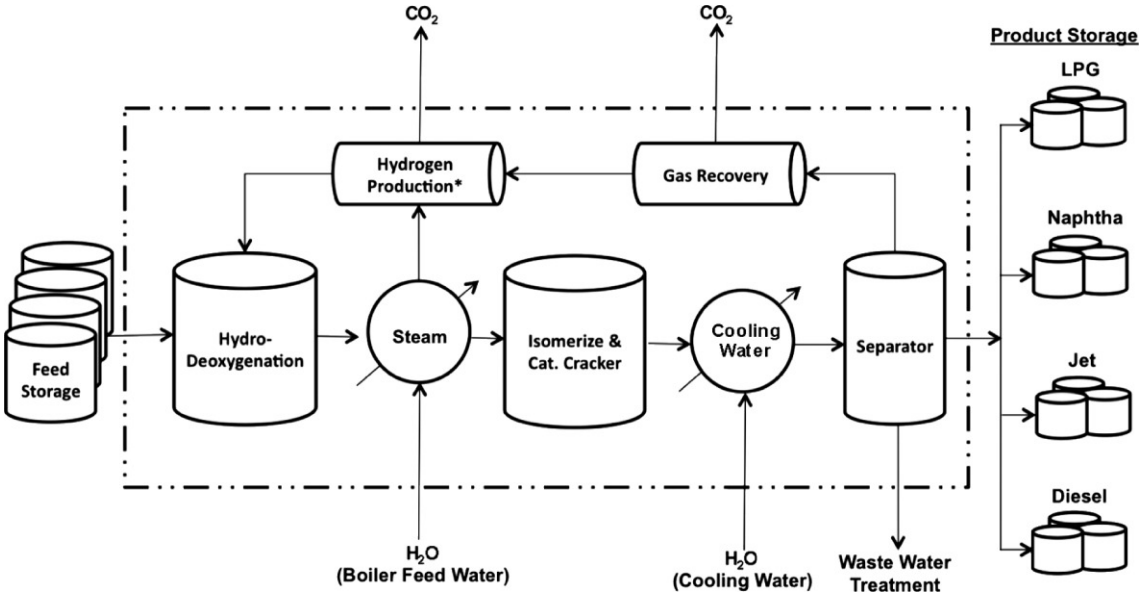

Figure 5: Simplified hydroprocessed esters and fatty acids (HEFA) process design. [14]

According to the studies of Pearlson et al. [14], the baseline costs for HEFA production range between $1.01 and $1.16 per liter, with an additional cost of $0.07 per liter if jet fuel production is maximized. Pearlson cites technological advantages being the biggest motivator behind HEFA production, with the limited availability of inexpensive feedstocks being the major drawback. [14]

2.2.2 Fischer-Tropsch

As a GTJ pathway, Fischer-Tropsch processes conventionally involve biomass gasification to produce syngas for the FTS. FTS can be used to produce synthetic paraffinic kerosene (SPK), which can be used as a liquid fuel in place of CJF. FT pathways

have reached a FRL of 7, while progressing towards level 8, and the fuels produced via this pathway have achieved ASTM certifications. FT processes have been successfully used with natural gas and coal as feedstock, but the application of the technology to use biomass derived feedstocks still requires development, particularly in biomass gasification and syngas production. [13] However, within the scope of this thesis, these problems are not considered, as the feedstock is a readily upgraded biogas consisting entirely of biomethane.

According to the techno-economic analyses of Wang et al. [15], the production costs for FT-to-jet fuels is $2.20 per liter. However, this analysis included natural gas as the raw feedstock, which accounted for 49% of the total operating costs. [15] As the feedstock in this thesis is upgraded biogas, the upgrading processes may increase the feedstock price to an even higher level than conventional natural gas. This price increase may be partially offset by simplifying the distribution and using the gas near the site at which it is upgraded.

2.2.3 Direct sugars to hydrocarbons

Direct sugars to hydrocarbons (DSHC) is a STJ pathway that produces alkane-type fuels directly via anaerobic fermentation. A commercial DSHC process is operated by Amyris and Total, with an annual capacity of 40 000 tonnes per year of biofuels. While Amyris has been able to reach a FRL of 7, other companies have provided insufficient data on their respective DSHC processes. According to Mawhood et al. [13], other companies are not pursuing ASTM certifications, allowing them to have a maximum FRL of 5.

2.2.4 Alcohol-to-jet

The ATJ pathway covers several technologies in which jet fuels are produced from biomass via alcohol intermediates. The alcohol intermediates go through dehydration, oligomerization and hydrogenation to produce jet fuels. Generally, the processes to produce the alcohol intermediates are well documented, while less development and maturity has been reached in upgrading the intermediates to jet fuels. [13]

ATJ technologies have the potential to produce SAF at a relatively low cost at a range of $0.68–1.17 per liter. However, as the technology for the alcohol intermediate upgrading processes is lacking, the technology is not currently applicable for large-scale industrial production. [16]

2.2.5 Hydrotreated depolymerized cellulosic jet

Hydrotreated depolymerized cellulosic jet (HDCJ) pathways include pyrolysis, hydrothermal liquefaction and hybrid processes. The common factor for these processes is the conversion of biomass to bio-oils with high oxygen contents. The bio-oil production processes are well-documented, but due to the high oxygen content, the upgrading processes are relatively expensive. However, due to the inexpensive and plentiful feedstocks, the processes have ongoing development by companies such as Licella. Fuels produced via this pathway have not yet been ASTM certified. [13]

2.2.6 Aqueous phase reforming

Aqueous phase reforming (APR) processes catalytically convert plant sugars into chemical intermediates, which may be further processed into liquid fuels. APR technologies are in early R&D stages, with little information available on the processes. The company Virent is a leading developer of APR fuels, having achieved a FRL of 6 due to their established process demonstration facilities. [13]

3 Economics of SAF production

Currently, the production capacities of SAFs are still negligible in comparison to the total annual consumption of CJFs. According to a McKinsey insight report, the global production of SAFs in 2019 was 200 000 metric tonnes, accounting for less than 0.1% of the total global annual aviation fuel consumption. [17]

According to an ICAO stocktaking seminar, the global annual production capacity of SAF is projected to increase to 13.6 billion liters, which would account for nearly 4% of the total global fuel consumption compared to the pre-pandemic value of 359.6 billion liters in 2019. [18, 19] The projected increase in global SAF production is presented in Figure 6.

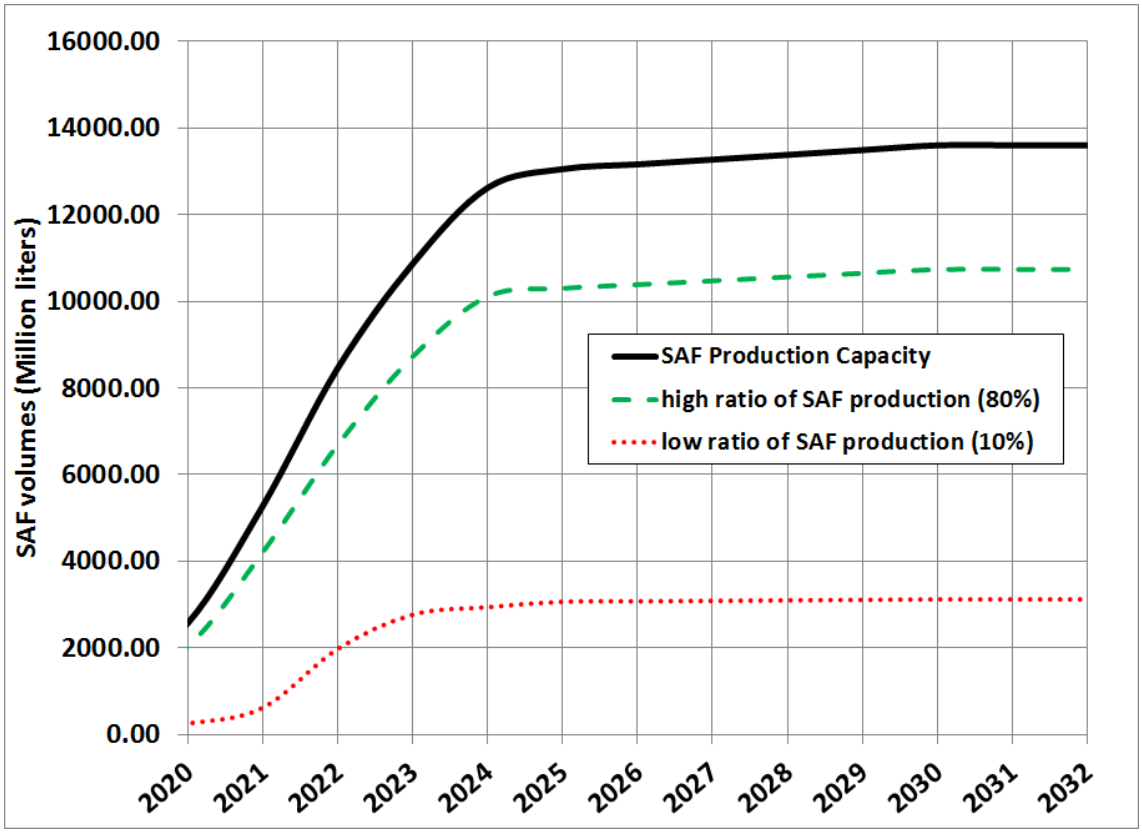

Figure 6: Projected scenarios for the production of SAFs. [18]

The total capital investment (TCI) and minimum fuel selling price (MFSP) for different SAF production pathways were studied by de Jong et al. [20]. The MFSP value is the price for SAF, at which the net present value (NPV) of the project reaches

zero. This feasibility study found significant differences between greenfield plant investment prices, with HEFA having the highest TCI with HDCJ and hydrothermal liquefaction (HTL) pathways following. The TCI values for different pathways are presented in Figure 7. [20]

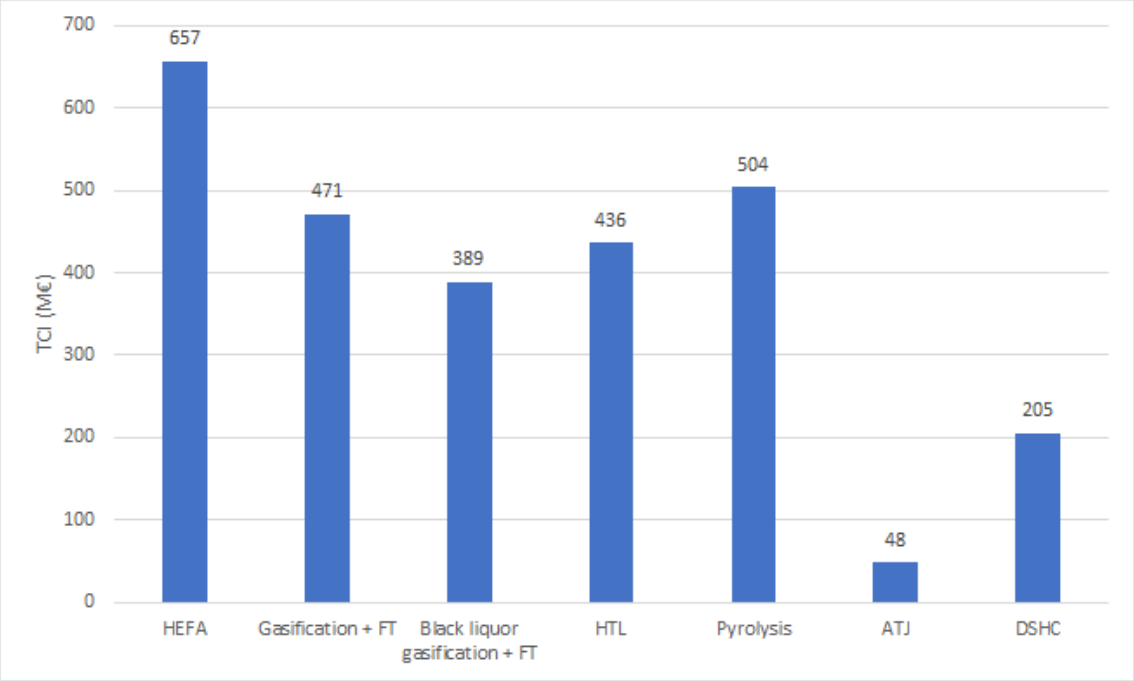

Figure 7: Total capital investment (TCI) values for different SAF pathways (data obtained from: [20]).

More importantly, the feasibility study found MFSPs for the different pathways. For HEFA, the study employed used cooking oil (UCO) as a feedstock and forest residues for the other pathways. [20] The MFSP values from this study were compared to the latest fuel prices obtained from the IATA website [21]. From the values of the feasibility study, it can be seen that HTL is theoretically able to achieve a MFSP lower than the current jet fuel price of 1008 €/t, with HEFA and pyrolysis pathways following. The FT pathway would require an MFSP of 63% higher than the current price. However, it should be noted, that the jet fuel prices have likely increased due to global uncertainties, and the 108% annual price increase reported by IATA may not be an accurate indicator for the future of jet fuel prices. The results from the feasibility study's MFSP values compared against the current jet fuel price are

presented in Figure 8. [20, 21]

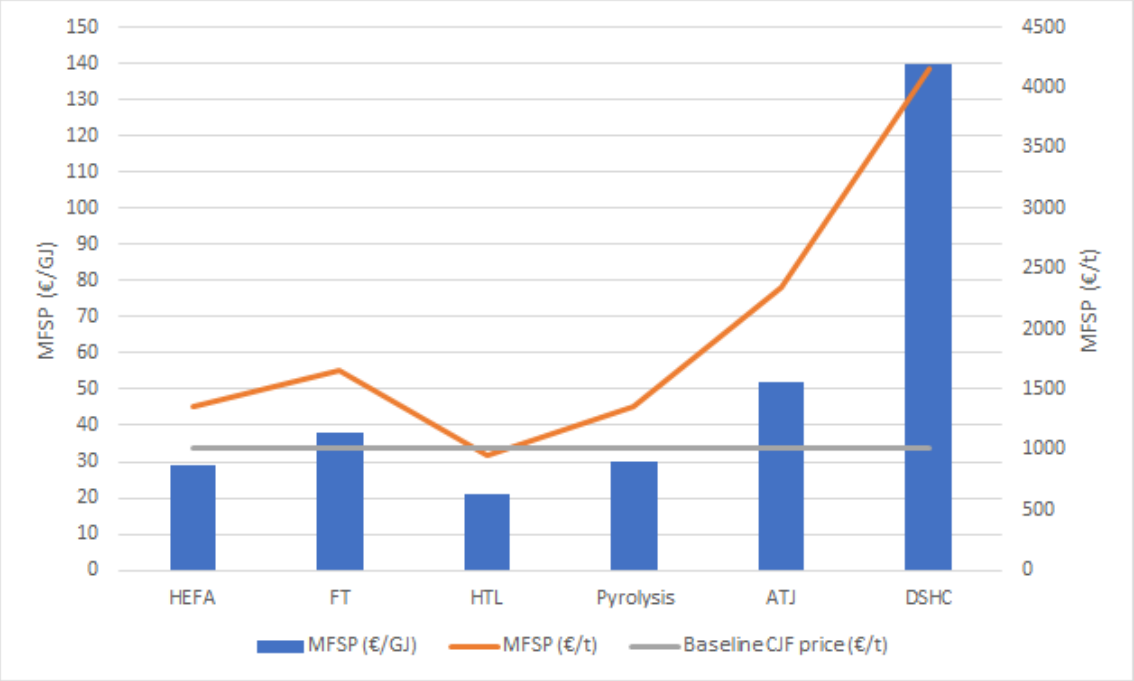

Figure 8: Minimum fuel selling prices compared against the current baseline jet fuel price represented by the grey horizontal line (data obtained from: [20, 21]).

It should be noted, that the FT technologies studied by de Jong et al. [20] used gasification technologies, which significantly increase both the capital and operational expenditure. In this thesis, gaseous biomethane is readily supplied to the process, eliminating the need for separate gasification processes.

4 Method selection

The motivation behind this study is to evaluate the economic feasibility of producing SAFs by using biogas as a feedstock. This production route falls under the GTJ pathway, for which FT pathways are an attractive choice due to their mature technology and extensive research behind them. The FT process, however, can be energy-intensive, leading to high operating costs. Producing the syngas feedstock for the FT process is also a particularly energy intensive part of the process.

Compared to HEFA, which is currently the most technologically mature pathway for the production of SAFs, FT has the clear advantage of having a more abundant feedstock. This enables the potential for expansion of production and better future prospects, and a generally lower feedstock price. According to a 2018 study, UCO prices are 33.3 €/GJ, while the price of natural gas, to which the feedstock in this process is comparable to, has a price of 5.02 €/GJ in June 2022. [16, 22] Other waste fats, oils and greases may also be used for HEFA processes, the availability of which will at most yield 1.2 Mt of SAF, accounting for only 1.9% of the total jet fuel demand in the year 2030. [23]

Based on the technological maturity of the FT processes and the opportunities the abundant feedstock provides, the production of SAF with this pathway is easily justified. As a company, St1 has a growing biogas production portfolio, for which upgrading can provide significant value for the company. St1 has an increasing interest towards using biogas as a feedstock for the production of renewable liquid fuels, as they have production plants where biogas can be collected from. [24, 25] In order for SAFs to be produced from this biogas, the gaseous product must be first processed into synthesis gas, which can then be processes in an FT reactor and subsequently distilled into liquid biofuels.

4.1 Biogas as a feedstock

Biogas is a desirable feedstock for the production of renewable fuels, as it is an abundant bioproduct from several different processes and industries. Biogas composition

depends mainly on the feedstock used for the fermentation or digestation process, and the amount of organic load available to be metabolized into biogas. [26] The main components in biogas include methane, carbon dioxide, oxygen and nitrogen, with trace amounts of hydrogen sulfide, benzene and toluene, which may be considered as contaminants. [27] While the composition of biogas can be complex, in this work it is assumed that the biogas is cleaned at the source. Biogas contaminant cleaning processes are mature technologies, for which solutions and equipment are readily available from vendors. [28] Higher heating values (HHV) of biogas constituents, as well as relevant GTL components such as carbon monoxide and hydrogen are presented in Table 3.

Table 3: Higher heating values for different biogas and GTL components.

Component	Chemical formula	Energy density
Methane	CH4	55.5 MJ/kg
Carbon dioxide	CO2	–
Oxygen	O2	–
Nitrogen	N2	–
Carbon monoxide	CO	9.2 MJ/kg
Hydrogen	H2	142.1 MJ/kg

4.2 Biogas upgrading

Biogas upgrading commonly refers to the removal of carbon dioxide to yield a gas with a high methane content, with a concentration up to 97%. Generally, there is little incentive to transport carbon dioxide as it has little value as a chemical. By separating CO_2 from the methane at the source, the transportation of the biogas as liquefied methane becomes more efficient in terms of the calorific content transported. Readily available mature technologies such as water scrubbing, pressure swing adsorption and amine scrubbing are in wide-scale industrial use in the upgrading of biogas. [29]

The main constituents of biogas are methane and carbon dioxide, with methane being the component containing the most chemical energy within the mixture.

Upgraded biogas is generally referred to as biomethane. Carbon dioxide can be used on its own as a feedstock for the production of renewable fuels, which would require significant amounts of hydrogen to produce a liquid fuel. Fuels produced with hydrogen sourced from electrolysis using renewable electricity are commonly referred to as efuels, which differ from the renewable fuels produced in this work.

Carbon dioxide is a required feedstock for the DMR and RWGS reactions, presented in Equations 4 and 5. The consumption of CO_2 gives a carbon tax credit, which may be accounted for in the economic evaluation. [30] Carbon dioxide produced in the process may be recycled, requiring a separate cleaning process before recycling it into the process.

While it is assumed that the liquefied biogas is mostly methane in order to make transportation easier, the carbon dioxide required by the process may be supplemented from other operations. It is assumed, that there are plants and processes nearby, from which carbon dioxide may be fed into the process.

In this work it is assumed that the biogas is readily upgraded to pure biomethane before feeding it into the process. Thus, pure methane is considered the feedstock of this process.

5 Syngas generation

To produce synthetic crude oil from FT, the methane must first be reformed into carbon monoxide (CO) and hydrogen (H_2). This mixture is often referred to as synthesis gas, or syngas. This process route of producing liquid fuels from gaseous feedstocks is considered a gas-to-liquid (GTL) process. The molar ratio of hydrogen to carbon monoxide (H_2/CO) in the syngas will affect the operation of the FT reactor [31], and the composition of the syngas is determined by the process used.

There are different process unit options for the reforming of methane; steam methane reforming (SMR), dry methane reforming (DMR), catalytic partial oxidation (CPOX) and autothermal reforming (ATR). These process units may be operated in series or simultaneously to achieve the desired H_2/CO ratio. Reverse water-gas shift (RWGS) processes can also be utilized to further control the H_2/CO ratio. For example, according to Baltrusaitis et al. [30], SMR alone would produce a H_2/CO ratio of 3, which would be too rich in hydrogen to be used in a FT reactor [30]. According to the research of Ostadi et al. [31], the highest total syncrude production and carbon efficiencies while minimizing the required FT reactor volume are achieved with a H_2/CO ratio of 2.05 [31]. The effect of the H_2/CO ratio is presented in Figure 9.

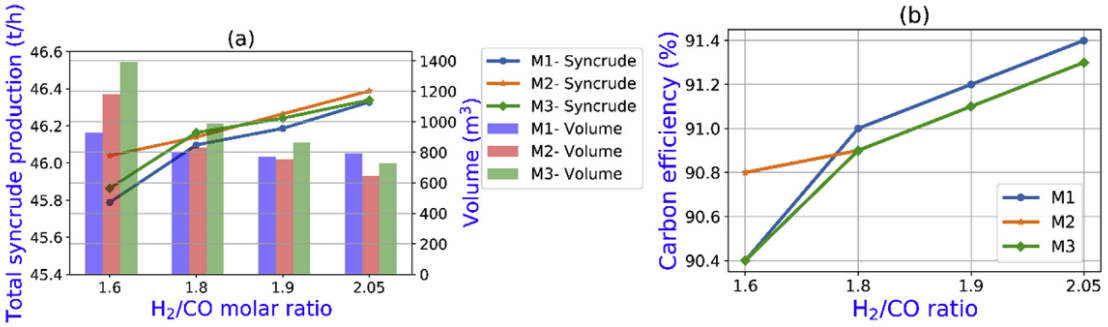

Figure 9: a) Total syncrude production and required FT reactor volume with constant CO feed with varying H_2/CO ratios, b) carbon efficiencies of the process [31].

5.1 Steam methane reforming

The SMR process is a catalytic process for the reforming of methane to syngas that has stood as the benchmark reforming process for decades. It has been used as a common method for producing hydrogen. [32] The primary reaction of SMR is presented in Equation 1 [30].

$$\mathrm{CH_4 + H_2O \rightleftharpoons CO + 3\,H_2} \qquad \Delta \mathrm{H_{298K}} = 205.6\,\mathrm{kJ/mol} \tag{1}$$

The SMR is an endothermic process, requiring heat which is commonly supplied in the form of natural gas. As the aim of the SMR reactor is to produce carbon monoxide and hydrogen, undesired water-gas shift (WGS) reactions may take place, in which carbon monoxide reacts with the steam in the reactor to form CO_2 and hydrogen. This WGS reaction is presented in Equation 2. [33]

$$\mathrm{CO + H_2O \rightleftharpoons CO_2 + H_2} \qquad \Delta \mathrm{H_{298K}} = -41\,\mathrm{kJ/mol} \tag{2}$$

As can be seen from Equation 1, the SMR reaction alone produces a H_2/CO ratio of 3, which is unsuitable for the production of syncrude from FT reactors. [31] Hence the SMR process must be coupled with a hydrogen consuming process in order to obtain a suitable feed for FT reactors when liquid fuels are the desired end product.

Steam reforming (SR) reactions may also be utilized for other hydrocarbons with more than a singular carbon atom. In this case, the SR reaction effectively first produces methane which is then converted into CO and H_2. This reaction can be presented as a single-step reaction shown in Equation 3.

$$\mathrm{C}_n\mathrm{H}_m + \mathrm{nH_2O} \longrightarrow \mathrm{nCO} + (\mathrm{n} + m\,/\,2)\,\mathrm{H_2} \qquad \Delta \mathrm{H_{298K}} > 0\,\mathrm{kJ/mol} \tag{3}$$

5.1.1 SMR process equipment and conditions

The process flow diagram of a typical SMR process used to produce syngas for FT reactors, as presented by Santos et al. [33] is shown in Figure 10.

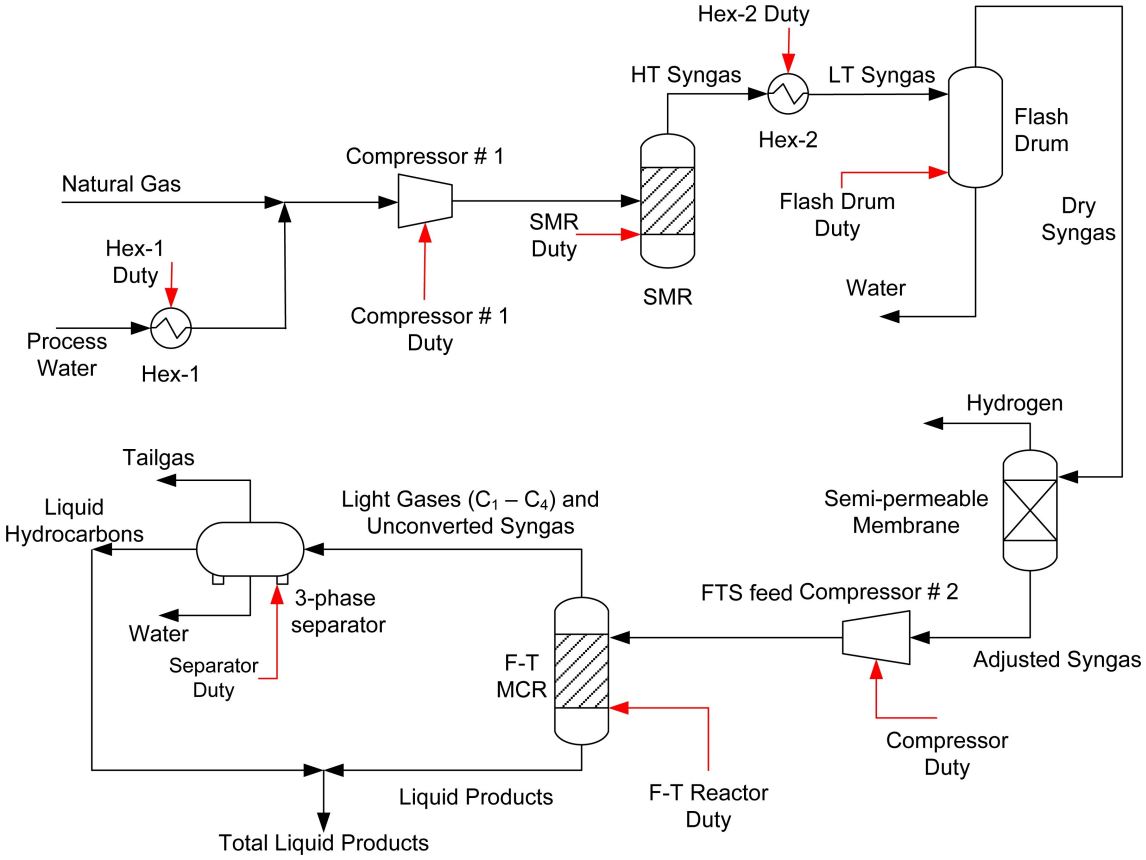

Figure 10: Process flow diagram of an SMR unit used to produce syngas for an FT reactor. [33]

The SMR unit presented in Figure 10 is operated at a pressure of 20 bar and a temperature of 860 °C with a molar steam/CH_4 ratio of 1.5:1. [33] A slightly different SMR reactor configuration is presented by Baltrusaitis et al. [30], presented in Figure 11. The SMR process illustrated in Figure 11 operates with a molar steam/CH_4 ratio of 3:1. The SMR reactor itself operates at 800–900 °C and 15-30 bar. The process employs a prereactor operated at 34 bar, fed with methane heated to 210 °C. The 240 °C steam used in the process is generated by feeding high-pressure liquid water into a vaporizer. The output temperature of the SMR reactor may be set to a desired level depending on the application and subsequent processing steps. Unless the SMR unit is used alongside a carbon dioxide consuming unit, the carbon dioxide formed in the unwanted WGS reaction presented in Equation 2 must be removed from the process with an absorber. The absorber is fed with a lean solvent, with 5

mol-% monoethanolamine diluted with water. [30]

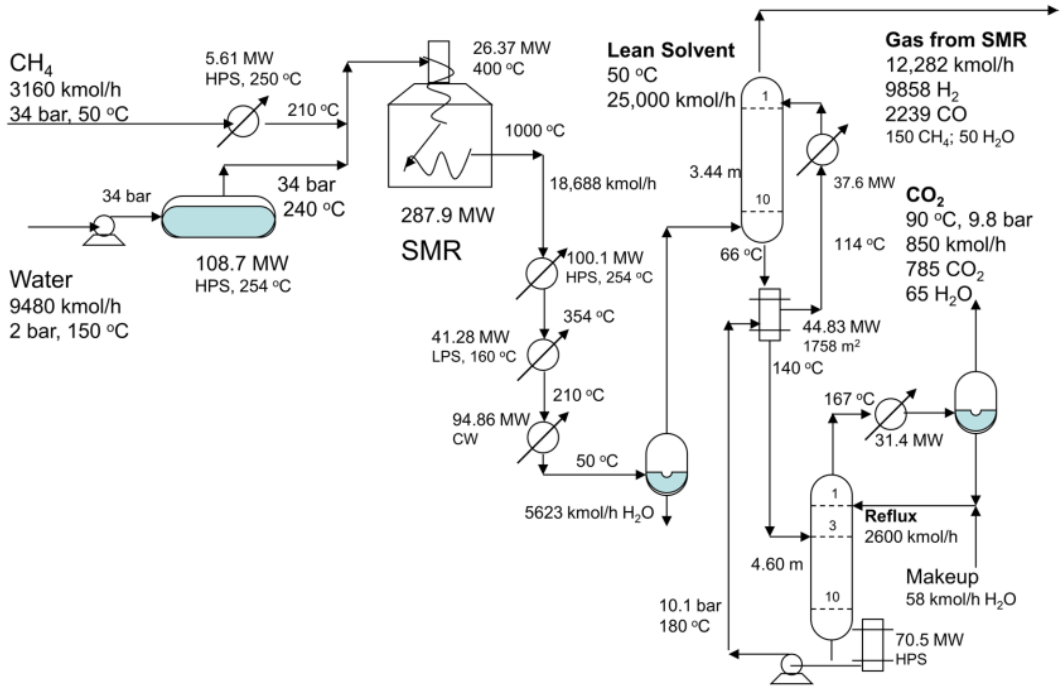

Figure 11: Process flow diagram of an SMR unit used to produce syngas for FT (modified from source: [30]).

.

5.1.2 SMR catalysts

The SMR process modelled by Baltrusaitis et al. [30] used a nickel-based catalyst and was able to reach a 95% conversion of methane to carbon monoxide, with the rest of the methane remaining unreacted. Carbon dioxide formation happens simultaneously following Equation 2. This carbon dioxide formation adds a necessary carbon dioxide removal step, increasing the operating costs and footprint of the production plant. To minimize the effect of this undesired WGS reaction while simultaneously maximizing the production of carbon monoxide and hydrogen through Equation 1, noble metal catalysts, such as γ -Al_2O_3, $CaAl_2O_4$ or MgO supported ruthenium and rhodium catalysts, are the optimal catalysts for SMR reactors as they provide high activity of Equation 1 and low activity of Equation 2. Relative activity of different catalyst materials are presented in Figure 12. However, despite the superior qualities of the

noble metal catalysts, nickel-based catalysts supported on the same metal oxide supports are preferred due to their significantly lower costs in industrial applications. [33]

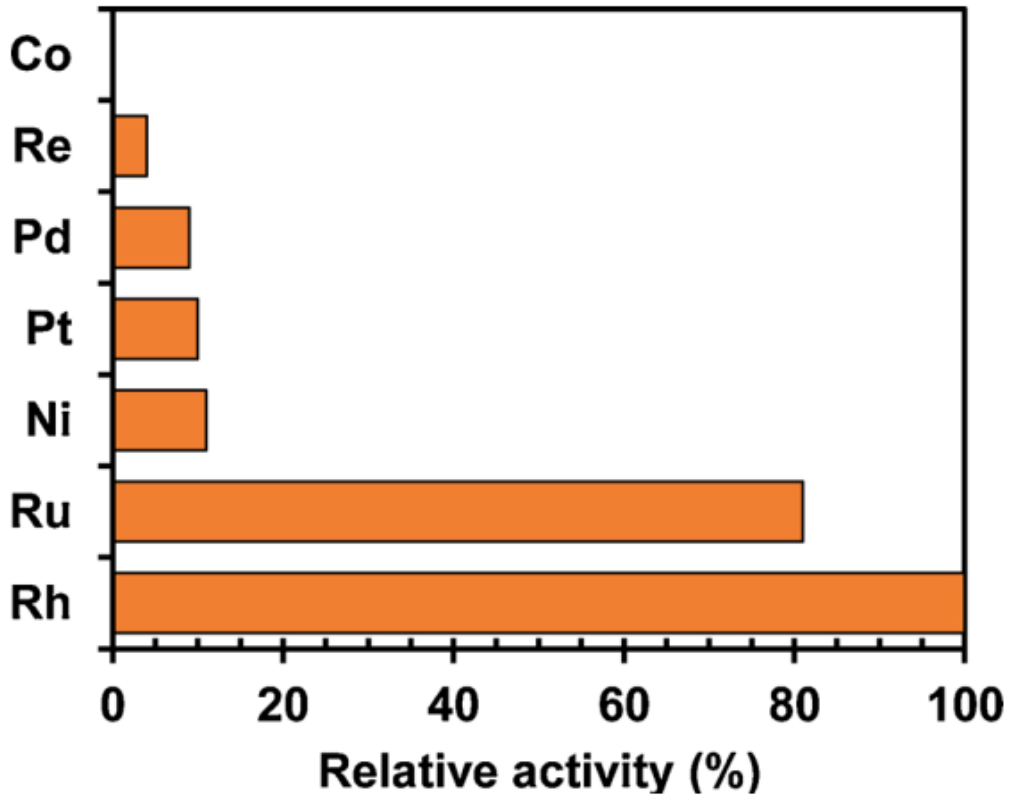

Figure 12: Summarization of the relative activities for different metal catalysts used in SMR [33].

5.2 Dry methane reforming

Dry methane reforming is a process in which methane reacts with carbon dioxide to produce carbon monoxide and hydrogen. The DMR reaction is presented in Equation 4. [30]

$$\mathrm{CH_4 + CO_2 \rightleftharpoons 2\,CO + 2\,H_2} \qquad \Delta \mathrm{H_{298K}} = 247.3\,\mathrm{kJ/mol} \tag{4}$$

As the DMR process consumes CO_2 while producing a syngas with a H_2/CO

ratio of 1 it is well-suited to be used in combination with the SMR process in order to obtain the desired H_2/CO ratio of 2. A combination of SMR/DMR also introduces steam into the reaction, eliminating most of the coking problems associated with nickel-based catalysts, enabling their use in an industrial application [34]. Similar to the case with SMR reactions, an unwanted reverse water-gas shift reaction (RWGS) may happen due to the simultaneous presence of carbon dioxide and hydrogen in the reactor. [30]. The RWGS reaction is presented in Equation 5.

$$CO_2 + H_2 \rightleftharpoons CO + H_2O \qquad \Delta H_{298K} = 41.2\,\mathrm{kJ/mol} \tag{5}$$

5.2.1 DMR process equipment and conditions

The general process equipment is presented by Baltrusaitis et al. [30] in the process flow diagram in Figure 13. [30]

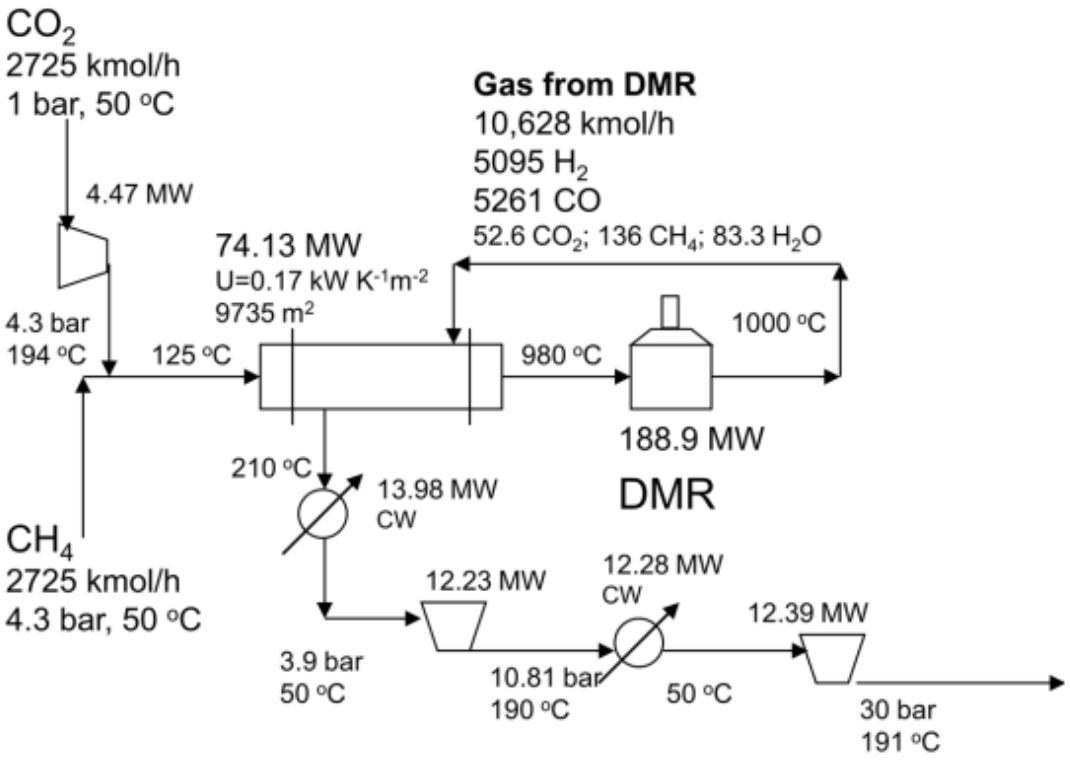

Figure 13: Process flow diagram of a DMR unit used to produce syngas for FT (modified from source: [30]).

The process modelled by Baltrusaitis et al. [30] is operated at a temperature of 980 °C and pressure of 4.2 bar to minimize possible RWGS reactions in the reactor. The carbon dioxide fed into the reactor is compressed to 4.3 bar and fed through a feed-effluent heat exchanger (FEHE), which preheats the feed to the reactor to the desired temperature of 980 °C. The exiting gas stream from the DMR reactor passes through the FEHE once more and is put through a two-stage compressions system to raise the pressure to 30 bar to be suitable for being fed into a FT reactor. [30]

5.2.2 DMR catalysts

Nickel-based catalysts are common catalysts for endothermic reactions, which have garnered interest for use in DMR reactions as well, but their industrial application is limited by coking in the DMR process. Coking happens through the decomposition of methane over the nickel catalyst, presented in Equation 6, or by the Boudouard reaction, shown in Equation 7. [35]

$$CH_4 \longrightarrow C + 2\,H_2 \qquad \Delta H_{298K} = 75.0\,kJ/mol \tag{6}$$

$$2\,CO \longrightarrow C + CO_2 \qquad \Delta H_{298K} = -172.0\,kJ/mol \tag{7}$$

The catalysts for the DMR reaction require stable and effective catalysts that can resist coking. [36] Ruthenium and rhodium catalysts present an attractive choice used in most industrial dry reforming applications due to their resistance to coking. [34] Platinum catalysts also offer a possible alternative due to their high coking resistance, long lifetime and better selectivity compared to nickel based DMR catalysts. [36] However, due to the high costs of these noble metal catalysts, the development of a nickel-based catalyst that is resistant to coking has been the subject of extensive studies. According to Guo et al. [37], the coking resistance can be greatly affected by the type of support and its modifiers. The most common supports for nickel-based catalysts used in DMR are γ -Al_2O_3, with developing interest towards other metal oxide supports. [37]

5.3 Catalytic partial oxidation

Syngas generation via catalytic partial oxidation of methane is based on the partial oxidation (POX) reaction of methane and oxygen over a catalyst bed. The reaction follows Equation 8 [33].

$$\mathrm{CH_4} + 0.5\,\mathrm{O_2} \rightleftharpoons \mathrm{CO} + 2\,\mathrm{H_2} \qquad \Delta \mathrm{H_{298K}} = -35.6\,\mathrm{kJ/mol} \tag{8}$$

The CPOX reaction is an attractive alternative to the SMR and DMR reactions due to several reasons; the reaction is exothermic as opposed to the SMR and DMR reactions, eliminating the need for expensive superheated steam, the generated syngas has a H_2/CO ratio of 2, which would enable its direct use in FT synthesis and the CPOX process yields little CO_2 compared to other options. [38]

5.3.1 CPOX process equipment and conditions

CPOX processes utilize a reactor, to which methane and oxygen are fed at a ratio slightly higher than the stoichiometric value to avoid carbon deposition. The gaseous components mix in a mixing layer and pass through the catalytic zone, where the reaction presented in Equation 8 takes place. An illustration of a CPOX reactor is presented in Figure 14. [39]

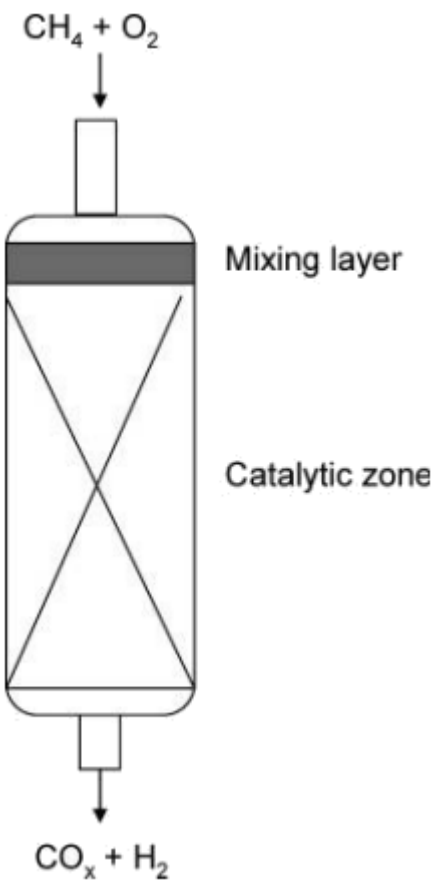

Figure 14: Illustration of a CPOX reactor. [39]

Fixed-bed reactors are the most commonly used reactor configurations for CPOX processes [40]. However, using fixed bed-reactors have been shown to produce undesired hot spots and temperature gradients on the catalyst surface by Enger et al. [41], which may affect the stability of the catalyst and reactor materials as well as enable the formation of binary species in the reactor. These temperature gradients and hot spots may be overcome by using a fluidized-bed reactor or a conical spouted-bed reactor. [41]

Typical CPOX reactions are operated at a temperature range of 400–1000 °C, depending on the catalyst used. At temperatures below 177 °C, no conversion is achieved due to the kinetic barrier of the reaction not being reached. In the temperature range 227–847 °C the reaction products may be accurately predicted from thermodynamics, with the conversion of methane and the selectivity of carbon

monoxide and hydrogen increasing with increasing temperature. [41, 38]

The conversion of methane and the selectivities to carbon monoxide and hydrogen have been shown to decrease with increasing pressures, so the CPOX reactors are typically operated at atmospheric pressure. [41] This effect is explained entropically by York et al. [38] to happen due to the reformation reactions becoming less favorable as they result in gas expansion, while the total combustion reactions such as carbon dioxide and water formation are affected much less by the increase in pressure. [38]

The effect of the reactant ratio and flow rate have also been studied. A CH_4/O_2 reactant ratio of 2 has been shown to be optimal for the POX reactions. If the ratio is decreased from this value, the reactions in the reactor become more favorable towards total combustion reactions producing carbon dioxide and water. An increased methane ratio results in an excess of methane, which hinders further conversion of methane. The CPOX reactions have been shown to favor low gas hourly space velocities (GHSV), with equilibrium product distributions being achieved at a GHSV value as low as $4 \times 10^4 h^{-1}$. At increased GHSV the kinetics of the reaction become a limiting factor. Using noble metal catalysts enable the use of a higher GHSV value, with ruthenium and rhodium enabling the highest flow rates due to their high activities. [38]

Generally, the optimal operating conditions for the CPOX process favor high temperatures at atmospheric pressure with a non-stoichiometric CH_4/O_2 at flow rates. A reaction operated at a temperature of 777 °C and a pressure of 1 bar reached a methane conversion of 99%, with carbon monoxide and hydrogen selectivities being 97% and 99% respectively. [38] The combined effects of different operating conditions studied by York et al. [38] are presented in Figure 15.

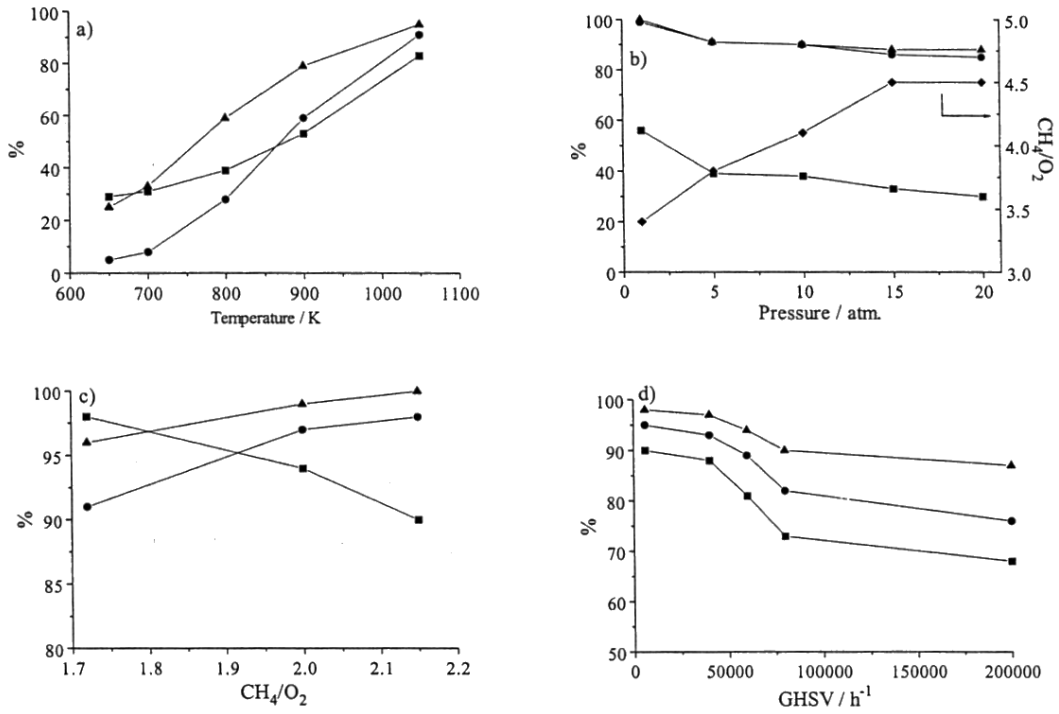

Figure 15: Effect of reaction conditions on the oxidation of methane over a ruthenium catalyst operated at T = 777 °C, p = 1 atm, $CH_4/O_2 = 2$ and GHSV = $4 \times 10^4 h^{-1}$ unless otherwise stated. (■) = X_{CH_4}, (•) = S_{CO}, (▲) = S_{H_2}. a) Effect of temperature, b) Effect of pressure, c) Effect of reactant ratio, d) Effect of GHSV. (modified from source: [38]).

5.3.2 CPOX catalysts

The main challenges for utilizing CPOX reactors in an industrial scale are associated with the catalysts used in the process. Controlling the selectivity of the reaction towards total combustion is a persisting problem [42], as there are a total of 11 reactions that may take place in a CPOX reactor according to Enger et al. [41]. The overall reactions observed in a methane oxidation system are presented in Table 4 [41].

Table 4: Overall reactions in the methane partial oxidation system. Reactions involving oxygen have been presented as irreversible for practical purposes [41].

$CH_4 + 2\,O_2 \longrightarrow CO_2 + 2\,H_2O$	(a)
$CH_4 + 0.5\,O_2 \longrightarrow CO + 2\,H_2$	(b)
$CH_4 + O_2 \longrightarrow CO_2 + 2\,H_2$	(c)
$CO + H_2O \rightleftharpoons CO_2 + H_2$	(d)
$CH_4 + H_2O \rightleftharpoons CO + 3\,H_2$	(e)
$CH_4 + CO_2 \rightleftharpoons 2\,CO + 2\,H_2$	(f)
$CO + H_2 \rightleftharpoons C + H_2O$	(g)
$CH_4 \rightleftharpoons C + 2\,H_2$	(h)
$2\,CO \rightleftharpoons CO_2 + C$	(i)
$CO + 0.5\,O_2 \longrightarrow CO_2$	(j)
$H_2 + 0.5\,O_2 \longrightarrow H_2O$	(k)

According to Enger et al. [41], all of the reactions presented in Table 4 play important roles in the partial oxidation of methane, and that there have not been any studies presenting indisputable evidence for a direct route to synthesis gas via the reaction presented in Equation 8. [41]

The POX reactions have been studied over various catalytic materials and supports, and as is the case with SMR reactions, noble metal and nickel catalysts have been the most commonly studied catalysts for the process. [41] All of the commonly utilized catalyst materials have been studied and shown to catalyze the POX reaction to thermodynamic equilibrium, with minimal carbon formation and no discernible carbon depositions on the catalyst materials. The rate of carbon formation over different catalyst materials is presented in Figure 16. [38]

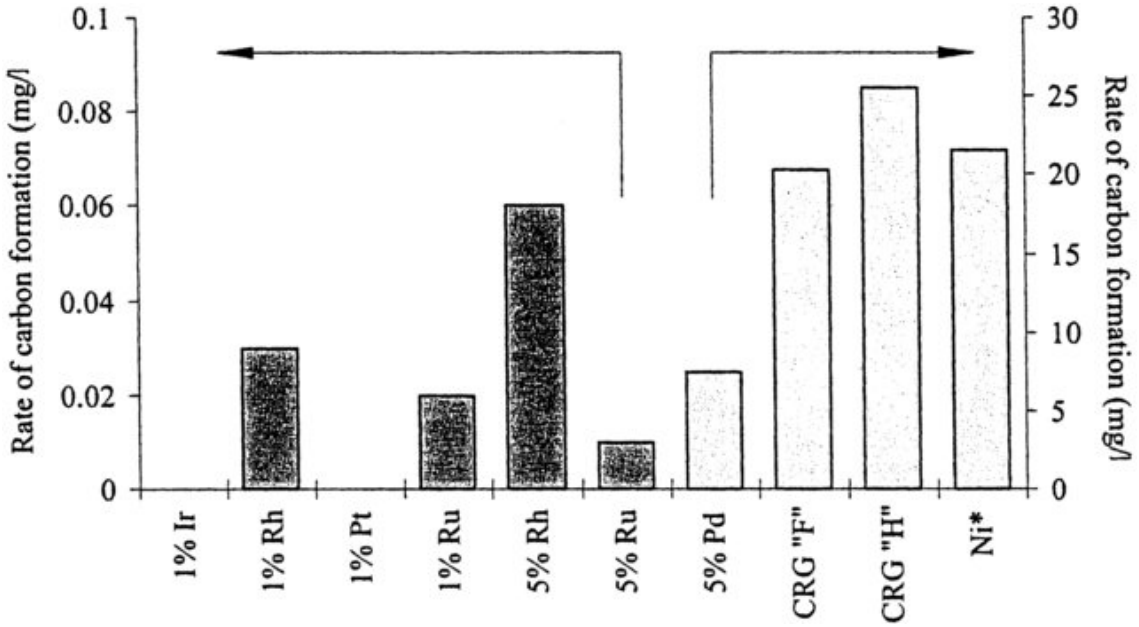

Figure 16: Carbon formation over different catalyst materials in CPOX reactions. [38]

CPOX processes of methane have been well documented and the catalysts have been studied since the 1990s [41]. However, as a catalyst that would present 100% activity towards the desired reaction presented in Equation 8 has still not been developed, combined with the need for expensive oxygen as a reagent, the process can be deemed as unsuitable for use as a standalone process for the production of syngas. However, POX reactions are an integral part of the ATR process.

5.4 Autothermal reforming

Autothermal reforming of methane is based on the combination of a partial oxidation (POX) reaction of methane and the SMR reaction presented in Equations 1 and 8. The output of an ATR reactor depends on the composition of the feed streams. If methane is reacted with oxygen and steam, the reaction can be done in a single chamber according to the Equation 9. [43]

$$\mathrm{CH_4} + 0.5\,\mathrm{H_2O} + 0.25\,\mathrm{O_2} \rightleftharpoons \mathrm{CO} + 2.5\,\mathrm{H_2} \qquad \Delta\mathrm{H_{298K}} = 84\,\mathrm{kJ/mol} \qquad (9)$$

If the feed streams include carbon dioxide, the ATR reaction follows Equation 10.

$$CH_4 + 0.5\,O_2 + 0.5\,CO_2 \rightleftharpoons 1.5\,CO + 1.5\,H_2 + 0.5\,H_2O \qquad \Delta H_{298K} = -15\,kJ/mol \tag{10}$$

The principle of the ATR reaction is that the exothermic POX reaction provides the heat required for the endothermic SMR reaction. As can be seen from Equation 9, the total ATR process is endothermic.

5.4.1 ATR process equipment and conditions

The general process equipment used in ATR is presented by Baltrusaitis et al. [30] in the process flow diagram in Figure 17.

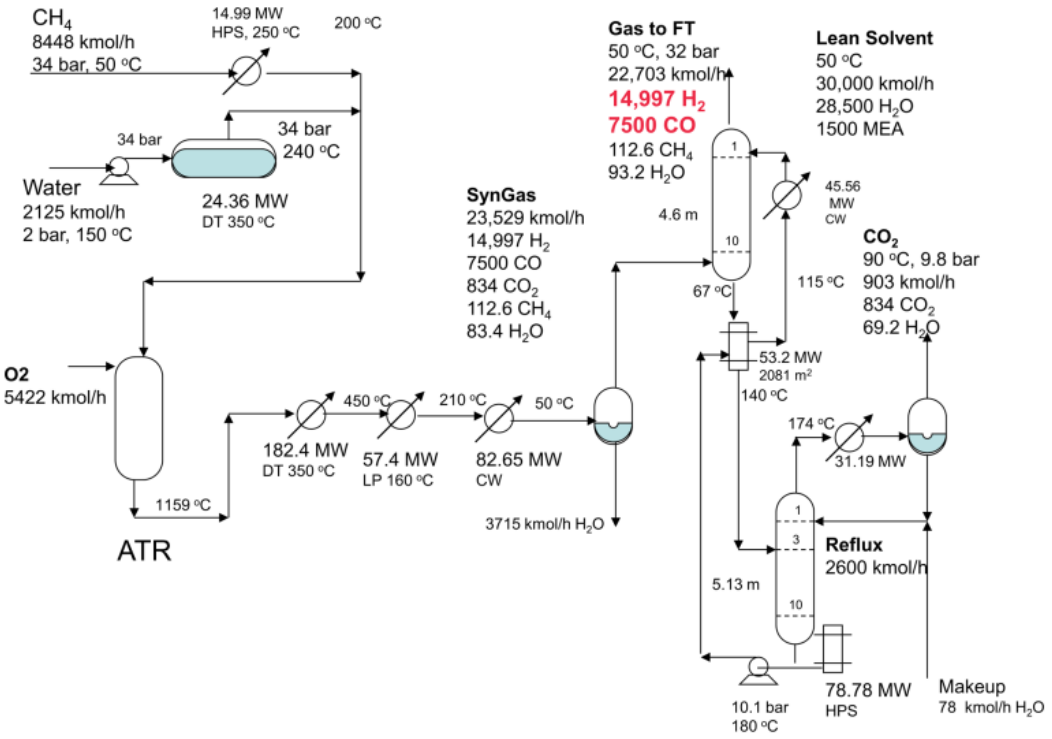

Figure 17: Process flow diagram of an ATR unit used to produce syngas for FT. [30]

According to Speight [44], a typical ATR reactor consists of three zones. First is the burner, which provides mixing for the feed streams in a turbulent diffusion

flame. Second is the combustion zone, where the POX reactions produce the desired mixture of carbon monoxide and hydrogen. Lastly comes the catalytic zone, in which the gases leaving the combustion zone reach thermodynamic equilibrium. [44] An illustration of an ATR reactor is presented in Figure 18.

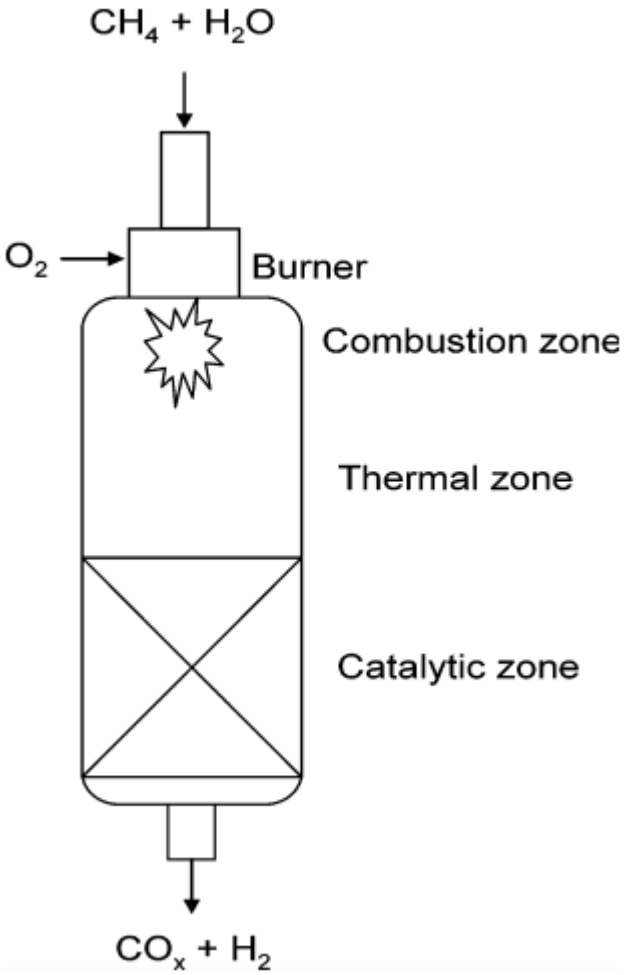

Figure 18: Illustration of an ATR reactor. [39]

The reaction is typically carried out in a temperature range of 900–1150 °C and pressures between 1 and 80 bar. [43]

5.4.2 ATR catalysts

Catalysts used in the ATR process are similar to those that are used in the SMR process, namely nickel and noble metals, with nickel catalysts being the most attrac-

tive choice. However, as the reactor temperature in ATR is significantly higher than in SMR, the catalyst requires higher resistance to high temperatures with high thermal stability. This thermal stability may be increased by using temperature-stable supports for the nickel catalysts, such as magnesium alumina spinel. Studies have also proposed using bimetallic catalysts, such as nickel-platinum catalysts to achieve the desired thermal stability. [39]

5.5 Reverse water-gas shift

For process configurations that produce an excess of hydrogen, reverse water-gas shift reactions can be utilized to convert the excess hydrogen to carbon monoxide while consuming unwanted carbon dioxide. The reaction follows Equation 5 as presented earlier [45]. As methane is the desired feedstock in the process, RWGS reactors can not be used as a standalone method for producing synthesis gas.

The RWGS reaction where carbon monoxide is formed competes with the Sabatier reaction presented in Equation 11. While methane is the feedstock in the process, it is an undesired product in the syngas stream, as it complicates the subsequent separation processes before the syngas can be fed into the FT reactor. [46]

$$\mathrm{CO_2} + 4\,\mathrm{H_2} \rightleftharpoons \mathrm{CH_4} + 2\,\mathrm{H_2O} \qquad \Delta \mathrm{H_{298K}} = -164.7\,\mathrm{kJ/mol} \tag{11}$$

5.5.1 RWGS process equipment and conditions

Baltrusaitis et al. [30] present two different process configurations for using a RWGS process alongside a SMR reactor. The first, presented in Figure 19, utilizes a FEHE condenser to cool and condense the outlet gas from the SMR reactor to remove water before the RWGS reactor. Removing water contributes to the overall conversion of carbon dioxide and hydrogen, as water pushes the reaction in the opposite direction as seen from Equation 5. The removal of water also means less fresh carbon dioxide is required. However, this configuration requires an excessive heat exchanger area, which increases both the capital investment and the overall plant footprint. [30]

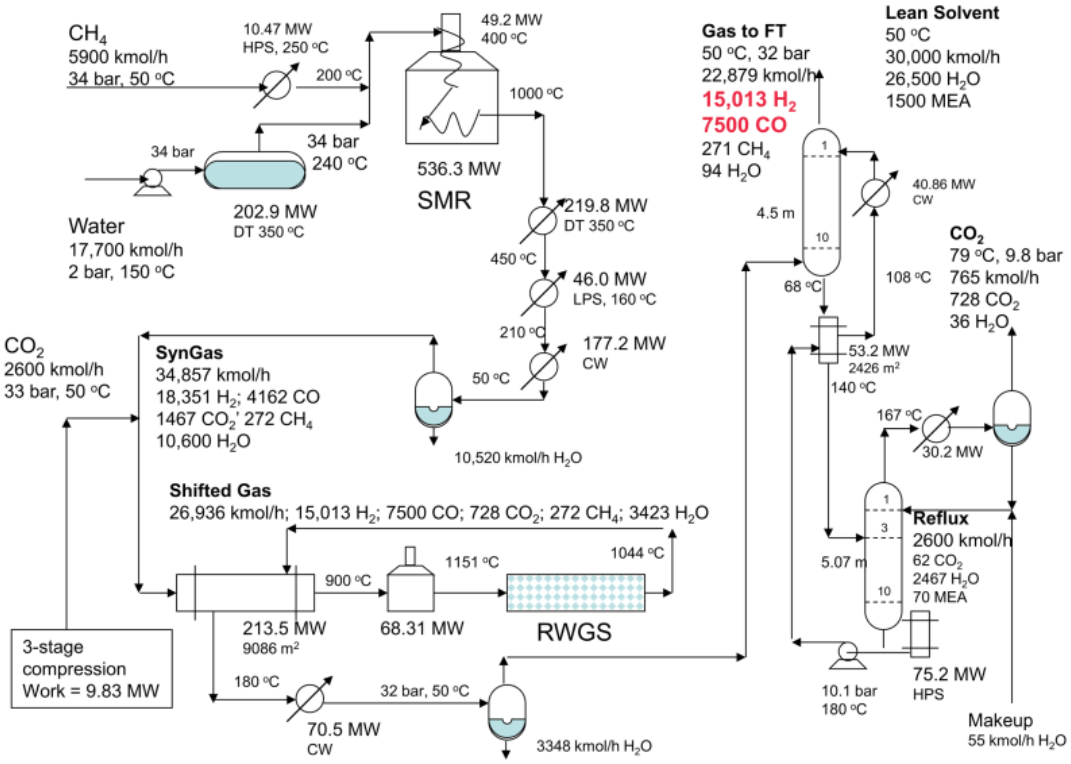

Figure 19: Process flow diagram of a RWGS unit with an intermediate cooler between the SMR and RWGS reactors. [30]

The second RWGS configuration, presented in Figure 20, sends the outlet gas from the SMR reactor directly to the RWGS reactor. This configuration requires more fresh carbon dioxide, meaning the possible amine treatment units to clean carbon dioxide may become a concern regarding the plant capital investment. [30]

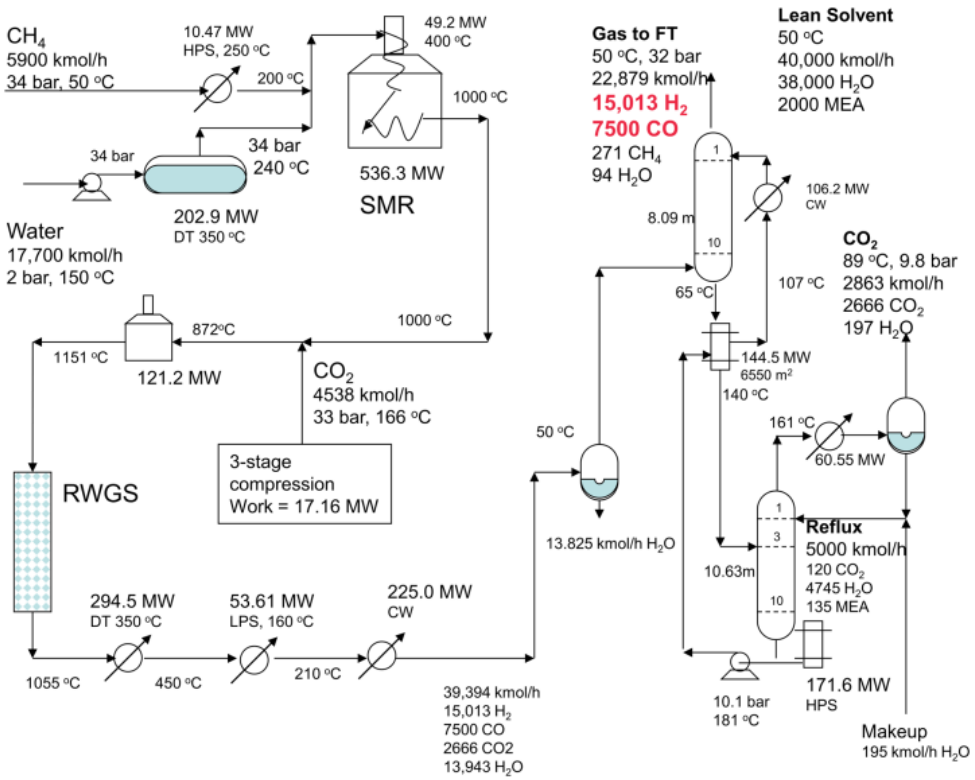

Figure 20: Process flow diagram of a RWGS unit with direct inlet feed from an SMR reactor. [30]

The RWGS reaction is mildly endothermic, meaning a relatively inexpensive adiabatic reactor should be sufficient for the reaction. The temperatures required by the process depend on the amount of carbon dioxide fed into the process, with the required temperature decreasing with increasing carbon dioxide feed. The RWGS processes modelled by Baltrusaitis et al. [30] operate with a H_2O/CH_4 ratio of 3, with the SMR reactor outlet temperature set at 1000 °C. The SMR outlet stream is cooled to 50 °C with energy-recovering heat exchangers. The RWGS reactor inlet feed is heated back up to 900 °C by the effluent stream of the reactor through a FEHE, followed by a furnace heating the stream up to 1151 °C before entering the RWGS reactor. The process operates at a pressure of 33 bar.

5.5.2 RWGS catalysts

Currently, no catalysts have been developed to ensure 100% selectivity towards carbon monoxide formation. Zhu et al. [46] suggest that the development of such catalysts is the milestone that has to be reached before RWGS may be employed in a process where carbon monoxide is the desired product. [46]

While there is debate on the mechanisms of RWGS with no clear consensus according to Zhu et al. [46], the RWGS catalyst requires two functionalities; adsorption of CO_2 and the disruption of the C–O bond and the disassociation of H_2 on the catalyst surface. [46] Even without a consensus on the mechanisms of the RWGS reaction, the active and selective RWGS catalyst should have both an active metal as well as a metal-oxide support that participates in the reaction. Copper, iron and noble metal catalysts supported on different metal-oxide supports have been studied extensively, operated at a temperature range of 200–700 °C and pressures between 1–50 bar depending on the catalyst. [47]

5.6 Process selections for Fischer-Tropsch

Baltrusaitis et al. [30] studied different process configurations to produce syngas for FT synthesis. These configurations include the combination of SMR and DMR, SMR and RWGS (with both process configurations presented in Section 5.5.1) and ATR as a standalone process. These configurations were studied in terms of total annual cost (TAC) and capital costs of the process. A summarization of the TAC and capital cost studies are presented in Table 5. [30]

Table 5: Summarization of the TAC and capital costs for different syngas production configurations (modified from source: [30]).

Configuration	TAC (M€/a)	Capital (M €/a)	Total (M€/a)
SMR/DMR	337.648	46.7086	384.3566
SMR/RWGS	350.62	53.7398	404.3598
SMR/ATR	359.268	20.4732	379.7412
SMR/RWGS$_{MOD}$	363.31	53.0912	416.4012
ATR	375.906	17.1362	393.0422

As can be seen from Table 5, the process configurations do not have significant variance in terms of their total costs annually. The configurations utilizing ATR processes have the lowest capital costs for total project times, while the configurations using SMR processes have the highest costs.

Besides economic analyses, the maturity of the processes must also be evaluated. Out of the available technologies, the SMR and DMR processes can be considered mature processes, as there is industrial production using those technologies. As was mentioned in Section 5.3, CPOX processes have not been utilized in industrial scale due to challenges with the catalyst materials. As such, they have been left out of consideration. ATR processes present a possible alternative for syngas production in terms of maturity, however, the requirement for expensive oxygen in the process may make them an economically unviable choice. RWGS process units partly suffer from undeveloped catalysts, but can still be a viable choice for the production of syngas. The use of RWGS reactors would require gas cleaning steps between the syngas production and FTS.

Based on these, the process configuration assessed in this work is the SMR/DMR configuration. Other configurations should be looked over in future works, but for the sake of this work, SMR/DMR is chosen due to its technological maturity and extensive available literature on the processes.

6 Fischer-Tropsch Synthesis

Fischer-Tropsch processes are catalytic hydrogenation processes in which synthesis gas comprised of carbon monoxide and hydrogen is converted into synthetic hydrocarbons of various chain lengths over a transition metal catalyst. [48] The FT process dates back to 1923, when Fischer and Tropsch first reported the production of liquid hydrocarbons over an iron catalyst. The main characteristics of the FTS is the production of a wide range of hydrocarbon products and the exothermic nature of the reactions. [49]

6.1 Fischer-Tropsch chemistry

FTS can be generalized as a polymerization reaction with five basic steps;

I the adsorption of CO onto a catalyst surface
II chain growth initiation by the dissociation and subsequent hydrogenation of CO
III chain propagation with additional CO molecules and subsequent hydrogenation
IV chain termination
V product desorption from the catalyst surface

The two main products from FTS are n-paraffins and α-olefins. Paraffin is a general term used to describe hydrocarbons consisting only of saturated hydrocarbons while α-olefin is used for hydrocarbons with double-bonded carbon atoms at the beginning of the hydrocarbon chain in the α-position. Differences between paraffin and α-olefin molecules is demonstrated in Figure 21.

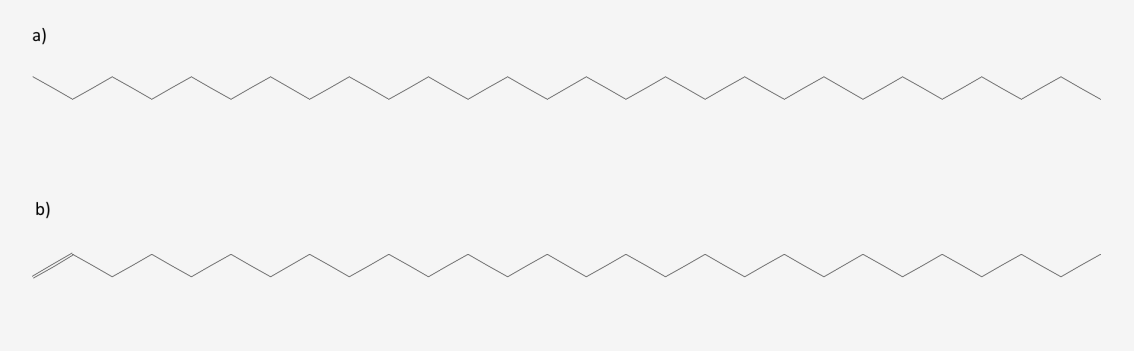

Figure 21: Differences in molecular structure between C28 chain-length paraffins and α-olefins. a) n-paraffin octacosane, b) α-olefin 1-octacosane (modified from source: [50, 51]

There is also a possibility of the formation of aromatics and alcohols in the process. The general FTS reaction is presented in Equation 12, and the n-paraffin and α-olefin reactions are presented in Equations 13 and 14 respectively. Generally, the definitions for the FTS products are set by their carbon numbers, with syncrude being defined as produced hydrocarbon chains with carbon numbers of 5 and above. [31]

$$\mathrm{CO} + 2\,\mathrm{H_2} \rightleftharpoons -\mathrm{CH_2}- + \mathrm{H_2O} \qquad \Delta \mathrm{H_{298K}} = -165\,\mathrm{kJ/mol} \tag{12}$$

$$\mathrm{nCO} + (2\,\mathrm{n} + 1)\,\mathrm{H_2} \longrightarrow \mathrm{C}_n\mathrm{H}_{2n+2} + \mathrm{nH_2O} \qquad \mathrm{n} = 1,2,...,\infty \tag{13}$$

$$\mathrm{nCO} + 2\,\mathrm{nH_2} \longrightarrow \mathrm{C}_n\mathrm{H}_{2n} + \mathrm{nH_2O} \qquad \mathrm{n} = 2,3,...,\infty \tag{14}$$

While the n-paraffin and α-olefin reactions are considered desired reactions, the formation of alcohols is an undesired reaction. The alcohol formation reactions are presented in Equation 15 [52].

$$\mathrm{nCO} + 2\,\mathrm{nH_2} \longrightarrow \mathrm{C}_n\mathrm{H}_{2n+1}\mathrm{OH} + (\mathrm{n\text{-}1})\,\mathrm{H_2O} \tag{15}$$

Other undesired reactions may also take place, including WGS and Boudouard

reactions, presented in Equations 2 and 7 respectively. Besides these, carbonaceous materials and bulk carbides may also form. Carbonaceous materials may form via the reaction of carbon monoxide, presented in Equation 16, while the bulk carbides may form from a reaction involving either carbon monoxide or carbon dioxide, presented in Equations 17 and 18 respectively. [52]

$$(\mathrm{x} + (\frac{\mathrm{y}}{2}))\mathrm{H_2} + \mathrm{xCO} \longrightarrow \mathrm{C}_x\mathrm{H}_y + \mathrm{xH_2O} \tag{16}$$

$$\mathrm{yCO} + \mathrm{xM} \longrightarrow \mathrm{M}_x\mathrm{O}_y + \mathrm{yC} \tag{17}$$

$$\mathrm{yCO_2} + \mathrm{xM} \longrightarrow \mathrm{M}_x\mathrm{O}_y + \mathrm{yCO} \tag{18}$$

The FTS is a kinetically controlled reaction, where the reactions can be generalized as polymerisation reactions of the CH_2-groups on a catalyst surface. The products of the FTS are determined by the catalyst's ability to propagate chain growth and inhibit chain termination reactions. As the propagation and termination reactions are independent of the chain length, the hydrocarbon chain growth can be predicted with the Anderson-Schultz-Flory (ASF) statistical distribution model, presented in Equation 19. [49]

$$W_n = n(1-\alpha)^2\alpha^{n-1} \tag{19}$$

where W_n = weight percentage of a product of n carbon atoms
n = number of carbon atoms
α = chain growth probability

The expected product distributions and hydrocarbon chain lengths according to the ASF model is presented graphically by Spath et al. [49] in Figure 22.

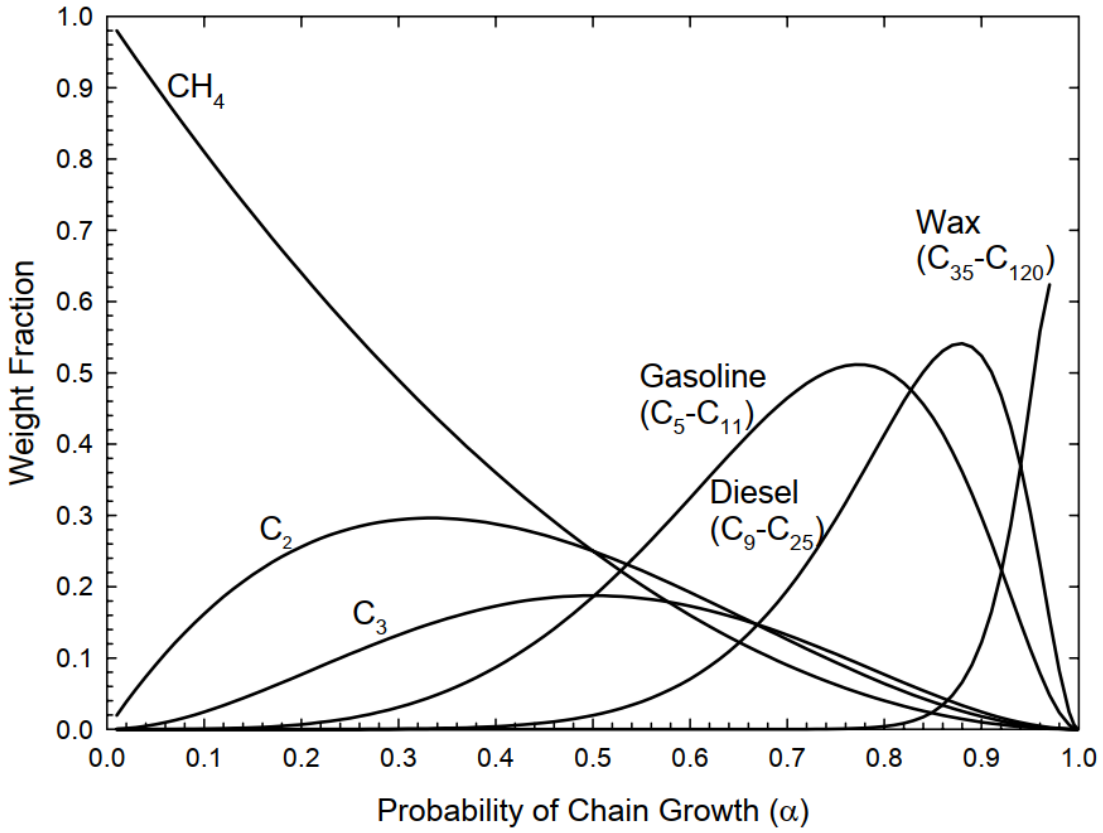

Figure 22: The Anderson-Schulz-Flory distribution presented graphically. [49]

The FTS always produces a range of olefins, paraffins and oxygenated compounds regardless of the operating conditions. However, the product distributions may be influenced by temperature, feed gas composition, pressure and the catalyst material used. With these, the selectivity of the reactions may be directed towards the desired outcome. For example, FTS can theoretically be directed towards having 100% selectivity towards methane. High selectivity towards heavy paraffin wax is also possible. According to Spath et al. [49], the maximum selectivities towards the gasoline and diesel product fractions are 48% and 40% respectively. [49] This means FTS is unable to direct selectivity completely towards jet fuel fractions, and other fractions are inevitable in the process. However, a part of the gasoline fractions fall within the jet fuel fraction and heavy fractions may be processed further to obtain jet fuels.

6.2 Process equipment

At the center of the Fischer-Tropsch process is the FTS reactor. Due to the high exothermicity of the FTS reactions, appropriate heat removal is crucial for controlling FTS selectivity and preserving the catalysts. Commercially, four different reactor setups have been used; multi-tubular fixed bed, circulating fluidized bed, fixed fluidized bed and fixed slurry bed reactors. These FTS reactors are presented in Figure 23. [49]

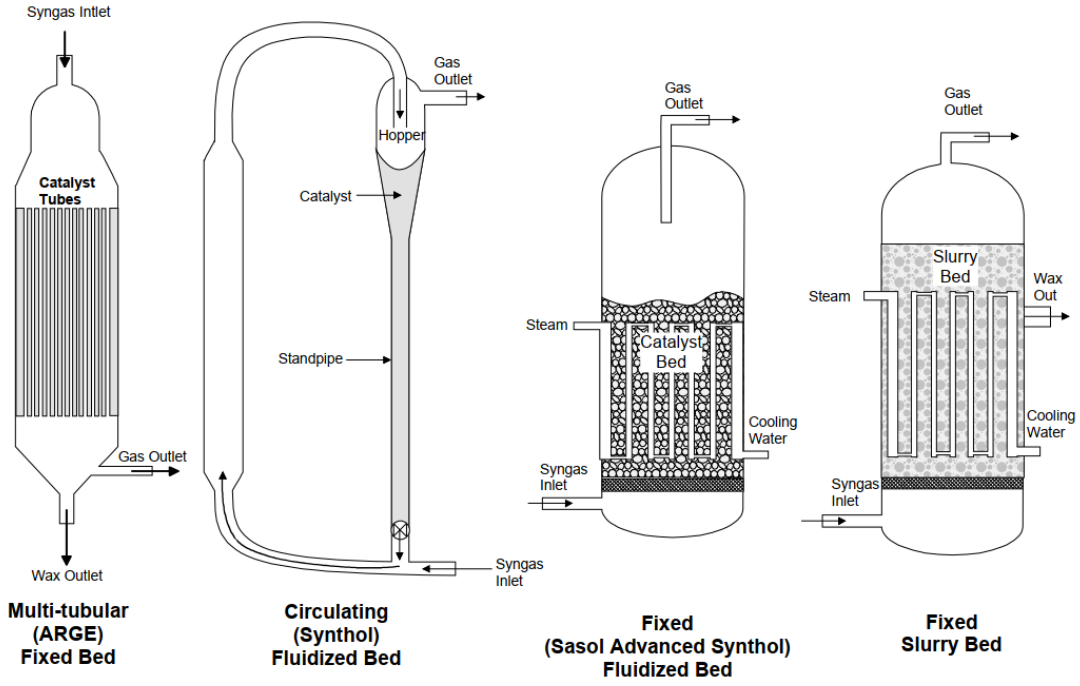

Figure 23: The four commercially used FTS reactor configurations. [49]

While slurry bed reactors are a proven technology with several favorable aspects compared to fixed and fluidized bed reactors, such as little down time and lower catalyst consumption, separating the catalyst slurry may be difficult in large-scale operation. [53] Other novel configurations such as micro channel systems and ionic suspensions for the FTS catalyst have been studied but have not been utilized in an industrial scale. [54]

The high exothermic nature of the FT reactors also means there is significant potential for energy integration in order to minimize the consumption of external

heat in the process. The heat from the FTS may also be used in other parts of the overall process, such as syngas generation.

6.3 Process conditions

FTS can be operated in several different modes, depending on the desired end products. High conversion of CO is a common goal for all modes of operation to ensure high productivity, but selectivity may depend on operation temperature, pressure and feed ratios.

6.3.1 Temperature

FTS is generally operated under two different temperature ranges; the low-temperature Fischer-Tropsch (LTFT) at a range of 200–250 °C and the high-temperature Fischer-Tropsch (HTFT) at a range of 320–350 °C. The LTFT operates as a three-phase gas-liquid-solid system, while the HTFT system operates as a gas-solid system under the reaction conditions. The LTFT synthesis processes favor hydrocarbon chains in the diesel-distillate and wax region, while the HTFT produces products in the gasoline region. [55]

6.3.2 Pressure

The operating pressure of FTS is also a significant factor affecting the conversion of CO. Over typical iron and cobalt catalysts, LTFT processes are carried out in a pressure range of 20–45 bar, while HTFT processes operate a range of 20–40 bar. [56] Akbarzadeh et al. [57] studied the effect of pressure on overall CO conversion and found that over bimetallic cobalt-catalysts, the optimal operating pressure was 20 bar, as is shown in Figure 24.

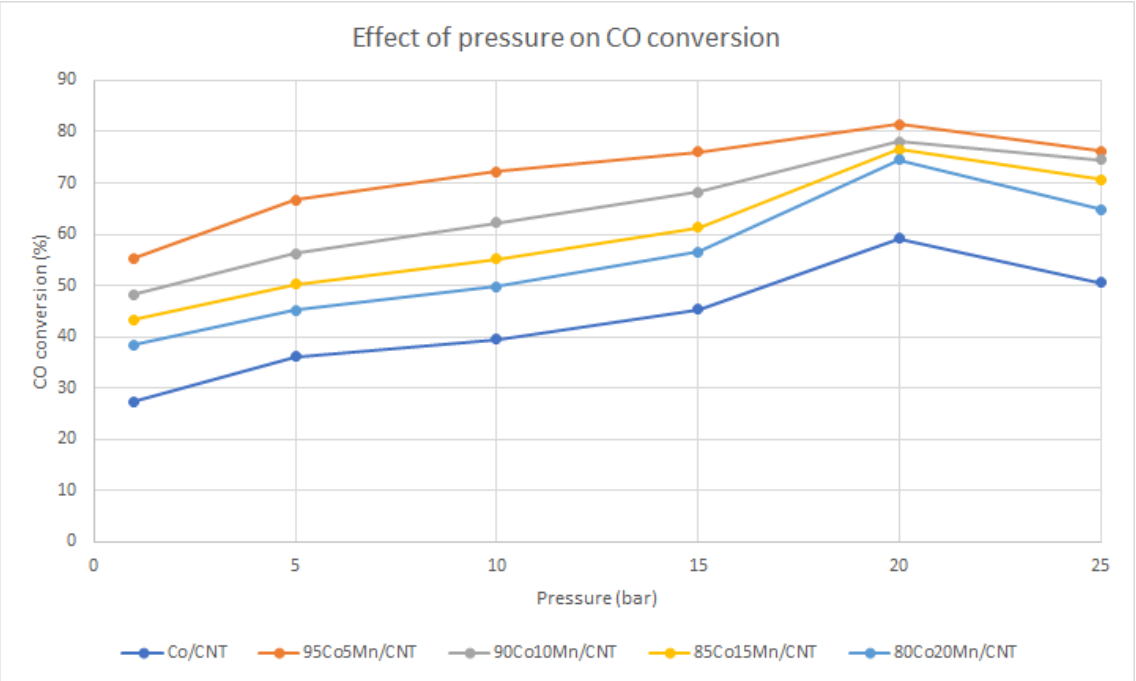

Figure 24: The effect of operating pressure on CO conversion over varying bimetallic cobalt catalysts (data from source: [57]). Co/CNT = carbon nanotube supported cobalt catalyst, 95Co5Mn/CNT = carbon nanotube supported 95% cobalt and 5% manganese catalyst, 90Co10Mn/CNT = carbon nanotube supported 90% cobalt and 10% manganese catalyst, 85Co15Mn/CNT = carbon nanotube supported 85% cobalt and 15% manganese catalyst, 80Co20Mn/CNT = carbon nanotube supported 80% cobalt and 20% manganese catalyst.

6.3.3 H_2/CO ratio

The ratio at which hydrogen and carbon monoxide is fed into the FT process is an important parameter for controlling FTS and its selectivity. The optimal H_2/CO molar ratio for CO conversion in FTS has been studied extensively, with most sources citing an optimal feed H_2/CO ratio of 2. [58, 31, 52, 55] These citations are supported by the studies of Akbarzadeh et al. [57], where the CO conversion was found to increase with increasing H_2/CO ratio over different catalyst materials up to a ratio 2, after which the conversions started decreasing. The results of the studies are presented in Figure 25. The studies also show, that the selectivity towards syncrude

increases with increasing H_2/CO ratio up until 2. [57]

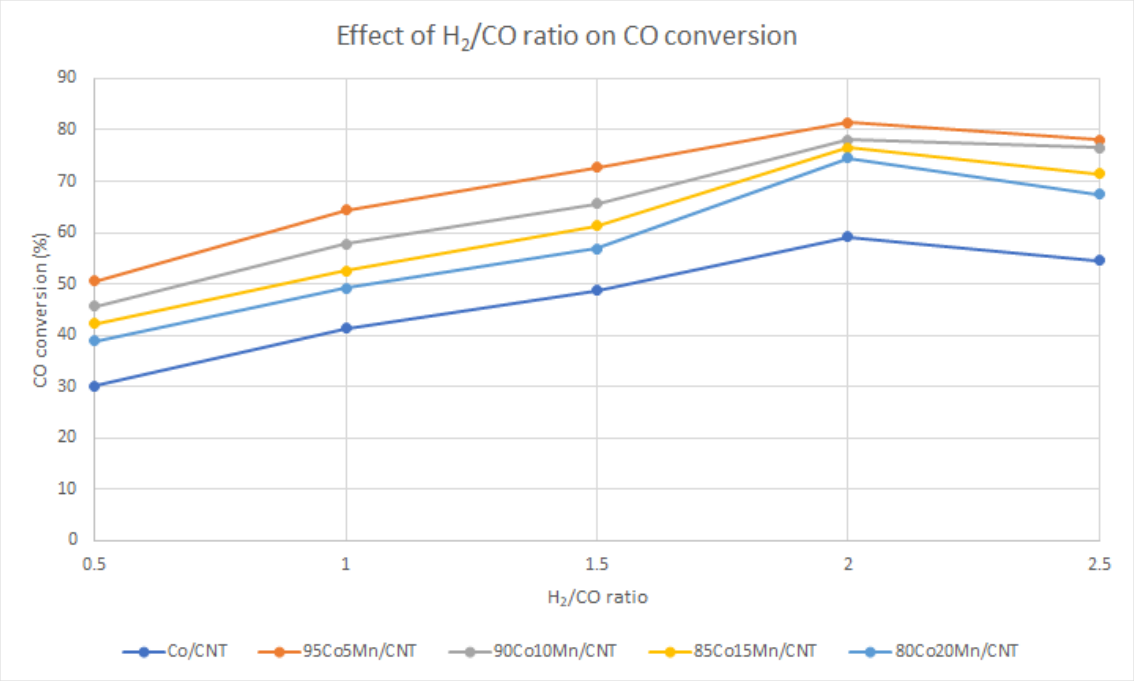

Figure 25: The effect of the H_2/CO molar ratio on CO conversion over varying bimetallic cobalt catalysts (data obtained from source: [57]).

The effect of the H_2/CO ratio on the selectivity towards different FTS products was studied using two different configurations for the production of syngas by Marchese et al. [58], showing increased selectivity towards middle distillates with increasing H_2/CO ratio. The results from these studies are presented in Figure 26. [58]

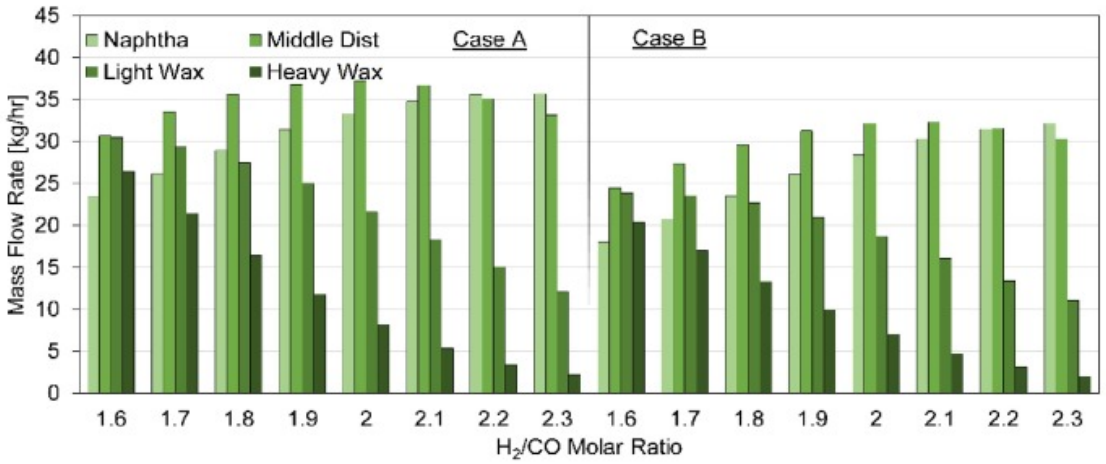

Figure 26: The effect of the H_2/CO molar ratio on the selectivity of FTS (modified from source: [58]).

The optimal H_2/CO ratio of 2 is not uniform for all FTS processes, but more a recommended starting point for optimization of the process. For example, the true optimal H_2/CO ratio for industrial operations depends heavily on the catalyst, with a ratio of 2 being optimal for cobalt-catalysts while an iron-catalyst may operate in a H_2/CO ratio range of 0.5–2.5. [59]

6.4 Catalysts

Iron, cobalt, ruthenium and nickel are the main catalysts that catalyze FT reactions. Ruthenium is an expensive noble metal, and nickel only has selectivity towards methane, so they are not used in GTL applications. As a result, iron and cobalt catalysts are the ones that have seen widespread use in industrial applications. The two catalysts produce different products with varying operating conditions. [55]

6.4.1 Iron catalysts

Iron catalysts are the cheaper alternative of the two industrially used catalysts, with the price of raw cobalt materials being on average 250 times more expensive than raw iron. Comparatively, iron is more resistant to catalyst poisons and more responsive to selectivity manipulations with operating conditions. As such, iron

catalysts are capable of producing both light hydrocarbons as well as heavy FT waxes. Iron catalysts produce a chain-growth probability of 0.94 at LTFT conditions, within a temperature range of 220–250 °C. This LTFT operation yields mainly hydrocarbons with a chain length of 21 and above. At HTFT operation, the chain-growth probability decreases to 0.7 at a temperature range of 320–350 °C, while producing transportation fuel suitable lighter hydrocarbons. [55] The lighter fractions are especially of interest in GTL processes, where liquid biofuels are the end-goal.

The mechanisms through which FT reactions happen on iron-catalysts have been studied extensively, with several different mechanisms being proposed and being generally agreed upon throughout history. Currently, at LTFT conditions, it is agreed that iron catalyst operates following the carbide mechanism, presented in Figure 27. An oxygenate mechanism has also been proposed in the past, with recent interest rising towards the mechanism by Davis [60] in 2009. [60]

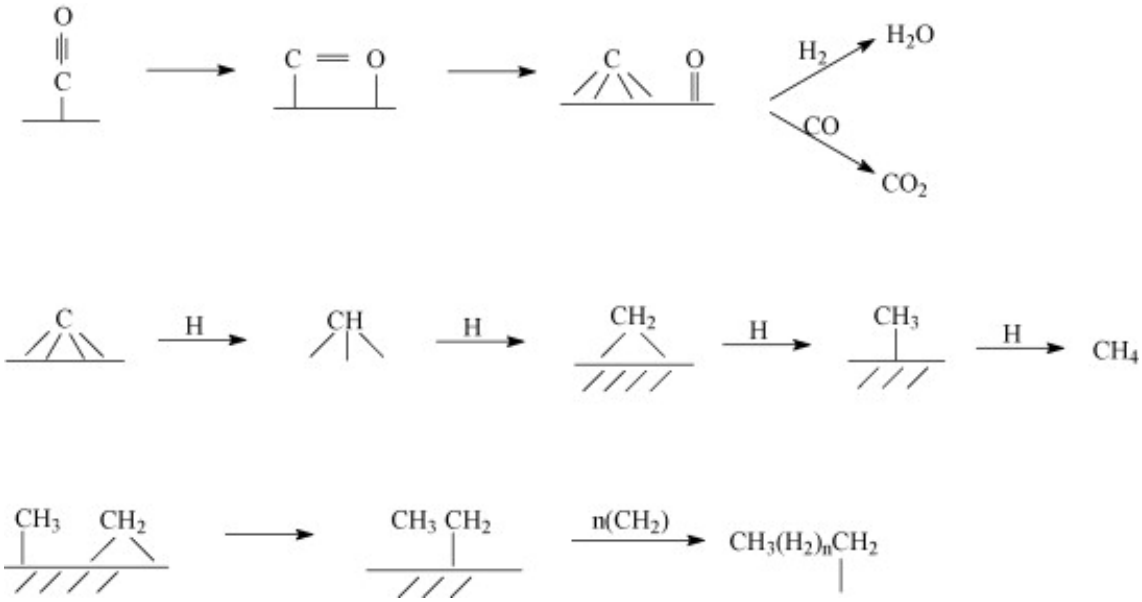

Figure 27: The carbide mechanism through which iron catalysts work in FTS. [60].

Under HTFT conditions, the direct CO dissociation seen in Figure 27 become a minor contributor, and the reactions happen through hydrogen-assisted CO dissociation. The difference between these two dissociation mechanisms is presented in Figure 28. [61]

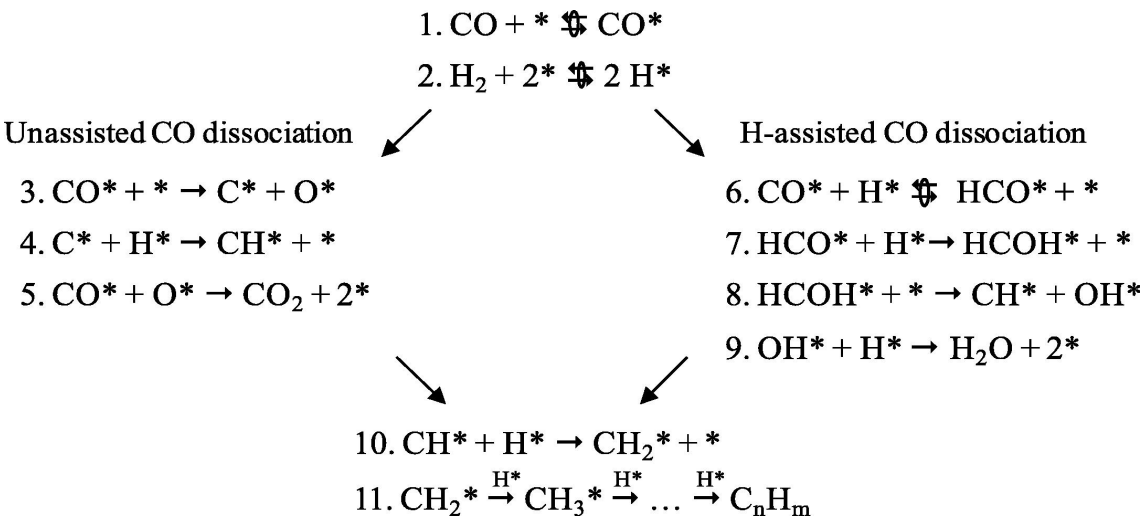

Figure 28: Direct and hydrogen assisted CO dissociation mechanisms [61].

6.4.2 Cobalt catalysts

Cobalt catalysts precede iron catalysts in terms of industrial usage. Cobalt catalysts are used exclusively in LTFT applications, typically in fixed-bed mode of operation. If operated at the HTFT region, cobalt catalysts would drive the selectivity towards essentially only producing methane, making the temperature range unsuitable for GTL applications. [55] LTFT cobalt-based GTL plants have been operated by Shell and Sasol, producing mainly naphtha, kerosene and distillates. Compared to iron catalysed HTFT processes, the liquid fuels produced from cobalt catalysed LTFT synthesis have a higher n-paraffin content, resulting in a higher cetane number. [62]

Similar to iron catalysts, cobalt catalysts work with the carbide formation mechanism presented in Figure 27. The CO dissociation may be further increased with the introduction of support metals onto the catalyst, such as aluminum and noble metals, to increase CO conversion in the process. [63]

6.5 Fischer-Tropsch syncrude distillation

The distillation of the liquid syncrude produced in FTS is analogous to that of crude oils. The distillations are based on boiling points, with typical distillation setups involving several distillation steps. The distillation configurations are typically

operated at atmospheric pressure. The FT distillation setup studied by Marchese et al. [58], presented in Figure 29, included a three-phase separator, to which the FTS product feed is first fed into to separate the water and FT products, followed by two distillation columns. The first distillation column separates the naphtha from middle distillates, waxes and residuals. The second distillation column separates the light waxes from the heavy waxes. [58]

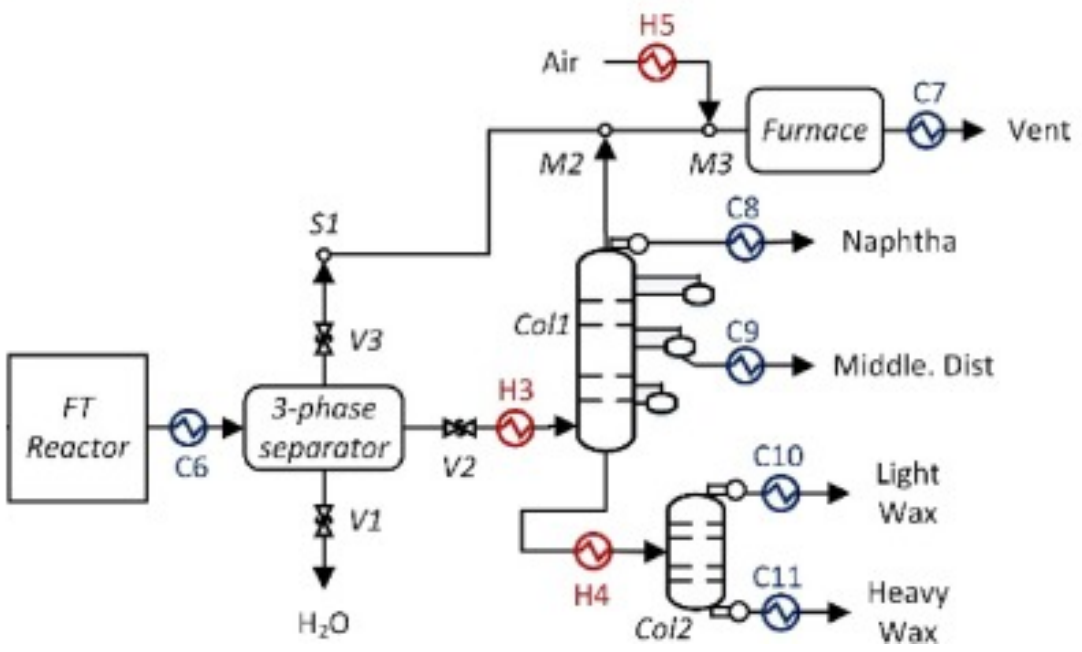

Figure 29: Typical FT syncrude distillation configuration (modified from source: [58]).

6.6 Selections for Fischer-Tropsch configuration

For the FT process studied in the experimental section, slurry bed FT reactors are used. As the goal of the process is to produce economically viable SAF, iron catalysts are used in LTFT operation due to their lower price. LTFT operation allows for the production of 10-15% mass percentage of directly SAF applicable C9-C15 fractions, with 45-50% of heavy distillate and waxes, which may be hydrotreated to obtain desired kerosene fractions. The operation temperature is set between 170–270 °C and the pressure between 20–45 bar depending on the catalyst and reactor setup.

[64] The H_2/CO ratio may be adjusted in the synthesis gas production phase of the simulation to achieve maximum product output, but a baseline of 2 will be the goal.

7 Hydrocracking

As the FTS yields a relatively high fraction of wax products unsuitable for use as liquid fuels, a hydrocracking process unit must be included in the process, when the aim of the process is to maximize the output of liquid fuels. Hydrocracking reactions are essentially any chemical reactions, where carbon-carbon bonds are broken to yield shorter hydrocarbon chains than in the reactant. The carbon-carbon bond breakage yields a free valency, which is saturated by hydrogen. Thus, hydrocracking processes consume hydrogen and are able to convert FTS waxes into shorter hydrocarbons, which may be usable as liquid fuels. [65]

Hydrocracking reactions may proceed via four different methods depending on the catalyst; bifunctional hydrocracking, hydrogenolysis, Haag-Dessau hydrocracking and thermal hydrocracking. Out of these four, hydrocracking over bifunctional catalysts is the one most commonly employed in petroleum refining. [65] Bifunctional catalysts typically consist of supported platinum, cobalt or molybdenum [66], nickel or cobalt over phonolite structures [67] or zeolite structures [68]. The classical mechanism of hydrocracking for alkanes is presented in Figure 30. The hydrocracking reaction starts with the dehydrogenation of the reactant, in this case the FT wax, on the catalyst metal sites. These dehydrogenated components desorb from the catalyst and diffuse to Brønsted acid sites where they undergo protonation to secondary alkylcarbenium ions, which can then undergo carbon-carbon bond rupture as well as skeletal rearrangement. The carbon-carbon bond rupture is generally accepted to proceed through β-scission. [65]

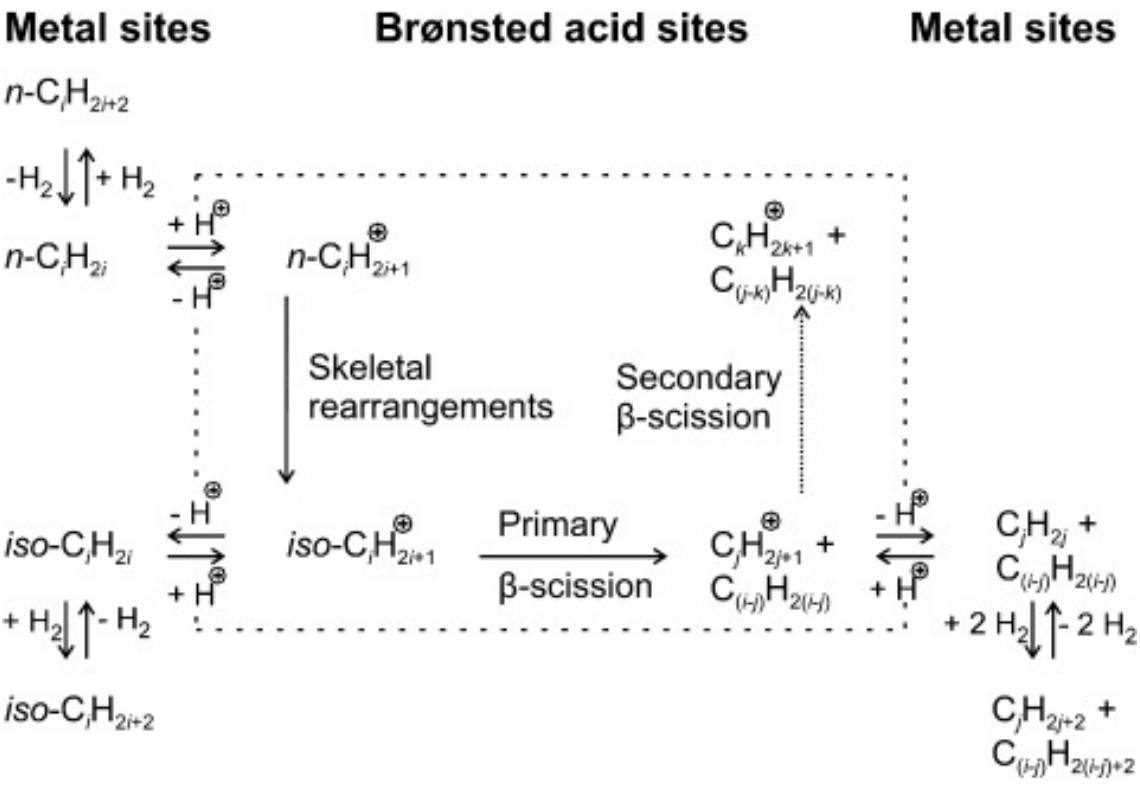

Figure 30: Classical mechanism for hydrocracking and isomerization over a bifunctional catalyst. [65]

β-scissions happen through different mechanisms depending on the carbon chain length and the possible branching of the hydrocarbon chain. This branching may occur prior to the carbon-carbon bond rupture. The different β-scission mechanisms are presented in Figure 31. It should be noted, that under mild conditions, the Type D reactions in Figure 31 are completely prohibited, resulting in the absence of methane and ethane in the product stream.

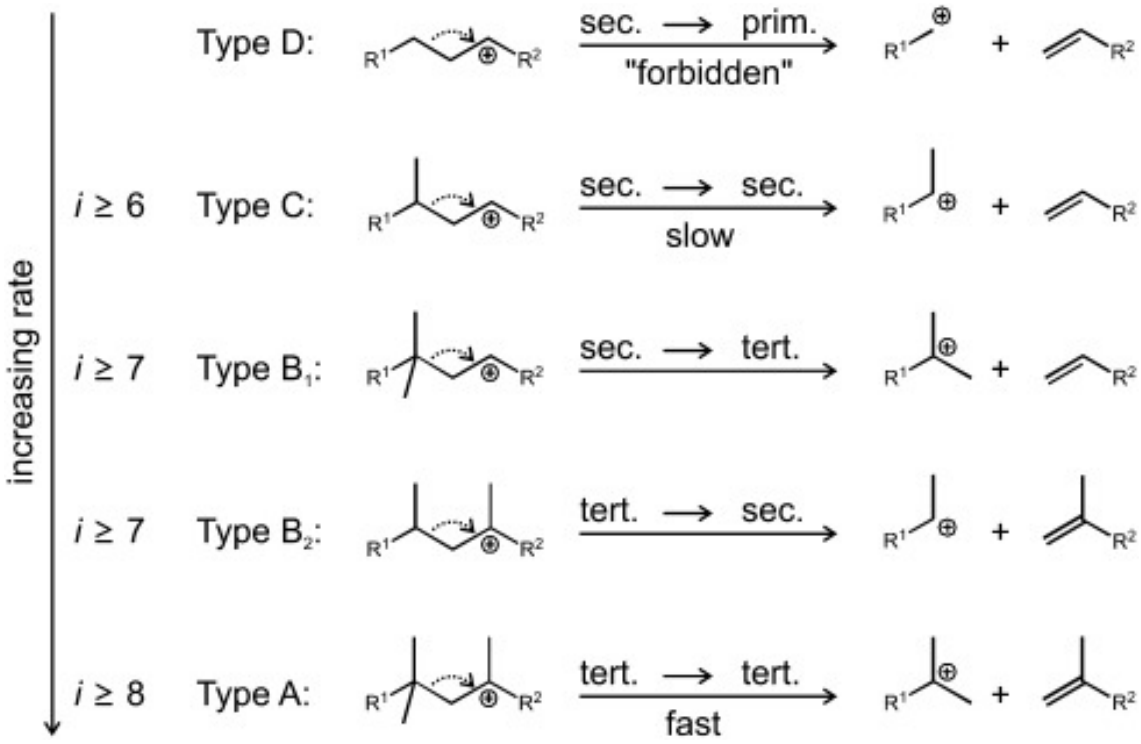

Figure 31: Different mechanisms for β-scission reactions and their respective reaction rates [65].

Based on this theory, a general chemical equation for hydrocracking may be formulated based on the reactions presented for each step in Figure 30. The steps of protonation, skeletal rearrangements, β-scissions and subsequent hydrogenations may be simplified to the form presented in Equation 20.

$$\text{n-C}_i\text{H}_{2i+2} + \text{H}_2 \longrightarrow \text{C}_j\text{H}_{2j+2} + \text{C}_{(i-j)}\text{H}_{2(i-j)+2} \tag{20}$$

In hydrocracking, the operating conditions affect the yield of different hydrocarbon chain lengths from the reactant. According to the studies of Hanaoka et al. [66], a temperature range of 200–350 °C and a reaction pressure range of 1–60 bar may be used depending on the desired product. According to the study, the optimal conditions to produce jet applicable hydrocarbons were a temperature range of 250–300 °C and a pressure of 15 bar. At the 250 °C temperature, the process yields a higher yield of liquid fuel product applicable hydrocarbons, while the 300 °C

temperature shifts this balance towards lighter hydrocarbons unusable as liquid fuels, making lower temperatures the more attractive choice for this process.

Experimental

8 Process simulation setup

This section presents different areas of the Aspen Plus simulation implementation of the process. The main emphasis of this work is to provide adequate values for mass and energy balances to provide the basis for OPEX and CAPEX calculations via simulation of the process. The Aspen Plus simulation in this thesis is primarily based on values obtained from simulations and experimental work from literature. The kinetics of the reactions involved in this process are complicated and require significant attention to detail to configure them correctly into Aspen Plus. The benefit of implementing kinetic models for the reactors is the ability to obtain data on the physical requirements for the reactor setups. As this work aims to formulate a basic structure for the design of the process in terms of used equipment, mass and heat balances and economics of the process, the kinetics are left out to simplify the evaluation of the process. However, these kinetic models could be applied to the same process and simulations in the future to obtain detailed design and dimensioning of process equipment.

The basis for the simulation and process evaluation setup is chosen as 8000 operating hours annually. The initial production capacity goal for the process was set as 200 ktonne of jet fuel annually. However, as recycling streams were implemented into the process to maximize the utilization of syngas, the production capacity ended up being higher. The capacity was also increased by the simulated distillation processes being unable to yield 100% mass-purity products in terms of hydrocarbon distribution, so the produced jet fuel fraction ended up being significantly higher than the 200 ktonne goal. This should be taken into account in future work, that the equipment and economical values would change, if the production was set at a lower value.

While the main reactors are modelled as RStoic blocks, where the obtained yields are manually entered from literature values, the simulation still provides valuable

information on the thermodynamics of the process. The Aspen Plus software is capable of calculating the heat requirements for the process, which are crucial information when estimating the overall cost-effectiveness of the process.

A simplified block diagram of the entire process is presented in Appendix C. The streams numbered in the block diagram are correspond to the streams in the process mass balance, presented in Appendix D. The Aspen Plus flowsheets are presented in Appendices E, F and G for different sections of the process. A complete equipment list from the Aspen Plus simulation is presented in Appendix H.

8.1 Property method

According to the AspenTech Physical Property System documentation, the Peng-Robinson Boston-Mathias (PR-BM) property method is recommended for refinery applications wherein light hydrocarbons are processed. [69] The PR-BM property method was also used by Dimitriou et al. [70] in their simulation of a FTS unit. The same property method is used throughout the simulation.

8.2 Components

The component list used for this process is presented in Appendix A. All of the components were readily available in Aspen Plus, with some of the longer hydrocarbon chain components missing some thermodynamical parameters such as heat of formation and combustion. However, as these components are not directly involved in the reactions due to the assumption that all the C20+ hydrocarbons are lumped together into the C28+, this should not cause any problems with the simulation. Aspen Plus does not yield an error even with these parameters missing.

8.3 Steam methane reforming reactor

The steam methane reforming (SMR) reactor is modelled as an RStoic reactor, with yields given for the products based on literature values by Gangadharan et al. [71]. The reactor block is fed with a feed of methane at -93.15 °C and 44 bar and steam

at a temperature of 130 °C and pressure of 2 bar. The extreme temperature and pressure of the methane feed is due to the conditions of the methane separation prior to feeding the methane. In these conditions, the methane is fed from liquefied storage conditions. [71] The reactant streams are mixed and passed through a heat exchanger, where the temperature rises to 687 °C. The heated stream is fed to the reactor operating at 627 °C. The outlet stream of the reactor passes through a heat exchanger which transfers heat to the inlet side heat exchanger, effectively making a FEHE configuration.

As the reactor block is not based on kinetics, the yield of the reactor is presented as a fractional conversion from methane based on values obtained from the study of Gangadharan et al. [71]. The SMR reaction is implemented as it is presented in Equation 1, but the WGS reaction presented in Equation 2 must be given in a form where methane is the reagent. This is obtained by combining both Equations 1 and 2 to obtain Equation 21. The reactor operates at a temperature of 627 °C and a pressure of 1.97 bar. [71]

$$CH_4 + 2\,H_2O \longrightarrow CO_2 + 4\,H_2 \tag{21}$$

The SMR reaction presented in Equation 1 has a fractional conversion of 90.7% of the fed methane and the WGS reaction presented in 21 has a fractional conversion of 7.2% of methane.

The SMR reaction is highly endothermic and the reactor requires a significant heat input. As mentioned by Gangadharan et al. [71], furnaces burning off-gases from the process may be used to heat this reactor. Off-gases from this process can be used to supply some of the required heating, but additional heat is still required. Fired heat may be utilized to heat this reactor.

8.4 Dry methane reforming reactor

The dry methane reforming (DMR) reactor is modelled as an RStoic reactor block, with yields given for the products based on literature values by Gangadharan et al.

[71]. The reactor block is fed with a feed of methane at -93.15 °C and 44 bar and a CO_2 stream at 137 °C and 2 bar. The conditions for the methane feed are the same as in SMR, as it is fed in a liquefied state. The reactant streams are mixed and passed through a heat exchanger, where the temperature of the feed stream is increased to 615 °C. This stream is then fed into the reactor operating at 600 °C. Just like in the SMR reactor, a FEHE configuration is used where the outlet stream of the reactor passes through a heat exchanger, from which heat is transferred to the inlet side of the heat exchanger.

While the DMR reaction can produce H_2O in the process, the process modelled by Gangadharan et al. [71] utilizes a catalyst that effectively removes water forming reactions. Thus, only synthesis gas is formed in the reaction as per the reaction presented in Equation 4. The fractional conversion from methane to synthesis gas is 98.9%.

The DMR reaction, much like the SMR reaction, is highly endothermic, requiring significant heating to maintain the reactor. This heat may be provided by a fired heater.

8.5 Syngas pretreatment

As the synthesis gas leaves the SMR and DMR reactors, it contains components such as water and CO_2, which should not enter the FT reactor. After mixing the reactor outlet streams, the gaseous syngas stream first enters a flash column, where water is removed from the stream. After this, the stream is directed to a CO_2 separation column, in which CO_2 is stripped from the stream. As per the study of Selvatico et al. [72], the CO_2 separation happens in a Rectisol column, which operates by absorbing acid gases and CO_2 from the syngas stream with cold methanol. The CO_2 stripping process is modelled as a simple Sep block in Aspen Plus, as the simulation of a CO_2 stripper is complicated and it is assumed that the technology is well enough developed that a complete solution may be readily purchased from a vendor. The study of Selvatico et al. [72] used the same approach of presenting the stripper with a simple separator block, citing the Rectisol process as a commercially readily available

solution for CO_2 removal.

8.6 Fischer-Tropsch synthesis

The FT reactor is modelled using a RStoic block in Aspen Plus. The reactor operates at a temperature of 240 °Celsius and a pressure of 25 bar as per the studies of Selvatico et al. [72], where high conversions of jet fuel were obtained with these conditions. This constitutes as LTFT operation, where waxes are the primary product and liquid products, such as jet fuel and diesel, are produced in smaller quantities.

As the reactor model in the simulation does not follow actual kinetics, the yields for different hydrocarbons are calculated manually and inserted into the RStoic block. The theoretical yield is calculated using the ASF statistical distribution model presented in Equation 19. Using the ASF model, it is possible to calculate the weight fraction for each carbon chain length in the product stream. The chain growth factor α in LTFT is given a range of 0.85–0.95 by Loosdrecht et al. [55], with current LTFT technologies having an α value of 0.9 [73], which is used as the basis for the theoretical yield. In reality, this chain growth factor may change when longer hydrocarbon chains are formed. For example, the studies of Todic et al. [74] showed that the chain growth factor increased from 0.8 to 0.95 at the C3–C15 range over a cobalt catalyst in a slurry reactor. The theoretical carbon chain distribution in the FTS product stream as calculated from the ASF model using a constant chain growth probability of 0.9 is presented in Figure 32. The corresponding product fractions and the total weight fractions for each of those products are presented in Table 6.

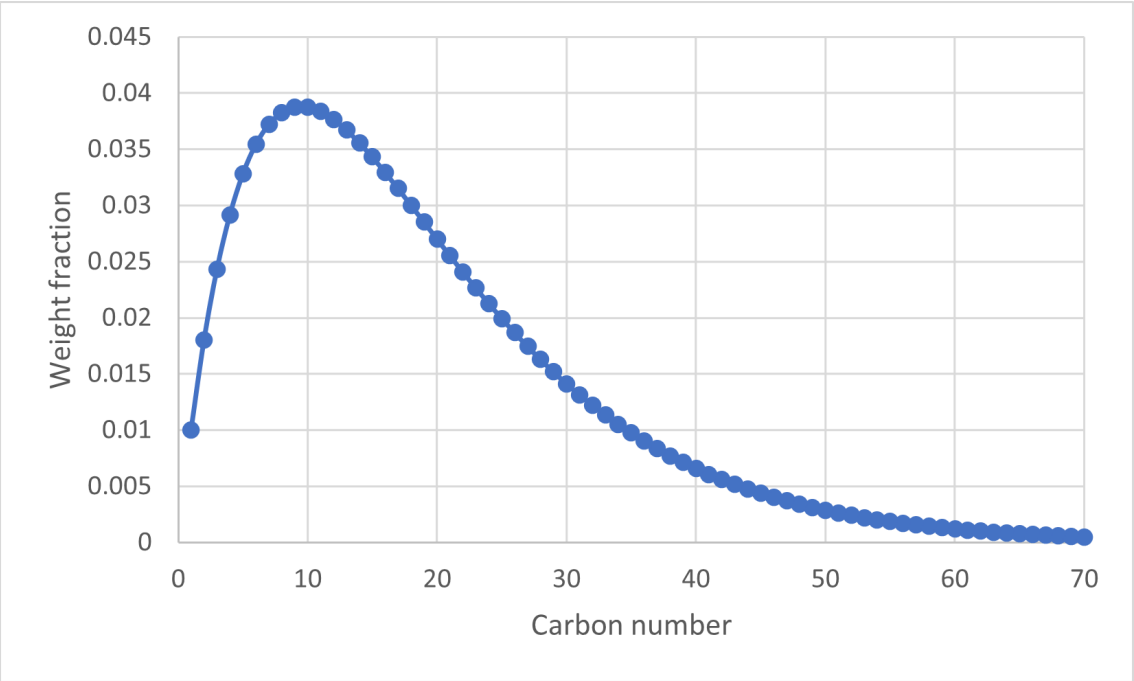

Figure 32: Weight distributions for different hydrocarbon chain lengths calculated using the ASF model with chain growth probability $\alpha = 0.9$.

Table 6: Weight fractions for each product fraction obtained from FTS according to the ASF statistical model.

Carbon chain length	Corresponding product	Weight fraction in product (wt-%)
C1-C8	Light gases, naphtha	22.52%
C9-C15	Jet fuel	26.01%
C16-C19	Diesel	12.3%
C20+	Waxes	39.17%

The components used in the FTS simulation are all readily available in the Aspen Plus simulation software. For this simulation, only olefins and paraffins are considered for the sake of brevity. The FTS also produces alcohols, aldehydes, carboxylic acids and methyl alkanes. These products are deemed to be side-products of the synthesis and are not formed in the same scale as olefins and paraffins are. [72]

The hydrocarbon chains in the range of C1–C8 are considered to be light gases that may be recycled into the process and naphtha [72]. The C9–C15 range is the

range for jet fuel applicable hydrocarbons [55]. The C16–C19 fraction is considered to be diesel. [75] The hydrocarbon chains with a chain-length of C20 and over are considered to be waxes, that are sent to the hydrocracker in order to obtain jet fuel applicable hydrocarbon chains. However, as there is little difference in how the different hydrocarbon chain lengths behave in the C20+ region, they are all presented as a single component in the simulation for the sake of brevity. As the wax fraction accounts for 39.17% of the total product fraction, the carbon chain length at which the cumulative weight fraction in the wax fraction is half of the total wax fraction percentage is chosen. By using this method the chosen hydrocarbon chain length is C28. This choice is further supported by the studies of Hanaoka et al. [66], where the same hydrocarbon chain length is used to model components for hydrocracking. [66]

Besides the hydrocarbon chain length, the ratio at which olefins and parafins are produced in the FTS is also crucial for evaluating the process feasibility for jet fuel production. Generally, a higher paraffin content is preferable for aviation fuels, due to their higher chemical energy in comparison to olefins due to the lack of double bonds. According to Maitlis et al., [73] typical LTFT synthesis configurations produce a mixture of 85–90% linear paraffins with the rest being olefins and oxygenates. For this simulation, the FTS product is assumed to be 90% paraffins and 10% olefins.

The conversion of carbon monoxide is the primary factor in determining the total hydrocarbon yield of the process. According to Hamelinck et al. [76], the total conversion from synthesis gas in once-through operation can reach 90% in typical LTFT operation, if a large enough FT reactor is employed. [76] While 10% of the synthesis gas remains unreacted throughout the FTS process, recycling this fraction back into the process is possible to improve overall carbon conversion efficiency. Selvatico et al. [72] proposed a recycling configuration consisting of an ATR and WGS reactors to recycle both light hydrocarbons and syngas back into the FTS syngas feed.

By using both the theoretical mass fractions for each hydrocarbon chain length and the overall syngas conversion, the theoretical yields in terms of syngas conversion for

each component can be calculated for both paraffins and olefins. These are presented in Appendix B. Each reaction for both paraffin and olefin reactions according to the Equations 13 and 14 respectively with their corresponding fractional conversions from carbon monoxide. This allows the RStoic block to calculate the process' thermodynamics and give theoretical yields for all of the hydrocarbon products.

While an actual FT reactor is capable of separating the liquid and wax fractions from the gaseous streams at the outlet, the RStoic block only has one outlet stream. To account for this, a simple Flash2 block is inserted after the RStoic block to separate these fractions from the gaseous stream. The liquid and wax stream is directed to the Fischer-Tropsch product (FTP) distillation, while the gaseous stream goes through a flashing process.

8.7 Fischer-Tropsch product flashing

The FTP exiting the FT reactor contains a large portion of water due to the reactions presented in Equations 13 and 14. This water must be removed from the stream before entering the product distillation. This is done by utilizing a three-phase separator modelled as a Flash3 block in Aspen Plus, operating at a temperature of 80 °C and a pressure of 25 bar. The three-phase separator removes the water from the hydrocarbon stream, which is removed from the bottom of the separator. The block also separates gaseous components from the FTP stream, consisting mainly of light hydrocarbons and the unreacted syngas from the FTS. This gaseous stream passes through one more flash drum modelled with a Flash2 block, which separates as much of the liquid hydrocarbons from the unreacted syngas stream as possible. The light hydrocarbons are passed back to the stream, continuing to the FTP distillation column, while the gaseous stream containing syngas continues to the recycling section of the process.

8.8 Recycling

As the FT reactor has a syngas conversion of 90%, there is relatively high percentage of unreacted syngas in the outlet stream. In order to optimize the total production process, this unreacted syngas should be recycled. As the stream contains short hydrocarbons as well, the unreacted syngas stream must be processed before it can be fed back into the FT reactor.

As the synthesis gas exits the flash drums, it is passed through a splitter. This splits 10% of the stream as a purge stream to keep unwanted components from accumulating in the process with time. The split is set at 10% based on an assumption that it is enough to ensure no unwanted components are able to accumulate in the stream. The purge stream is directed to a furnace, where it is burned for process heat. 90% of the dirty syngas stream is directed to a steam reforming reactor, where the hydrocarbons react as per the reaction presented in Equation 3. The SR reactor is also fed with water, and the inlet stream passes through a heat exchanger which is connected to a heat exchanger in the outlet side in a FEHE configuration. The reactor operates at a temperature of 700 °C and a pressure of 1 bar.

The SR reactor is modelled with reactions up to octane, as components with higher hydrocarbon chain lengths are present in relatively negligible amounts. As per Al-Musa et al. [77], octane has a conversion of nearly 100% at a temperature of 700 °C, complete conversion is assumed. The studies of Schädel et al. [78] present conversion for hydrocarbon chain lengths up to butane to have a conversion of 100% at 700 °C, so they are also assumed to be completely converted in the reactor.

The resulting recycling stream consists mainly of syngas components CO and H_2, with some CO_2, CH_4 and some residual water from the SR reactor. This stream is reconnected and mixed with the clean syngas before the syngas flash and CO_2 separation steps, where the recycled stream goes through the same cleaning procedures as syngas from SMR and DMR before entering the FT reactor.

8.9 Fischer-Tropsch product distillation

The liquid products from the FTS reactor are fed into a fractionation column to separate the product fractions from one another. Before this, the product stream goes through a simple three-phase separator, which separates the excess syngas and water from the product stream.

The fractionation column is modeled with a PetroFrac Aspen Plus block. As per the operating conditions presented by Selvatico et al. [72], the 54-stage column operates with a mass-based reflux ratio of 1.8 and a bottom stage pressure of 2 bar, dropping to 1 bar at the top of the column. [72, 79] The bottoms rate is specified as the amount of C_{28} hydrocarbons in the feed stream of the column. The main column feed is set to stage 38. The top stage is specified as stage 1, with the bottom stage being stage 54.

The condenser of the column operates at a temperature of 60 °C. The gaseous distillate from the column is directed to a furnace that utilizes the light hydrocarbons from the process to produce heat. The liquid distillate is directed to another distillation column, as it contains a significant portion of jet fuel. The jet fuel is separated from the lighter components in the second distillation column, yielding a naphtha product stream from the top and a jet fuel stream from the bottom.

The fractionation column has a single side stripper, where jet fuel is recovered from the main column. The liquid side draw from the column is from stage 18 based on the composition curves of the main column. The composition curves for the liquid phase are presented in Figure 33. The vapor return from the side stripper is set at stage 2. The bottoms rate of the stripper is set based on the amount of jet fuel components in the fractionation column inlet. The stripper is fed with stripping steam at a rate of 2.27 kg/bbl jet product [79]. Jet fuel is the main product of the side stripper.

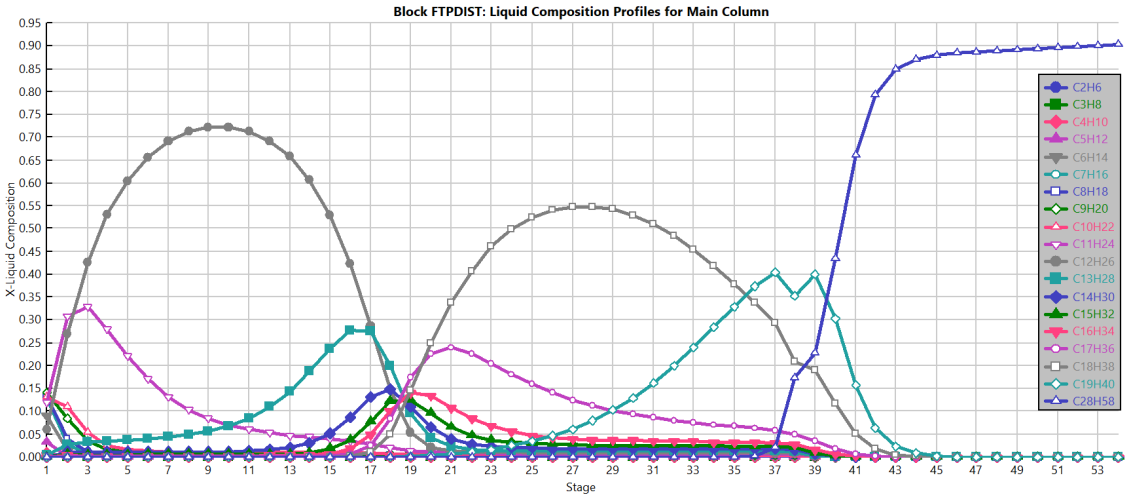

Figure 33: Liquid composition on different stages of the fractionation column.

The column has a single direct side draw for the diesel fraction on stage 40, the rate of which is determined from the total amount of diesel in the FTP stream. In the scale of the entire process, diesel is not a significant product in the stream, but is still removed as a product as it still has value as a liquid fuel.

The heavy waxes from the bottom of the column are directed to the hydrocracking process. The bottoms of the column pass through a counter-current heat exchanger connecting the inlet of the column in a FEHE configuration to minimize the reboiler's required duty.

8.10 Hydrocracking

The hydrocracking reactor is modelled with an RStoic block in Aspen Plus. A study by Hanaoka et al. [66] found, that the highest yield of 29.2 wt-% for jet fuel from analytical grade n-$C_{28}H_{56}$ was achieved over a 0.5 wt-% Pt-loaded β-type zeolite catalyst at reaction temperatures of 250–350 °C and pressure of 9–14 bar. The study of Hanaoka et al. [66] tested actual FT products produced via a biomass-to-liquid (BTL) process. In these tests, the maximum jet fuel yield was 21.5% at reaction conditions of 250 °C and 15 bar over a 0.1 wt-% platinum catalyst. The remaining yields are 36.7% C1-C8 and 41.8% C16+ hydrocarbons, corresponding to mainly naphtha and diesel fractions respectively. The total conversion from the hydrocarbon

reactant was nearly 100%. [66]

As the product yields are presented as ranges without the specific component yields, model components for each of these hydrocracking product (HCP) fractions must be chosen. While there are olefins and parafins present in the reactor, it is assumed that all olefins yield paraffinic products in the process. Olefins are formed as intermediates in the hydrocracking process, which are then hydrogenated to yield paraffins [80], same is assumed to happen for olefins readily available in the FT wax. As there is a large portion of C16+ hydrocarbons in the hydrocracker outlet stream, which mainly consist of waxy components [66], this is chosen to be represented as an unreacted fraction of the inlet C28 hydrocarbon stream. The remainder of the C28 hydrocarbon stream is cracked to yield the jet and naphtha components.

As the reactant is assumed to be composed of only C28 hydrocarbons, it is assumed to be hydrocracked in half, yielding two hydrocarbon molecules with a hydrocarbon chain length of C14. These reactions are used to present the jet fuel yielding reactions, presented in Equations 22 and 23 for paraffinic and olefinic reactants respectively, with a fractional conversion of 0.215 of the C28 components for both reactions.

$$C_{28}H_{58} + H_2 \longrightarrow 2\,C_{14}H_{30} \tag{22}$$

$$C_{28}H_{56} + 2\,H_2 \longrightarrow 2\,C_{14}H_{30} \tag{23}$$

The naphtha fraction is assumed to be formed by cracking a C28 hydrocarbon into four C7 hydrocarbons. While this assumption is quite optimistic compared to the actual random hydrocarbon chain cracking in the reactor, it is used to simplify the implementation of hydrocracking reactions into the simulation. These reactions for both paraffinic and olefinic components are presented in Equations 24 and 25 respectively, with a fractional conversion of 0.367 of the C28 components for both reactions.

$$C_{28}H_{58} + 3\,H_2 \longrightarrow 4\,C_7H_{16} \tag{24}$$

$$C_{28}H_{56} + 4\,H_2 \longrightarrow 4\,C_7H_{16} \tag{25}$$

The resulting hydrocracked hydrocarbons exit the reactor and are passed through a heat exchanger where the pressure is reduced to 2 bar while maintaining the outlet temperature of 250 °C.

8.11 Hydrocracking distillation

The hydrocracked products are passed on to a distillation column, modelled as a RadFrac block in Aspen Plus. The block operates with 15 stages and a bottom stage pressure of 2 bar increasing to 1 bar at the top as per the studies of Selvatico et al. [72]. The convergence for the column is set as Petroleum/Wide-boiling to help the simulation converge. The bottoms rate of the column is calculated from the fraction of wax products in the column inlet stream. The reflux rate is also specified on a mass-basis in the column, calculated from the amount of hydrocarbon chains in the column inlet with a sufficient boiling point to be returned to the column as liquid from the top of the column. The condenser in the column operates at a temperature of 55 °C. The gaseous distillate from the column is directed to the same furnace as the gaseous products from the FTP fractionation column. The liquid distillate, consisting mainly of naphtha is directed as a liquid product and mixed with the naphtha from the FTP fractionation column.

The column has a liquid side draw for the jet fuel fraction, determined from the amount of jet fuel components in the inlet stream of the column. The draw is from stage 3. This jet fuel fraction is directed forward as a product and mixed with the jet fuel fraction from FTP fractionation column.

The bottom product of the column is effectively the same FT wax as it was exiting the FTP distillation column. In reality, the hydrocracker would likely produce products with a hydrocarbon chain length applicable in the diesel product region, but due to the highly simplified reactions in the hydrocracking reactor in this work, the diesel fraction is assumed to be all waxes. This wax product could be recycled

into the hydrocracker or used analogously to traditional heavy oil fractions. In this work, the wax product is obtained as such from the bottom of the hydrocracking distillation, and assumed to be comparable to conventional heavy oil fractions.

8.12 Furnace

As the overall heat demand of the process is very high and there are gaseous products exiting from different parts of the process, a furnace can be implemented to burn off these gases to cover part of the process heat requirements. The furnace is fed with gases from the purge stream of the syngas recycling and the gaseous distillates from both the FTP and HCP distillations. The furnace is fed with air alongside these gases. The furnace is modelled as a RGibbs block in Aspen Plus. Aspen Plus calculates the value for the outlet heat duty from the furnace, but due to the limitations of how Aspen Plus handles heat streams, this heat stream is not directly connected to either of the reactors, as it is not enough to heat them on its own, and the reactors can only be connected with one heat source.

Results

9 Aspen Plus simulation results

This section presents simulation results from the main parts of the process in terms of simplified mass and molar balancess as well as the required heat duties for each specified process.

9.1 Syngas generation

The syngas generation step is the first in the process, where methane is converted into syngas in the SMR and DMR reactors. The syngas generation step contains most of the heating requirements of the process.

9.1.1 SMR reactor

The SMR reactor is fed with CH_4 and steam. The stream results of the SMR reactor block are presented in Table 7.

Table 7: SMR reactor mass and molar balances.

	Feed		Output	
Component	(tonne/hr)	(kmol/hr)	(tonne/hr)	(kmol/hr)
CH4	51.25	3194	1.025	63.86
H2O	69.08	3834	8.518	472.8
CO2	0	0	10.18	231.2
CO	0	0	81.21	2900
H2	0	0	19.40	9622

The heat balance of the SMR process is presented in Table 8.

Table 8: SMR process heat balance.

Process unit	Duty (MW)	Notes
Inlet heat exchanger	62.3	In FEHE configuration with outlet
SMR reactor (627 °C)	186.6	Requires fired heat
Outlet heat exchanger	-62.3	In FEHE configuration with inlet

Overall, the SMR process has considerable heating requirements, which likely should be covered mostly with fired heat, as the reactor requires a high temperature of 627 °C.

9.1.2 DMR reactor

The SMR reactor is fed with CH_4 and CO_2. The stream results of the SMR reactor block are presented in Table 9.

Table 9: DMR reactor mass and molar balances.

	Feed		Output	
Component	(tonne/hr)	(kmol/hr)	(tonne/hr)	(kmol/hr)
CH4	51.25	3194	1.025	20.68
CO2	79.59	1809	1.333	30.30
CO	0	0	99.62	3556
H2	0	0	7.170	3556

The heat balance of the DMR process is presented in Table 10.

Table 10: DMR process heat balance.

Process unit	Duty (MW)	Notes
Inlet heat exchanger	31.8	In FEHE configuration with outlet
DMR reactor (600 °C)	127.6	Requires fired heat
Outlet heat exchanger	-31.8	In FEHE configuration with inlet

The DMR process, much like the SMR process, requires significant heating, likely requiring the same fired heat as the heating utility for the reactor.

9.2 Syngas cleaning

The syngas stream from both the SMR and DMR reactors as well as the syngas recycled from the FT reactor, passes through a two-step cleaning process, in which water and CO_2 are removed from the syngas stream before being passed to the FT reactor. The mass and molar balances of the cleaning process are presented in Table 11. The balance assumes the entire cleaning section as one operation, including the removal of water and the Rectisol process for CO_2 removal. The balance of the Rectisol unit itself is not presented, as it is not simulated in the work but rather given as a simplified Sep-block that removes CO_2 from the stream.

Table 11: Syngas cleaning mass and molar balances.

	Feed		Output	
Component	(tonne/hr)	(kmol/hr)	(tonne/hr)	(kmol/hr)
CH4	20.67	1288	20.67	1288
CO2	11.61	263.8	0.116	2.638
CO	214.4	7654	214.4	7654
H2	29.64	14705	29.64	14705
H2O	9.320	517.4	3.028	168.1

The overall heat requirements of the syngas cleaning process are relatively small, with small heat exchange happening between the inlet and outlet heat exchangers in FEHE configuration. The heat balance of the syngas cleaning process is presented in Table 12.

Table 12: Syngas cleaning process heat balance.

Process unit	Duty (MW)	Notes
Inlet heat exchanger	-5.91	In FEHE configuration with outlet
Outlet heat exchanger	5.91	In FEHE configuration with inlet

9.3 FT reactor and outlet stream separators

The FT reactor in the process is fed with the clean syngas stream from the previous process step. The stream passes through a heat exchanger heating up the stream slightly, but generally it is assumed that the exothermic nature of the FT reactions remove any heating requirements for the incoming stream. The FT reactor is also fed with a 100 kmol/hr stream of supplementary clean H_2. The exiting wax stream is directly directed to the fractionation step, while the gaseous stream goes through a series of heat exchangers and flashes to separate the unreacted dirty syngas from the product stream to enable dirty syngas to be recycled. The total mass and molar balances of the FT reactor and the separations steps are presented in Table 13.

Table 13: Fischer-Tropsch synthesis and downstream separation mass and molar balances.

	Feed		Output	
Component	(tonne/hr)	(kmol/hr)	(tonne/hr)	(kmol/hr)
CO2	0.116	2.638	0.004	0.1
CO	214.4	7654	0.148	5.288
H2	29.84	14805	0.004	2.075
H2O	3.028	168.1	1.34	74.42
C1-C4	0	0	1.565	44.48
C5-C8	0	0	11.78	124.9
C9-C15	0	0	25.40	154.6
C16-C19	0	0	11.97	48.78
C20+	0	0	38.03	96.38

The FT unit as well as the heat exchanger preceding the flash both have a significant negative heat duty, which may be harnessed to either produce steam and electricity within the plant area or could even be sold to a local heat grid. Due to the relatively low temperature of the FT reactor, the heat duty cannot be used to heat up the SMR or the DMR reactors. Whichever the method for utilization of the outlet heat, it must be utilized somehow, as the heat should not be released

directly back to the environment as warm effluent water as it may cause damage to the surrounding nature. This is also not economically viable, as the heat is a valuable asset if sold to a local heating grid. The heat balance of the FT unit and the separation processes are presented in Table 14.

Table 14: Fischer-Tropsch reactor and downstream separation heat balance.

Process unit	Duty (MW)	Notes
FT reactor (250 °C)	-285.5	May be used to produce steam
FT outlet heat exchanger (80 °C)	-101.2	Heat utilizable elsewhere

9.4 Syngas recycling

The recycling stream is fed with the gaseous components leaving the FTS product separation steps consisting mainly of syngas and light hydrocarbons. The light hydrocarbons need to be converted into syngas in a SR reactor before re-entering the FT inlet stream. 10% of the incoming recycle stream is purged off the process and burned off for energy. Syngas is recycled by converting the light hydrocarbons in the incoming stream into syngas (H_2 and CO). The mass and molar balances of the SR reactor are presented in Table 15.

Table 15: Syngas recycling process mass and molar balances.

	Feed		Output	
Component	(tonne/hr)	(kmol/hr)	(tonne/hr)	(kmol/hr)
CH4	19.31	1204	19.31	1204
CO2	0.100	2.280	0.100	2.280
CO	19.16	684.1	33.57	1199
H2	0.718	356.3	3.078	1527
H2O	10.07	558.9	0.802	44.53
C1-C8	7.514	156.4	0.013	0.132

The reactions involved in the SR reactor are similar to those in the SMR reactor, meaning they are endothermic in nature. This means the reactor requires a high heat

duty capable of maintaining 700 °C temperature in the reactor. The heat balance of the recycling section is presented in Table 16.

Table 16: Syngas recycling process heat balance.

Process unit	Duty (MW)	Notes
Inlet heat exchanger (526 °C)	25.27	In FEHE configuration with outlet
SR reactor (700 °C)	32.77	Requires fired heat
Outlet heat exchanger (700 °C)	-25.27	In FEHE configuration with inlet

9.5 Fischer-Tropsch product fractionation

The FTP is distilled in a fractionation column, where the crude FTP is fed through a heat exchanger. The column aims to separate the inlet into different product fractions based on the boiling points of different fractions. The feed composition is presented in the yield column of Table 13. The yields for the different fractions are presented in terms of hydrocarbon yields.

The yields for the distillate products are presented in Table 17. The vapor distillate is directed to the furnace where it is burned for heat, while the liquid distillate continues to a secondary distillation column where naphtha and jet are separated from one another.

Table 17: FTP fractionation distillate yields.

	Vapor distillate		Liquid distillate	
Fraction	(tonne/hr)	(kmol/hr)	(tonne/hr)	(kmol/hr)
C1-C4	1.434	42.03	0.131	2.442
C5-C8	4.292	49.28	7.487	75.60
C9-C15	0.495	3.674	12.85	88.20
C16-C19	0	0	0.005	0.024
C20+	0	0	0	0
H2O	1.553	86.23	0.126	7.006

The yields for the different liquid products from different stages of the column

are presented in Table 18.

Table 18: FTP liquid product yields.

	Jet fuel (through side stripper)		Diesel (through side draw)		Wax (bottom product)	
Fraction	(tonne/hr)	(kmol/hr)	(tonne/hr)	(kmol/hr)	(tonne/hr)	(kmol/hr)
C1-C4	0	0	0	0	0	0
C5-C8	0	0	0	0.001	0	0
C9-C15	11.20	62.43	0.051	0.256	0	0
C16-C19	7.972	33.54	3.994	15.21	0	0
C20+	0	0	5.955	15.09	32.07	81.29
H2O	0.029	1.590	0	0	0	0

The heat balance of the fractionation step is presented in Table 19.

Table 19: FTP fractionation heat balance.

Process unit	Duty (MW)	Notes
Inlet heat exchanger	6.15	In FEHE configuration with outlet
Column reboiler (460 °C)	17.2	Requires fired heat
Column condenser (60 °C)	-14.12	Cooling water used
Outlet heat exchange (460 °C)	-6.15	In FEHE configuration with inle

9.6 Naphtha distillation

The liquid distillate from the top of the column contains a significant portion of jet fuel, which needs to be removed from the lighter hydrocarbons of naphtha in order to be collected as a liquid product. The mass and molar balances of the naphtha distillation are presented in Table 20.

Table 20: Naphtha distillation mass and molar balances.

	Naphtha		Jet fuel	
Fraction	(tonne/hr)	(kmol/hr)	(tonne/hr)	(kmol/hr)
C1-C4	0.131	2.442	0	0
C5-C8	7.296	73.90	0.191	1.697
C9-C15	0.048	0.374	12.80	87.83
C16-C19	0	0	0.005	0.024
C20+	0	0	0	0

As the hydrocarbon fractions entering the column have relatively low boiling points, the heat duty of the column is not significant compared to the rest of the process. The heat balance of the naphtha distillation is presented in Table 21.

Table 21: Naphtha distillation heat balance.

Process unit	Duty (MW)	Notes
Column reboiler (216 °C)	2.62	Steam may be used
Column condenser (60 °C)	-1.88	Cooling water used

9.7 Hydrocracking

The hydrocracking reactor processes FT wax into shorter chain-length hydrocarbons. The mass and molar balances of the hydrocracking reactor are presented in Table 22.

Table 22: Hydrocracking mass and molar balances.

	Feed		Output	
Component	(tonne/hr)	(kmol/hr)	(tonne/hr)	(kmol/hr)
H2	0.232	115	0.007	3.481
C1-C4	0	0	0	0
C5-C8	0	0	11.96	119.3
C9-C15	0	0	6.935	34.95
C16-C19	0	0	0	0
C20+	32.07	81.29	13.41	33.98

The heat balance of the hydrocracking reactor is presented in Table 23.

Table 23: Hydrocracker heat balance.

Process unit	Duty (MW)	Notes
Hydrocracking reactor (250 °C)	-1.44	Low heat duty
Outlet heat exchanger (250 °C)	0.87	Used as a pressure changer

9.8 Hydrocracker product distillation

The inlet feed of the hydrocracker product distillation is presented on the yield column of Table 22. Mass and molar balances of the vapor and liquid distillates from the top of the column are presented in Table 24.

Table 24: HCP distillate yields.

	Vapor distillate		Liquid distillate	
Component	(tonne/hr)	(kmol/hr)	(tonne/hr)	(kmol/hr)
C1-C4	0	0	0	0
C5-C8	0.142	1.417	11.59	115.6
C9-C15	0	0	0.589	2.971
C16-C19	0	0	0	0
C20+	0	0	0	0

The liquid products obtained are presented in Table 25.

Table 25: Hydrocracking liquid product yields.

	Jet fuel (side draw)		Product wax (bottom product)	
Component	(tonne/hr)	(kmol/hr)	(tonne/hr)	(kmol/hr)
C1-C4	0	0	0	0
C5-C8	0.228	2.274	0	0
C9-C15	5.772	29.09	0.573	2.888
C16-C19	0	0	0	0
C20+	0	0	13.41	33.98

The heat balance of the hydrocracking product distillation is presented in Table 26.

Table 26: HCP distillation heat balance.

Process unit	Duty (MW)	Notes
Column reboiler (429 °C)	3.44	Fired heat required
Column condenser (55 °C)	-4.17	Cooling water used

9.9 Furnace

As the two columns and the syngas purge stream yield gaseous components that are likely not as valuable as end products as other liquid products from the process, they are burned off for heat to accommodate for some of the required high heat duties for both SMR and DMR reactors. Purge gas from the syngas cleaning and recycling loop is also fed into the furnace. Mass and molar balances for the furnace are presented in Table 27.

Table 27: Furnace mass and molar balances..

	Feed		Output	
Component	(tonne/hr)	(kmol/hr)	(tonne/hr)	(kmol/hr)
CH4	2.460	153.3	0.169	10.51
CO2	0.015	0.352	3.564	80.99
CO	2.277	81.29	17.42	622.09
H2	0.091	45.05	1.796	890.9
H2O	1.641	91.11	1.706	94.67
O2	11.29	352.8	0	0
N2	36.71	1310	36.71	1310
C1-C4	1.715	36.76	0	0
C5-C8	4.672	53.75	0	0
C9-C15	0.497	3.688	0	0
C16-C19	0	0	0	0
C20+	0	0	0	0

The outlet heat stream from the furnace is obtained as -15.6 MWh by using a heat exchanger block after the furnace block. However, due to how the Aspen Plus simulation handles heat streams, this heat stream could not be directly connected to either of the high temperature reactors, as it didn't have a high enough heat duty to heat the reactors on its own. The heat exchanger is left out of the simulation, as in real operation the hot flue gas could be directed to the reactor heating systems directly, without having a heat exchanger in between the furnace and the reactor. While the furnace can supply some of the heat required for the process, it is clear that it would require an external fuel source in order to supply enough heat for all of the high temperature reactors. This fuel requirement is further evaluated in the economic evaluation section.

9.10 Total product yields

The total process mass balance in terms of incoming feedstock streams and exiting product streams is presented in Table 28. Some of the major exiting streams, such as water and oxygen and their balances are presented in Sections 9.2 and 9.9 respectively.

Table 28: Total product yields.

	Total process feed	Naphtha yield	Jet fuel yield	Diesel yield	Wax yield
Component	(tonne/hr)	(tonne/hr)	(tonne/hr)	(tonne/hr)	(tonne/hr)
CH4	80.10	0.001	0	0	0
H2O	78.72	0.126	0.028	0	0
CO2	79.59	0	0	0	0
H2	0.433	0	0	0	0
O2	11.29	0	0	0	0
N2	36.71	0	0	0	0
C1-C4	0	0.131	0	0	0
C5-C8	0	18.88	0.419	0	0
C9-C15	0	0.637	30.57	0.051	0.573
C16-C19	0	0	7.978	3.994	0
C20+	0	0	0	5.955	13.41
Total	286.9	19.65	38.97	10	13.98

The product distributions in terms of percentages are visualized in Figure 34.

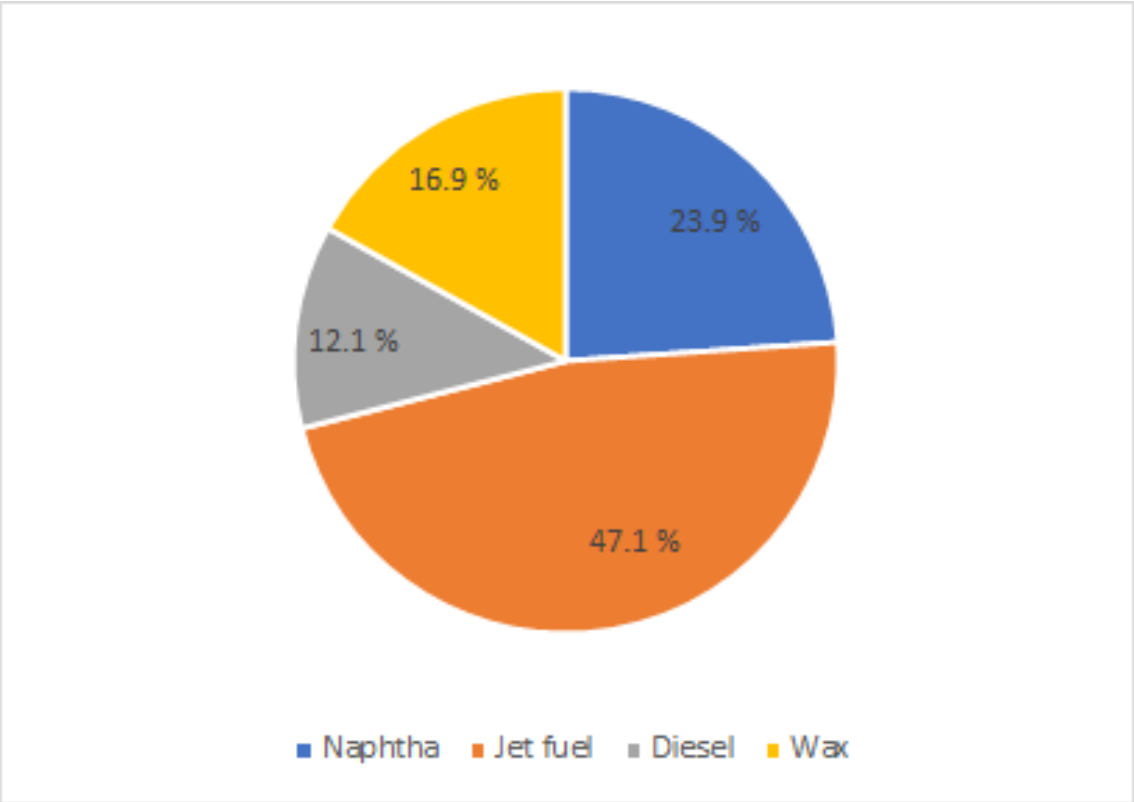

Figure 34: Product fraction mass distributions from the process.

As can be seen from Table 28, the desired product fraction, jet fuel, also contains hydrocarbons (app. 22 w-%) outside of the jet fuel range with 78.3% of the total mass being actual jet fractions (C9-C15 hydrocarbons). According Pries et al. [81], this jet fuel resembles AJF 9 type alternative jet fuel, in which similar amounts (20+ w-%) of C16 and above fractions are found. However, the fuel compostion can likely be altered by processing the fraction further to separate more hydrocarbons outside of the C9-C15 range, but for the sake of this work this product fraction is accepted as such as a jet fuel product.

As can be seen from Table 28, 80.10 tonne/hr of CH_4 is fed into the process while yielding a total of 30.57 tonne/hr of jet fuel applicable hydrocarbons, meaning a 38.2% mass yield from feedstock to product. For the total jet fuel fraction, also including other hydrocarbon chain lengths, this conversion is 48.7%. In terms of chemical energy conversion, using a higher heating value (HHV) of 55.5 MJ/kg for methane and 47.3 MJ/kg for typical alternative jet fuels [81], we can obtain a total

heating value of 4.44 TJ/h for methane and 1.84 TJ/h for jet fuel, meaning a 41.5% yield from methane to jet in terms of energy content. While jet fuel is not directly specified by the hydrocarbon chain length, for the sake of this work, it is used as the specification when determining possible yields from the FT reactor. In reality, the jet fuel would require isomerization and hydrocracking to improve its jet fuel properties, for it to meet specifications for SAF [82]. These isomerization processes would increase the costs of the process, but for the sake of this work, these unit operations are left outside of the scope of the project and the C9-C15 fraction is considered a product comparable to jet fuels.

Naphtha (C5-C8) is produced in the process with a high purity in terms of hydrocarbon chain length distribution. While renewable naphtha may not have a market as such, it can be used as a feedstock to produce light olefins such as ethene and propene via steam cracking. [83] The naphtha could, in theory, also be recycled directly back into the process as a feedstock for syngas generation in the SR reactor.

The produced diesel is assumed to be usable as such, as diesel fuels originating from a FT process typically have hydrocarbon chain lengths well beyond the typical diesel hydrocarbon chain length region [84]. The diesel produced in this process is assumed to be comparable to commercial renewable diesel.

Due to the relatively high HHV of the wax product [72], it is likely to be usable as a liquid fuel. Theoretically, this wax could be recycled into the hydrocracker to yield more of the desired liquid fuel products.

The product fractions produced could be further refined by optimizing the distillation columns' structures and operation parameters to obtain product fractions with even higher mass purity in terms of the hydrocarbon content.

10 Economic analysis

All the monetary values are given as euros, using a conversion rate of 0.94 € to $1. The entire economic analysis is based upon the assumption that the plant operates at 8000 hours annually. The initial goal for the plant capacity was set at 200 ktonne/a, but this value increased as recycling streams were included in the process.

10.1 Capital expenditure

For calculating the capital expenditure (CAPEX), the Aspen Process Economic Analyzer (APEA) is used for most process equipment. However, some of the primary process units cannot be evaluated using APEA, so these units are given CAPEX prices based on literature values. These literature values are scaled up using a formula presented by Chauvel et al. [85], presented in Equation 26.

$$\frac{C_1}{C_2} = (\frac{V_1}{V_2})^X \tag{26}$$

where C_1 = CAPEX of the first plant
C_2 = CAPEX of the second plant
V_1 = capacity of the first plant
V_2 = capacity of the second plant
X = scale-up factor

Scale-up factors for different process units are presented in Table 29.

Table 29: Scale-up factors for different process equipment [85].

Equipment	Factor	Equipment	Factor
Pressure vessels:		Crystallizers	0.65
columns and reactors	0.65-0.70	Basket centrifuges	1.00-1.25
tanks	0.60-0.65	Evaporators:	
Exchangers:		standard	0.55
standard	0.65	forced circulation	0.70
reboilers	0.50	Mills	0.65
Air coolers	0.80	Tanks:	
Compressors	0.80-0.85	<150 m^3	0.30
Pumps:		>150 m^3	0.65
centrifugal	0.40-0.50	Pressure storage:	
others	0.60-0.70	horizontal	0.65
Motors	0.90-1.00	spherical	0.70
Furnaces	0.80-0.85	Steam generation	0.80
Stirring reactors	0.45-0.50	Electrical generation	0.75
Steam ejectors	0.45-0.55	Cooling tower	0.60
Mixers:		Refrigeration	0.70
propeller	0.50		
turbine	0.30		
Dryers	0.45-0.50		
Filters	0.60-0.65		

10.1.1 Equipment evaluated by APEA

APEA is used to evaluate the equipment prices to the extent that it can evaluate them automatically. Some equipment, such as the reactors and the cleaning and recycling equipment cannot be evaluated automatically without specifying physical dimensions or parameters for the equipment. As this work does not include specific process design to evaluate these unit operations based on dimensions, they are evaluated based on literature values. The process equipment that are evaluated using literature values are discussed in the following sections. The equipment prices obtained from APEA and literature are combined at the end of the section. The list of equipment evaluated by APEA is presented in Table 30. The same equipment are listed in Appendix H, where brief explanations for each unit is given.

Table 30: Process equipment evaluated by APEA.

Equipment name	Equipment cost (k€)	Installed cost (k€)
2NDFLASH-flash vessel	30.5	119.9
JETHX	35.1	132.1
HXFTS	687.6	1198.7
FTPHXI	145.2	315.8
3PSEP-flash vessel	64.7	209.7
HCHX	20.2	112.7
HXPF	115.6	256.2
SRRHXOUT	74.1	245.2
PHC	50.9	99.9
DMRHXDS	430.6	780.7
FTPHXO	21.4	124.8
SMRHXDS	869.3	1390.6
FTPDIST - MAIN COLUMN-cond	57.2	175.6
FTPDIST - MAIN COLUMN-cond acc	35.0	163.4
FTPDIST - MAIN COLUMN-reflux pump	12.0	64.1
FTPDIST - MAIN COLUMN-tower	5783.5	9785.9
HCDIST-cond	24.2	118.5
HCDIST-cond acc	24.3	118.0
HCDIST-reflux pump	7.0	44.2
HCDIST-tower	283.9	905.1
SRHX	69.5	194.9
WAXHX	30.9	216.4
FTPDIST - MDIST-tower	148.9	402.5
NAPHCOL-cond	24.3	118.6
NAPHCOL-cond acc	25.2	119.1
NAPHCOL-reflux pump	7.8	49.6
NAPHCOL-tower	210.7	545.7
PREFLASH-flash vessel	90.2	230.2
Total	9448.6	18455.2

The total price of this equipment is 18.5 M€ including installation costs.

10.1.2 SMR and DMR reactors

As the SMR and DMR reactors were not designed and sized in this work, their price cannot be directly obtained from Aspen Plus. In order to calculate the CAPEX for both the SMR and DMR reactors, literature sources are used.

Baltrusaitis et al. [30] studied the production of syngas from using a SMR and DMR in concurrent operation. The study presents CAPEX values of 9.8 M€ for the SMR reactor and 6.4 M€ for the DMR reactor and 4.6 M€ for the SMR catalyst and 2.9 M€ for the DMR catalyst. The methane feed rates in the study are 1728 kmol/h and 1134 kmol/h for the SMR and DMR reactions respectively, while in this work the flow rates are 3194 kmol/h and 1799 kmol/h. By using Equation 26 with a scale-up factor of 0.7, we can obtain CAPEX values of 15 M€ and 8.8 M€ for the SMR and DMR reactors respectively. The values for the catalysts are calculated by directly comparing production capacities and assuming the catalyst price increases linearly with the capacity. By calculating with this assumption catalyst prices of 8.0 M€ and 4.4 M€ are obtained for the SMR and DMR catalysts respectively. Based on the literature, the inlet heat exchangers for both processes are included within these values.

10.1.3 CO_2 separation

As discussed by Baltrusaitis et al. [30], the CO_2 separation in a syngas-FT process can be done with commercial Rectisol syngas cleaning equipment. The economic evaluation of Mevawala et al. [86] uses a Rectisol process unit for a similar process utilizing shale gas for syngas production. The study gives a CAPEX of 27.1 M€ for a Rectisol unit with a maximum hourly capacity of cleaning 200 000 m^3/hr syngas. The syngas feed rate in this work is 587 000 m^3/hr. Mevawala et al. [86] use the same equation as is presented in Equation 26 to scale the price of equipment, and a scale-up factor of 0.63 is given. By using Equation 26, a total CAPEX of 53.3 M€ is obtained for the Rectisol unit.

10.1.4 Syngas recycling

While no literature sources could be found for the economic evaluation of SR reactors used to reform hydrocarbons into synthesis gas, the process may be considered as analoguous to the SMR process. As such, the CAPEX for this unit is calculated based on the SMR reactor price of 10.4 M€ given by Baltrusaitis et al. [30]. The molar feed rate given by Baltrusaitis et al. [30] is equivalent to a mass flow of 27.72 tonne/hr for methane. The required feed rate for this process is 56.89 tonne/hr. By using the SMR reactor prices given by Baltrusaitis et al. [30] with a scale-up factor of 0.7, Equation 26 gives a CAPEX price of 16.2 M€ for the SR reactor unit. The price of the SR catalyst is calculated directly from the difference in production capacities, assuming the catalyst price increases linearly with the capacity. By calculating with this assumption, a catalyst price of 8.9 M€ is obtained.

10.1.5 Fischer-Tropsch synthesis

The FTS equipment prices are not readily available from Aspen Plus, so an estimation is made based on literature values. Comparing to the economic studies conducted by van Vliet et al. [87], the FTS process described in this work resembles advanced FT configurations, for which the cost is given as 18.1 M€ for a liquid output capacity of 79.5 m^3/h. The required capacity in this process is 168.3 m^3/h. By using Equation 26 with a scale-up factor of 0.7, we can obtain a CAPEX value of 30.7 M€ for the FTS unit.

10.1.6 Fischer-Tropsch product distillation

The FTS product distillation column is sized and cost estimated by APEA. The total equipment cost evaluated is 6.0 M€, with an installed price of 10.6 M€. According to the economic evaluation of Becker et al. [88], a distillation unit with the capacity of 1.82 kg/s has a cost of 0.44 M€. The required capacity in this work is 25 kg/s, meaning Equation 26 gives us a value of 2.8 M€. The discrepancy between these values is likely caused by the significant difference in production capacities between the cited process of Becker et al. [88] and this work. Based on this, it can be said

that the value given by Equation 26 is likely not reliable, so the APEA value of 10.6 M€ is chosen for this equipment.

10.1.7 Hydrocracker

The economic analysis of Becker et al. [88] provides a price of 4.05 M€ for a hydrocracking reactor with a capacity of 1.13 kg/s. The required capacity in this work is 10.28 kg/s. By using Equation 26 with a scale-up factor of 0.7, we receive a CAPEX value of 19 M€ for a hydrocracker of this capacity.

10.1.8 Furnace

The price for the furnace in which fired heat is produced from the off-gases of the process is calculated using an online calculator by Matches. For a furnace with a heat duty of 15.6 MW, a capital expenditure of 1.28 M€ is obtained. [89]

10.2 Total capital expenditure

The total CAPEX by process area is presented in Table 31. Some of the figures presented in Table 31 may vary from the figures given in previous chapters due to including heat exchangers in their respective process areas (for example, FTP distillation process area costs include the two heat exchangers before and after the column). To obtain the total investment cost, presented in Table 31, a contingency factor and a reservation for price escalation must be added to the CAPEX estimation. A contingency of 10% is used for this work based on the study of Hamelinck et al. [76] and a reservation factor for price escalation is estimated at 20%. With these factors, the total investment cost comes up to 242.8 M€. It should be noted, that this investment cost is for inside battery limits (ISBL) operations. The process would also require outside battery limits (OSBL) investments, such as storage vessels and loading docks, depending on the location of the plant. For this work, the OSBL costs are left out of the scope of the project, as there is no guarantee whether the project will be a greenfield or a brownfield project.

Table 31: Total equipment costs and investment for the process.

Process area	Equipment cost (M€)	Share of equipment costs (%)
Syngas generation	38.4	20.9 %
Syngas cleaning	53.8	29.3 %
Fischer-Tropsch	32.7	17.8 %
FTP distillation	11.0	6.0 %
Naphtha distillation	0.8	0.5 %
Hydrocracking	19.2	10.4 %
HCP distillation	1.2	0.6 %
Recycling	25.5	13.8 %
Furnace	1.3	0.7 %
Total equipment cost	183.9	100 %
Total investment	242.8	

These results are visualized in Figure 35 in terms of percentages of total CAPEX for each process area.

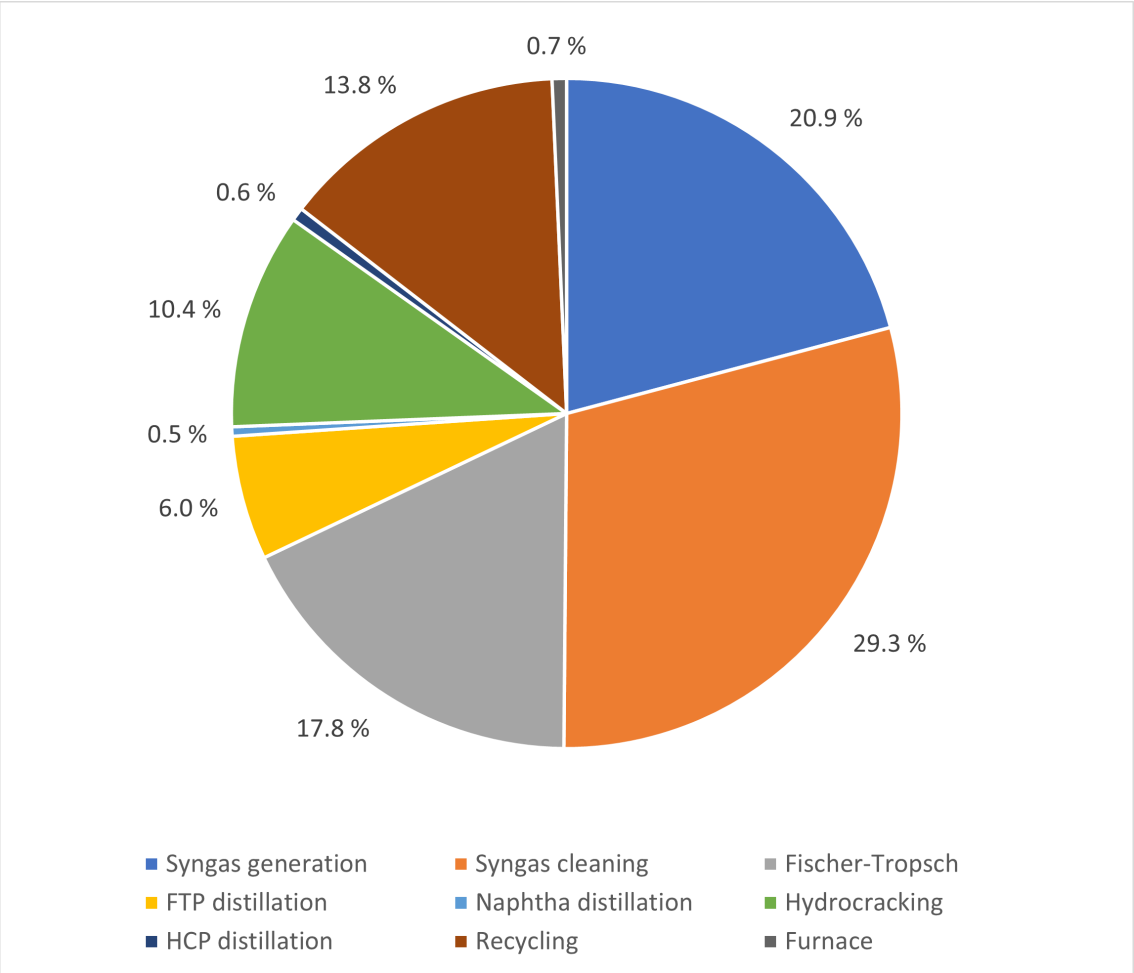

Figure 35: Distribution of CAPEX for each process area in terms of percentages.

As can be seen from the results, syngas generation and subsequent cleaning processes have the highest CAPEX in the process. The process configuration chosen for this work was the SMR/DMR setup, but the CAPEX could be lower, if another configuration was used. CPOX, for example, could be used as a standalone syngas production method, likely resulting in much lower CAPEX. ATR could also likely provide lower CAPEX costs, as the process is less energy intensive compared to the SMR and DMR processes. ATR, however, would require a separate oxygen generation plant, which would raise CAPEX costs.

The recycling step is another part of the process, where CAPEX could likely be lowered with another recycling configuration. The recycling process in this work not only recycles synthesis gas but also generates new syngas from the hydrocarbons

from the process. This is not necessarily required, and the recycling could be done with a process that simply separates hydrocarbons and other unwanted components from the syngas stream. This could, for example, be done with an absorber by using an appropriate absorbant.

Other parts of the process, however, likely have less room for savings in terms of the investment costs. Further optimizations could of course be done. The CAPEX values given in this section are assumed to contain the price of engineering and construction based on the APEA evaluation and the cited literature.

10.3 Operational expenditure

Operational expenditure (OPEX) is calculated for the entire process in terms of cost per annum. At the end of this section, the OPEX is also presented as a function of the product produced. All OPEX and income values are calculated with the assumption the plant operates 8000 hours a year.

10.3.1 Variable operating costs

The variable operating costs consist of the price of feedstock fed into the process, as well as the price of utilities consumed in the process. All the feedstocks, their feed rates and annual costs are presented in Table 32.

Table 32: Total raw material feeds and their prices annually.

Feedstock	Feed (tonne/hr)	Price (€/tonne)	OPEX (M€/a)
CH4	80.1	999.5	640.5
H2O	78.72	0.47	0.30
CO2	79.59	16.95	10.79
H2	0.433	6000	20.78
Total	238.8	351.9	672.3

The price for CH_4 is assumed to be the price of upgraded (purified and liquefied) biomethane. An IEA report from the year 2020 gives a price of 64.83 €/MWh for biomethane upgraded from biogas. This price accounts for the price of biogas itself as well as the required production steps and facilities for upgrading. This price decreases as the production capacity increases, with a price estimation of 47.8 €/MWh by the year 2040 assuming biogas production and upgrading capacities follow the current trend. [90]

The price of the methane used in this process is calculated from the mass-based HHV of methane, 55.5 MJ/kg, which is equivalent to 0.0154 MWh/kg. From this, the total hourly energy consumption in terms of methane is 1233.54 MWh. By using the biomethane prices above, this means an hourly cost of 80 057 € and an annual

cost of 640.5 M€.

The price of hydrogen is taken directly from the cost of producing it via electrolysis, as it is assumed that electrolysis equipment is readily available for St1. The production price of hydrogen is assumed at 6000 €/tonne, including the OPEX and CAPEX of the production. [91] From this, an OPEX of 20.78 M€/a for hydrogen is obtained. The price of water used in the process is assumed at 0.47 €/tonne [92]. The annual OPEX for water is 0.30 M€/a.

As it can be assumed, that raw CO_2 is not a commercially traded commodity, it is assumed that the CO_2 for the process has to be captured from St1's existing operations. Thus, the price of CO_2 is considered as the cost of capturing CO_2 from a stream. As it is already employed within the process, the Rectisol process is assumed to be used for the capture of CO_2 in this process. According to the study of Ma et al. [93], the price of CO_2 captured with the Rectisol process is 16.95 €/tonne. From this, an annual cost of 10.79 M€/a is obtained for CO_2 used in the process.

The required utilities, the required capacities and the OPEX they account for are listed in Table 33.

Table 33: Process utilities and their annual operational expenditure.

Required utility	Duty (MW)	Price (€/MW)	OPEX (M€/a)
High pressure steam	9.6	138.2	10.7
Fired heat	471.3	25.7	96.8
Cooling water	-32.6	20.2	5.3
Electricity	144.2	61.5	70.9
Total	657.7	34.9	185.8

The required electricity consumption given by APEA is 0.196 MW which is likely far from the actual electricity requirement of the process. For the OPEX calculations, the electricity consumption of the process is evaluated based on the study of Baltrusaitis et al. [30], where on-site consumption is cited as 95.94 MW. This includes pumps, compressors, the Rectisol unit and an air-separation unit (ASU), which is not included in this work. Without the ASU, the on-site consumption is

92.66 MW for a FT liquid product flow-rate of 58 tonne/hr. In this process the liquid product flow-rate is 90.2 tonne/hr. Assuming the electricity consumption scales linearly with the liquid product rate, this electricity consumption would equal 144.2 MW, which is used as the value in this work for electricity consumption. The other utility consumptions are taken directly from the simulation, with the fired heat duty being the total required heat duty and the heat duty from the furnace deducted.

For high pressure steam and fired heat, the utility prices are typically calculated by assuming they are generated using natural gas with a typical furnace efficiency of 85%. [92] With this, the required amount of heat supplied by natural gas is 564 MW. At current European natural gas prices of 117.5 €/MWh [94] this would cause an annual cost of over 530 M€. It should be noted, however, that natural gas price in Europe has inflated significantly in the year 2022 due to uncertainties over natural gas distribution. Even with a natural gas price of 70 €/MWh from the beginning of 2022, the OPEX would still be around 316 M€/a. It can be immediately stated that this is too high for the process to be economically viable, so some other method must supply the high temperature heat. One such method could be utilizing heat pumps to transfer the heat from the FT process and its subsequent flashing into the reactors and supplying the remaining heat by generating heat using natural gas. The FT reactor produces an excess of 285.5 MW of heat, meaning only 28.69 MW must be supplied from the flashing part of the process to cover the SMR and DMR reactor heating requirements.

In order to use heat pumps, the coeffecient of performance (COP) must be calculated for both the pump required for the FT reactor and the flashing stage heat exchanger. The COP may be calculated using Equation 27.

$$COP_{HP} = \frac{1}{1 - \frac{T_L}{T_H}} \tag{27}$$

where COP_{HP} = coefficient of performance for a heat pump
T_L = temperature of the incoming heat
T_H = temperature of the outgoing heat

Using Equation 27 with the outlet temperature of 250 °C for the FT reactor and 80 °C for the FTP heat exchanger, and using an outgoing heat temperature of 627 °C for both heat pumps, we can calculate a COP of 1.66 for the heat pump used for the FT reactor and 1.14 for the heat pump used with the FTP heat exchanger. With these COP values, the net amount of work required for the heat pump can be calculated using Equation 28.

$$W_{net} = \frac{Q_h}{COP_{HP}} \tag{28}$$

where W_{net} = net amount of work required
Q_h = heat delivered

By using Equation 28, we can obtain total work requirements to pump 386.7 MW of heat into the SMR and DMR reactors of 196.7 MW for both heat pumps combined. This would account for an annual OPEX of 96.78 M€ with an electricity price of 61.5 €/MWh [95]. While still a very high price, it is significantly more reasonable than producing fired heat with natural gas. By using heat pumps, the requirement to utilize the waste heat from the FT process is also covered, removing cooling water requirements from the process units. Other on-site electricity consumption of 144.2 MW accounts for an annual cost of 70.95 M€ with the same electricity price. Assuming the high pressure steam is still produced using natural gas and a typical furnace efficiency of 85%, the utility price comes up to 10.7 M€ annually. The price of the heat pumps is left out of the scope of this project in terms of investment costs.

The cooling water is assumed to be taken from the sea at 10 °C and released back into the nature at 30 °C to preserve the surrounding biosphere from possible complications relating to increased temperature. With this, an hourly cooling water

rate of 1400 tonne/hr is required to cover the cooling requirement of 32.56 MW. By using an estimation of 0.47 €/tonne of cooling water, the annual cooling water OPEX comes to 5.26 M€.

10.3.2 Fixed operating costs

The total fixed operating costs of the process are presented in Table 34.

Table 34: Total fixed operating costs of the process.

Item	Total cost (M€/a)
Maintenance costs	7.3
Personnel costs	9.16
Tax insurance costs	4.86
Total	21.3

The economic evaluation of Tijmensen et al. [53] presents a maintenance cost of 3% of the total investment and an annual personnel cost of 0.8225 M€/100 MW process inlet lower heating value (LHV) for a similar process of converting syngas into transport fuels via FT. The maintenance costs account for an annual cost of 7.3 M€. At an LHV of 13.9 MWh/tonne for methane, with the feed rate of this process the annual personnel costs are 9.16 M€/a. These personnel costs include health, safety and administrative costs for the process.

Tax and insurance are taken as of 2% of fixed investment. [96] This accounts for a total annual cost of 4.86 M€.

With these figures the total fixed operating costs come to 21.3 M€ annually.

10.3.3 Process income

While price projections for some products cannot be found online for free, estimations based on current prices are given for those products. The product prices are projected to the future 2035, where sustainable liquid fuel demand is expected to be the highest. The prices and annual incomes from the process are presented in Table 35.

Table 35: Total income from biofuels produced in the process.

Product	Output (ktonne/a)	Price (€/tonne)	Income (M€)
Naphtha	157.2	1024	160.9
Jet fuel	311.76	1690	526.8
Diesel	80	1880	150.4
Wax	111.84	558	62.4
Total	660.8		901

According to an S&P Global Commodity Insights report [97], the market price of bionaphtha has risen 8.9% between the years 2019 and 2021. If this trend continues, the price of bionaphtha is expected to reach 1024 €/tonne by the year 2035.

The economic study for SAF production by Hayward et al. [98] presents two scenarios for jet fuel price by the year 2035; a high estimation in the range of 1.42–1.65 €/litre and a low estimation of 0.86–1.1 €/litre. Out of these, the high estimation is used, as it is expected that SAF is in high demand in the future. The low end of the high estimation with the price of 1.42 €/litre would equal to a price of 1690 €/tonne of jet fuel. This is used as the value for this process.

According to an IEA renewable fuel market update, the price increase of renewable diesel has stagnated in Europe to a price of 1.6 €/l between January and March of 2022 [99]. This is equivalent to 1880 €/tonne, which is used as the price for this work.

While the heavy residual wax from the process has no current direct uses, its price is assumed to be comparable to that of bitumen produced in conventional refinery operations. The price of bitumen in Europe is quoted at 558 €/tonne. [100] It should be noted, however, that the price of renewable "biobitumen" would likely be higher than that of fossil fuel based bitumen.

11 Process valuation and sensitivity analysis

In order to valuate the process, some assumptions have to be made for the production. These assumptions are presented in Table 36.

Table 36: Assumptions for process valuation.

Parameter	Assumption
Plant life time	30 years
Investment decision	2023
Construction time	4 years
Production ramp-up	25%-units annually starting 2027
Discount factor	7%

The first assumption for the process is that the operational life-time of the plant is 30 years. For this case, it is assumed that the year 2023 can be counted as the first year of consideration for the entire plant, and 2052 as the last year of operation. The construction time is assumed as 4 years, meaning that after the initial investment, the year 2027 will be the first year in which production will be started at 25% of the maximum capacity. From here, the capacity will increase by 25%-units annually, until it reaches full capacity by the year 2030. Discount factor of 7% is used for the cash flows of the process.

Overall, the costs of the process are 877.23 M€ annually, with an income of 900.65 M€ with the assumed product prices. This means an annual earnings before interest, taxes, depreciation and amortization (EBITDA) of 23.43 M€.

With these parameters set, a non-discounted payback time of 19.2 years is obtained for the initial investment of 242.8 M€. The discounted payback time is 29 years. The internal rate of return (IRR) of the process is 3.3% over the 30-year period of investment total life time, falling short of the 7% discount factor requirement. The net present value of the process is calculated to be -119.6 M€, with an NPV per CAPEX being -0.492 $€_{NPV}/€_{CAPEX}$. A figure for the total cumulative discounted cash flow (DCF) is presented in Figure 36.

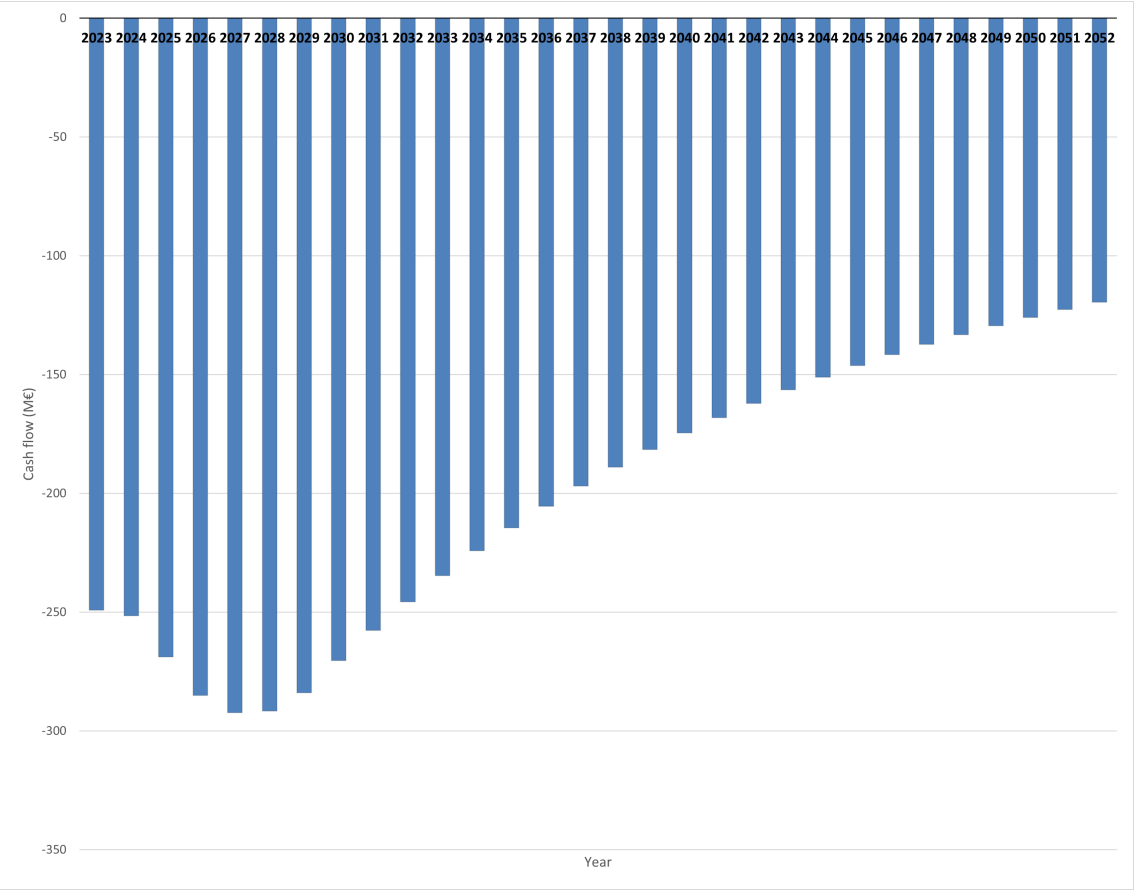

Figure 36: Discounted cash flow over investment operating time.

The overall OPEX over the 30 year investment total time is 21.59 G€. The total mass of liquid fuels produced during the investment total time is 16.189 Mtonne. By adding the total investment value of 242.8 M€ to the total OPEX, the total cost per tonne of liquid fuel produced over the total investment time is 1349 €/tonne.

The MFSP can be calculated as the required jet fuel price in order for the NPV of the project to become zero. [20] For this process, the MFSP would be 1738 €/tonne, meaning the jet fuel price would have to be 2.8% higher than the assumption made in this work. It should be noted, that an NPV of zero is the point at which the process starts to become profitable, so the price would actually have to be higher to obtain any real profit from the process.

The feedstock prices and the liquid fuel product prices are major factors affecting the overall profitability of the process. The biggest of these affecting the process

economics are the price of biomethane and jet fuel, presented in Tables 32 and 35 respectively. A sensitivity analysis based on these prices is presented in Figure 37.

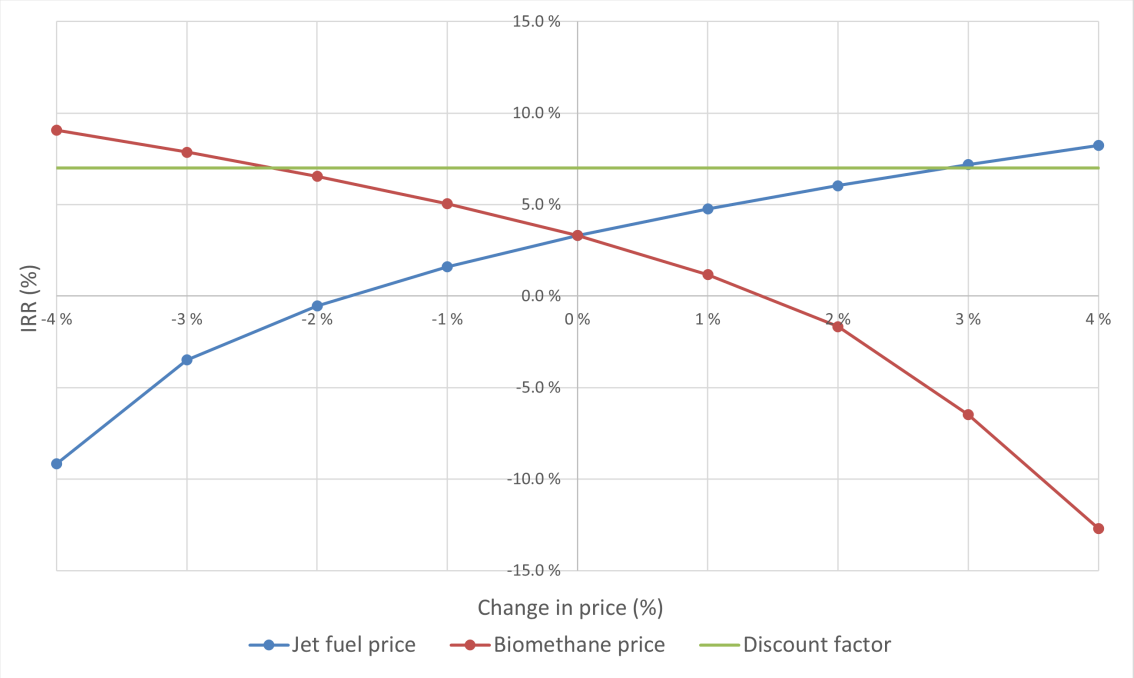

Figure 37: Sensitivity analysis of the effect of jet fuel and biomethane prices on the IRR.

Based on the sensitivity analysis presented in Figure 37, the price of jet fuel would have to be 2.8% higher and the price of biomethane to be around -2.25% lower in order for the process to fulfill the IRR requirement of 7%. The process would be significantly more profitable, with an IRR of 24.34%, NPV of 1226 M€ and a non-discounted payback time of 6.3 years if the price of biomethane was at 47.8 €/MWh, as was described as a possible scenario by the year 2040 in an IEA report on biomethane production [90].

The total investment of the process would also affect the profitability of the process. This requires evaluation, especially as the total investment estimated in this work may have some variance compared to the actual investment cost. However, as the difference between the income and the total costs of the process determines much of the profitability of the process, this sensitivity analysis is mainly used to determine that the overall economics do not rely heavily on the investment costs.

The effect of the production capacity on the IRR is also estimated, assuming that the investment costs increase with a factor of 0.7 per capacity increased. The sensitivity analysis for the effect of total investment and the production capacity on the IRR of the process is presented in Figure 38

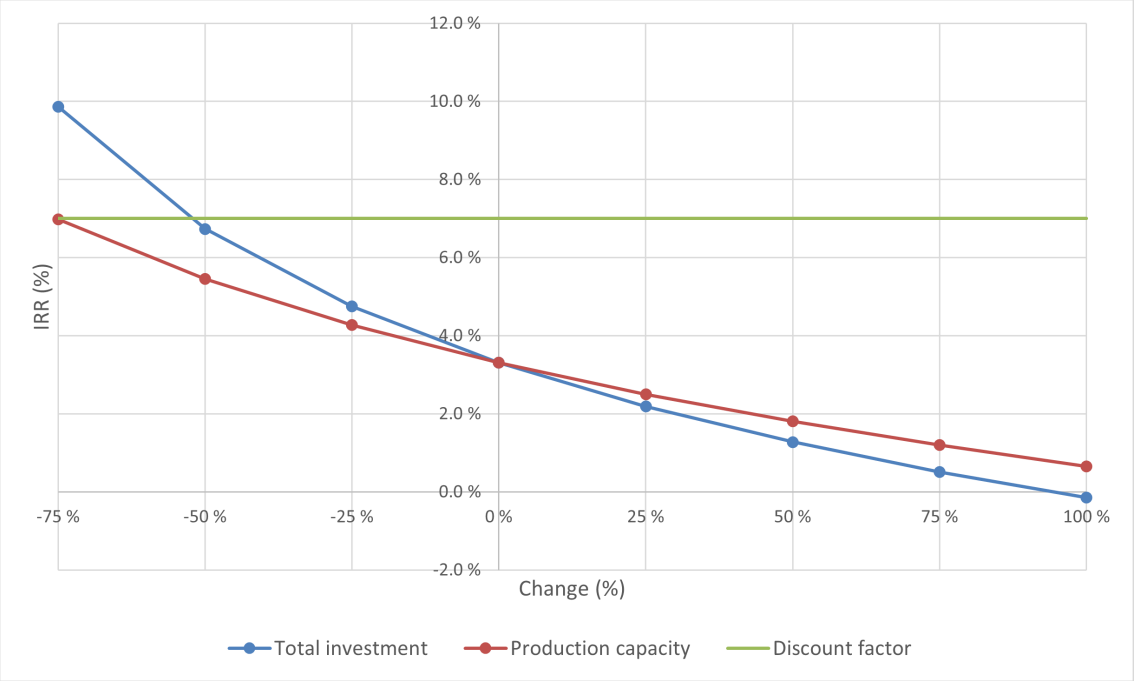

Figure 38: Sensitivity analysis of the total investment effect on the IRR.

As can be seen from the sensitivity analysis presented in Figure 38, the total investment does not radically change the IRR. Assuming that the investment cost is likely not lower than the current estimation, an increase in the investment costs slowly decreases the profitability of the process. Interestingly, decreasing the capacity of the process increases the economic performance of the process, with IRR reaching 7% and effectively achieving an NPV of zero if the capacity was 25% of the current capacity.

As can be seen from the figures presented in this section and the sensitivity analyses, the process is marginally profitable in its current state. However, as can be seen from the sensitivity analyses, the process may easily become more profitable, if the OPEX can be decreased, if the price of feedstocks decreased or if the price of produced jet fuel is higher than assumed.

12 Discussion and suggestions for future work

This work provides a basic analysis of the process and its economics for the production of SAF. As this work was conducted more as a conceptual design, more detailed engineering would be required for the process, especially for the reactors used in the process as in this work they were simulated as not following actual kinetics and being based on theoretical yields.

This work outlines reasons for the production of SAF in terms of potential markets and requirements in reducing CO_2 emissions in the industry. The work explores some of the possible alternatives for producing SAF and gives reasoning for why this syngas based FT process in particular could be used by St1. Economics of SAF production are also covered, opening important concepts behind understanding the economics of different production pathways.

The literature section covers the required theory behind the production of syngas, FTS, hydrocracking and distillation processes used in the process. Some alternatives are also given for parts of the process, outlining other possibilities for the process configuration. The section outlines the choices made for different process units that are used as the basis for building the Aspen Plus simulations.

The experimental section goes over the process areas and how they have been implemented in the Aspen Plus simulation. Literature sources for used values are given and the assumptions regarding the simulation are opened. The simulation was then evaluated on a mass and heat balance basis, from which economic analyses could be done.

The economic evaluation gives an overview of the expected economics of the process. While the process turned out to be somewhat profitable (IRR = 2.8%) in its current state with current prices, it could be even more profitable depending on the price of the biomethane feedstock as well as the product fractions, mainly jet fuel. This is determined via sensitivity analyses. Especially the price of biomethane may be subject to change in the future making the process even more profitable, as was described by the IEA report in 2020. [90] This price, however, relies heavily on

the global production scale of biomethane, meaning it may not be affected by the company itself, even if they are the ones to produce their own biomethane.

The overall process has a lot of potential for optimization, especially in terms of heat integrations. Within the scope of this work, only small heat integrations were able to be completed, mainly by implementing feed effluent heat exchangers for operation blocks with high temperatures and heat duties. Further heat integrations could be done in Aspen Plus by using the built in Aspen Energy Analyzer. These integrations could significantly decrease the heat requirements of the process, thus decreasing the overall cost of operation.

In terms of the process, areas that require special attention to detail would be the syngas production and the FT synthesis. The current proposed syngas production reactors, SMR and DMR both operate at very high temperatures meaning a significant heating requirement. These reactors should be looked into, to obtain possible savings in terms of energy consumption or even swapping the configuration out entirely for another, such as the SRM/ATR or SMR/RWGS configurations. The FT synthesis in this work also follows the completely theoretical ASF model yield for the products, meaning the actual hydrocarbon fractions produced could vary significantly. In order to proceed further with this process, parts of the process require more rigorous simulations and contacting equipment vendors to obtain more realistic evaluations for the equipment and their costs.

The scope of this work also leaves out some necessary downstream refining steps for the hydrocarbon products before they can be used as fuel products. Especially the jet fuel fraction would require isomerization, as the straight-chain hydrocarbons are not usable as such for aviation. This should be accounted for in the future, both in terms of investment costs and operational expenses.

It should also be noted, that as the process is modelled for the use of 100% mass purity methane, the process configuration may still require additional purification steps depending on the purity of the actual feedstock used by St1. If the biogas production, purification and distribution systems prior to the process evaluated here were included in the overall CAPEX and OPEX calculations, the figures might differ

significantly.

While the economics of the process are marginally profitable in its current state with prices obtainable at the time of writing in June 2022, there are certainly possibilities that the process may be able to turn more profitable in the future. This relies mainly on the price of biomethane as a feedstock and the price of renewable jet fuels. The process economics could also change significantly, if improvements to the FT and hydrocracking processes were developed. If the selectivity towards jet fuels could be increased, the income of the process would increase significantly. Developments in FT and hydrocracking technologies should be looked out for in the future. By keeping these factors in mind, this project should not be dismissed but instead kept as a possibility for obtaining maximal value from biomethane, should the market prices justify its use as a feedstock for renewable liquid fuels.

References

[1] Brandon Graver et al. "CO 2 emissions from commercial aviation , 2018". In: September (2019).

[2] Stefan Gössling and Andreas Humpe. "The global scale, distribution and growth of aviation: Implications for climate change". In: *Global Environmental Change* 65.November (2020). ISSN: 09593780. DOI: 10.1016/j.gloenvcha.2020.102194.

[3] David Chiaramonti. "Sustainable aviation fuels: The challenge of decarbonization". In: *Energy Procedia* 158 (2019), pp. 1202–1207. ISSN: 18766102. DOI: 10.1016/j.egypro.2019.01.308. URL: https://doi.org/10.1016/j.egypro.2019.01.308.

[4] Olivier Boucher et al. "On the contribution of global aviation to the CO2 radiative forcing of climate". In: *Atmospheric Environment* 267 (Dec. 2021). ISSN: 18732844. DOI: 10.1016/j.atmosenv.2021.118762.

[5] IATA. *Industry Domestic Russia Domestic Brazil Domestic India Domestic USA Domestic Japan Domestic China Sources: IATA Economics, IATA Monthly Statistics*. Tech. rep. 2021.

[6] Matteo Prussi et al. "CORSIA: The first internationally adopted approach to calculate life-cycle GHG emissions for aviation fuels". In: *Renewable and Sustainable Energy Reviews* 150.June (2021). ISSN: 18790690. DOI: 10.1016/j.rser.2021.111398.

[7] Qiang Cui, Yu-xin Hu, and Li-ting Yu. "Can the aviation industry achieve carbon emission reduction and revenue growth simultaneously under the CNG2020 strategy? An empirical study with 25 benchmarking airlines". In: *Energy* 245 (Apr. 2022), p. 123272. ISSN: 03605442. DOI: 10.1016/j.energy.2022.123272.

[8] Martin Cames et al. *DIRECTORATE GENERAL FOR INTERNAL POLICIES POLICY DEPARTMENT A: ECONOMIC AND SCIENTIFIC POLICY Emission Reduction Targets for International Aviation and Shipping STUDY*. Tech. rep. 2015.

[9] *THE PARIS AGREEMENT*. Tech. rep. 2016. URL: https://treaties.un.org/Pages/ViewDetails.aspx?src=TREATY&mtdsg_no=XXVII-7-.

[10] "IATA Aircraft Technology Roadmap to 2050". In: ().

[11] Wei Cheng Wang and Ling Tao. *Bio-jet fuel conversion technologies*. Jan. 2016. DOI: 10.1016/j.rser.2015.09.016.

[12] Libing Zhang, Terri L Butler, and Bin Yang. *5 Recent Trends, Opportunities and Challenges of Sustainable Aviation Fuel*. Tech. rep. 2020.

[13] Becky Mawhood et al. "Production pathways for renewable jet fuel: A review of commercialization status and future prospects". In: *Biofuels Bioproducts and Biorefining* Advance on (Apr. 2016). DOI: 10.1002/bbb.1644.

[14] Matthew Pearlson, Christoph Wollersheim, and James Hileman. "A techno-economic review of hydroprocessed renewable esters and fatty acids for jet fuel production". In: *Biofuels, Bioproducts and Biorefining* 7.1 (Jan. 2013), pp. 89–96. ISSN: 1932104X. DOI: 10.1002/bbb.1378.

[15] Wei Cheng Wang, Yu Cheng Liu, and Rusdan Aditya Aji Nugroho. "Techno-economic analysis of renewable jet fuel production: The comparison between Fischer-Tropsch synthesis and pyrolysis". In: *Energy* 239 (Jan. 2022). ISSN: 03605442. DOI: 10.1016/j.energy.2021.121970.

[16] Bruno Colling Klein et al. "Techno-economic and environmental assessment of renewable jet fuel production in integrated Brazilian sugarcane biorefineries". In: *Applied Energy* 209 (Jan. 2018), pp. 290–305. ISSN: 03062619. DOI: 10.1016/j.apenergy.2017.10.079.

[17] Christoph Wolff and Daniel Riefer. “Clean Skies for Tomorrow Sustainable Aviation Fuels as a Pathway to Net-Zero Aviation”. In: *World Economic Forum* November (2020), p. 43.

[18] *First ICAO Stocktaking Seminar toward the 2050 Vision for Sustainable Aviation Fuels*. 2019.

[19] E Mazarenau. *Total fuel consumption of commercial airlines worldwide between 2005 and 2022*. 2021.

[20] Sierk De Jong et al. “Life-cycle analysis of greenhouse gas emissions from renewable jet fuel production”. In: *Biotechnology for Biofuels* 10.1 (Mar. 2017). ISSN: 17546834. DOI: 10.1186/s13068-017-0739-7.

[21] IATA. *Jet Fuel Price Monitor*. 2022. URL: https://www.iata.org/en/publications/economics/fuel-monitor/.

[22] Trading Economics. *Natural gas price chart*. 2022. URL: https://tradingeconomics.com/commodity/natural-gas.

[23] Jane O’malley, Nikita Pavlenko, and Stephanie Searle. *Estimating sustainable aviation fuel feedstock availability to meet growing European Union demand*. Tech. rep. 2021. URL: www.theicct.org.

[24] St1. *St1 started biogas business in Sweden – the company’s biogas projects are also progressing in Norway and Finland*. 2021. URL: https://www.st1.com/st1-started-biogas-business-in-Sweden-the-companys-biogas-projects-are-also-progressing-in-norway-and-finland.

[25] St1. *Valio and St1 joint venture, Suomen Lantakaasu Oy, ready to increase domestic biogas production*. 2022. URL: https://www.st1.com/valio-and-st1-joint-venture-suomen-lantakaasu-oy-ready-to-increase-domestic-biogas-production.

[26] Siti Roshayu Binti Hassan, Mohamad Johari Abu, and Irvan Dahlan. “Industrial wastewater treatment: Recycled paper mill effluent treatment using Modified Anaerobic Hybrid Baffled (MAHB) bioreactor”. In: *Handbook of*

Research on Resource Management for Pollution and Waste Treatment (2019), pp. 318–338. DOI: 10.4018/978-1-7998-0369-0.ch014.

[27] S. Rasi, A. Veijanen, and J. Rintala. "Trace compounds of biogas from different biogas production plants". In: *Energy* 32.8 (2007), pp. 1375–1380. ISSN: 03605442. DOI: 10.1016/j.energy.2006.10.018.

[28] E. Ryckebosch, M. Drouillon, and H. Vervaeren. *Techniques for transformation of biogas to biomethane*. May 2011. DOI: 10.1016/j.biombioe.2011.02.033.

[29] Fredric Bauer et al. "Biogas upgrading - technology overview, comparison and perspectives for the future". In: *Biofuels, Bioproducts and Biorefining* 7.5 (Sept. 2013), pp. 499–511. ISSN: 1932104X. DOI: 10.1002/bbb.1423.

[30] Jonas Baltrusaitis and William L. Luyben. "Methane Conversion to Syngas for Gas-to-Liquids (GTL): Is Sustainable CO2 Reuse via Dry Methane Reforming (DMR) Cost Competitive with SMR and ATR Processes?" In: *ACS Sustainable Chemistry and Engineering* 3.9 (Sept. 2015), pp. 2100–2111. ISSN: 21680485. DOI: 10.1021/acssuschemeng.5b00368.

[31] Mohammad Ostadi, Erling Rytter, and Magne Hillestad. "Boosting carbon efficiency of the biomass to liquid process with hydrogen from power: The effect of H2/CO ratio to the Fischer-Tropsch reactors on the production and power consumption". In: *Biomass and Bioenergy* 127 (Aug. 2019). ISSN: 18732909. DOI: 10.1016/j.biombioe.2019.105282.

[32] James G. Speight. "Synthesis gas and the Fischer–Tropsch process". In: *The Refinery of the Future*. Elsevier, 2020, pp. 427–468. DOI: 10.1016/b978-0-12-816994-0.00012-9.

[33] Gustavo Rocha Silva Santos et al. "Techno-economic assessment of Fischer-Tropsch synthesis and direct methane-to-methanol processes in modular GTL reactors". In: *Catalysis Today* 371 (July 2021), pp. 93–112. ISSN: 09205861. DOI: 10.1016/j.cattod.2020.07.012.

[34] James G.. (2020) Speight. *Handbook of Gasification Technology - Science, Processes, and Applications - 11.1.* 2020, pp. 364–368.

[35] Muhammad Usman, W. M.A. Wan Daud, and Hazzim F. Abbas. *Dry reforming of methane: Influence of process parameters - A review.* 2015. DOI: 10.1016/j.rser.2015.02.026.

[36] M. García-Diéguez et al. "Transient study of the dry reforming of methane over Pt supported on different γ-Al2O3". In: *Catalysis Today* 149.3-4 (Jan. 2010), pp. 380–387. ISSN: 09205861. DOI: 10.1016/j.cattod.2009.07.099.

[37] Jianjun Guo et al. "Dry reforming of methane over nickel catalysts supported on magnesium aluminate spinels". In: *Applied Catalysis A: General* 273.1-2 (Oct. 2004), pp. 75–82. ISSN: 0926860X. DOI: 10.1016/j.apcata.2004.06.014.

[38] Andrew P E York, Tiancun Xiao, and Malcolm L H Green. *Brief overview of the partial oxidation of methane to synthesis gas.* Tech. rep.

[39] R. M. Navarro, M. A. Peña, and J. L.G. Fierro. *Hydrogen production reactions from carbon feedstocks: Fossil fuels and biomass.* Oct. 2007. DOI: 10.1021/cr0501994.

[40] Abdalwadood H. Elbadawi et al. "Catalytic partial oxidation of methane to syngas: review of perovskite catalysts and membrane reactors". In: *Catalysis Reviews - Science and Engineering* 63.1 (2021), pp. 1–67. ISSN: 15205703. DOI: 10.1080/01614940.2020.1743420.

[41] Bjørn Christian Enger, Rune Lødeng, and Anders Holmen. *A review of catalytic partial oxidation of methane to synthesis gas with emphasis on reaction mechanisms over transition metal catalysts.* Aug. 2008. DOI: 10.1016/j.apcata.2008.05.018.

[42] Consuelo Alvarez-Galvan et al. "Partial oxidation of methane to syngas over nickel-based catalysts: Influence of support type, addition of rhodium, and preparation method". In: *Frontiers in Chemistry* 7.MAR (2019). ISSN: 22962646. DOI: 10.3389/fchem.2019.00104.

[43] Mari Voldsund, Kristin Jordal, and Rahul Anantharaman. *Hydrogen production with CO2 capture*. Mar. 2016. DOI: 10.1016/j.ijhydene.2016.01.009.

[44] J. G. Speight. "Gasification processes for syngas and hydrogen production". In: *Gasification for Synthetic Fuel Production: Fundamentals, Processes and Applications* (Jan. 2015), pp. 119–146. DOI: 10.1016/B978-0-85709-802-3.00006-0.

[45] Gabriele Centi and Siglinda Perathoner. "Opportunities and prospects in the chemical recycling of carbon dioxide to fuels". In: *Catalysis Today* 148.3-4 (Nov. 2009), pp. 191–205. ISSN: 09205861. DOI: 10.1016/j.cattod.2009.07.075.

[46] Min Zhu, Qingfeng Ge, and Xinli Zhu. *Catalytic Reduction of CO2 to CO via Reverse Water Gas Shift Reaction: Recent Advances in the Design of Active and Selective Supported Metal Catalysts*. June 2020. DOI: 10.1007/s12209-020-00246-8.

[47] Marc D. Porosoff, Binhang Yan, and Jingguang G. Chen. *Catalytic reduction of CO2 by H2 for synthesis of CO, methanol and hydrocarbons: Challenges and opportunities*. Jan. 2016. DOI: 10.1039/c5ee02657a.

[48] James G. Speight. "Gasification of Unconventional Feedstocks - 5.1 Introduction." In: 2014, pp. 118–133.

[49] P L Spath and D C Dayton. *Preliminary Screening – Technical and Economic Assessment of Synthesis Gas to Fuels and Chemicals with Emphasis on the Potential for Biomass-Derived Syngas*. Tech. rep. Golden, CO (United States): National Renewable Energy Laboratory (NREL), Dec. 2003. DOI: 10.2172/15006100. URL: http://www.osti.gov/servlets/purl/15006100/.

[50] National Center for Biotechnology Information. *APA National Center for Biotechnology Information (2022). PubChem Compound Summary for CID 12408, Octacosane*. 2022. URL: https://pubchem.ncbi.nlm.nih.gov/compound/Octacosane.

[51] National Center for Biotechnology Information. *National Center for Biotechnology Information (2022). PubChem Compound Summary for CID 87821, 1-Octacosene*. 2022. URL: https://pubchem.ncbi.nlm.nih.gov/compound/1-Octacosene.

[52] A. K. Dalai and B. H. Davis. *Fischer-Tropsch synthesis: A review of water effects on the performances of unsupported and supported Co catalysts*. Sept. 2008. DOI: 10.1016/j.apcata.2008.06.021.

[53] Michiel JA Tijmensen et al. *Exploration of the possibilities for production of Fischer Tropsch liquids and power via biomass gasiÿcation*. Tech. rep. 2002, pp. 129–152.

[54] Vineet Singh Sikarwar et al. *Progress in biofuel production from gasification*. 2017. DOI: 10.1016/j.pecs.2017.04.001.

[55] J. Van de Loosdrecht et al. "Fischer-Tropsch Synthesis: Catalysts and Chemistry". In: *Comprehensive Inorganic Chemistry II (Second Edition): From Elements to Applications*. Vol. 7. Elsevier Ltd, 2013, pp. 525–557. ISBN: 9780080965291. DOI: 10.1016/B978-0-08-097774-4.00729-4.

[56] M. Gupta and James J. Spivey. "Catalytic Processes for the Production of Clean Fuels". In: *New and Future Developments in Catalysis: Catalysis for Remediation and Environmental Concerns* (Jan. 2013), pp. 87–126. DOI: 10.1016/B978-0-444-53870-3.00005-8.

[57] Omid Akbarzadeh et al. "Effect of Pressure , H 2 / CO Ratio and Reduction Conditions on Co – Mn / CNT Bimetallic Catalyst". In: *Symmetry* 12 (2020), pp. 1–14.

[58] Marco Marchese et al. "Energy Conversion and Management : X Energy performance of Power-to-Liquid applications integrating biogas upgrading , reverse water gas shift , solid oxide electrolysis and Fischer- Tropsch technologies". In: *Energy Conversion and Management: X* 6.January (2020), p. 100041. ISSN: 2590-1745. DOI: 10.1016/j.ecmx.2020.100041. URL: https://doi.org/10.1016/j.ecmx.2020.100041.

[59] A Y Khodakov, W Chu, and P. Fongarland. "Advances in the Development of Novel Cobalt Fischer-Tropsch.pdf". In: *Chemical Reviews* 107 (2007), pp. 1692–1744. ISSN: 0009-2665.

[60] Burtron H. Davis. "Fischer-Tropsch Synthesis: Reaction mechanisms for iron catalysts". In: *Catalysis Today* 141.1-2 (Mar. 2009), pp. 25–33. ISSN: 09205861. DOI: 10.1016/j.cattod.2008.03.005.

[61] Manuel Ojeda et al. "CO activation pathways and the mechanism of Fischer-Tropsch synthesis". In: *Journal of Catalysis* 272.2 (June 2010), pp. 287–297. ISSN: 00219517. DOI: 10.1016/j.jcat.2010.04.012.

[62] Dieter Leckel. "Diesel production from fischer - Tropsch: The past, the present, and new concepts". In: *Energy and Fuels* 23.5 (2009), pp. 2342–2358. ISSN: 08870624. DOI: 10.1021/ef900064c.

[63] Anna P. Petersen et al. "Cobalt-based fischer-tropsch synthesis: A kinetic evaluation of metal-support interactions using an inverse model system". In: *Catalysts* 9.10 (2019). ISSN: 20734344. DOI: 10.3390/catal9100794.

[64] A. de Klerk. "Aviation Turbine Fuels Through the Fischer–Tropsch Process". In: *Biofuels for Aviation*. Elsevier, 2016, pp. 241–259. DOI: 10.1016/b978-0-12-804568-8.00010-x.

[65] Jens Weitkamp. "Catalytic Hydrocracking-Mechanisms and Versatility of the Process". In: *ChemCatChem* 4.3 (2012), pp. 292–306. ISSN: 18673880. DOI: 10.1002/cctc.201100315.

[66] Toshiaki Hanaoka et al. "Jet fuel synthesis from Fischer-Tropsch product under mild hydrocracking conditions using Pt-loaded catalysts". In: *Chemical Engineering Journal* 263 (2015), pp. 178–185. ISSN: 13858947. DOI: 10.1016/j.cej.2014.11.042. URL: http://dx.doi.org/10.1016/j.cej.2014.11.042.

[67] Jakub Fratczak et al. “Hydrocracking of Heavy Fischer-Tropsch Wax Distillation Residues and Its Blends with Vacuum Gas Oil Using Phonolite-Based Catalysts”. eng. In: *Molecules (Basel, Switzerland)* 26.23 (Nov. 2021), p. 7172. ISSN: 1420-3049. DOI: 10.3390/molecules26237172. URL: https://pubmed.ncbi.nlm.nih.gov/34885761%20https://www.ncbi.nlm.nih.gov/pmc/articles/PMC8658968/.

[68] Christophe Bouchy et al. “Fischer-Tropsch waxes upgrading via hydrocracking and selective hydroisomerization”. In: *Oil and Gas Science and Technology* 64.1 (2009), pp. 91–112. ISSN: 12944475. DOI: 10.2516/ogst/2008047.

[69] Aspen Plus et al. “Part Number : Aspen Physical Property System 11 . 1 September 2001”. In: *Engineering* (2001), pp. 2–18. URL: http://www.aspentech.com.

[70] Ioanna Dimitriou et al. “Carbon dioxide utilisation for production of transport fuels: Process and economic analysis”. In: *Energy and Environmental Science* 8.6 (2015), pp. 1775–1789. ISSN: 17545706. DOI: 10.1039/c4ee04117h.

[71] Preeti Gangadharan, Krishna C. Kanchi, and Helen H. Lou. “Evaluation of the economic and environmental impact of combining dry reforming with steam reforming of methane”. In: *Chemical Engineering Research and Design* 90.11 (2012), pp. 1956–1968. ISSN: 02638762. DOI: 10.1016/j.cherd.2012.04.008. URL: http://dx.doi.org/10.1016/j.cherd.2012.04.008.

[72] Davide Selvatico, Andrea Lanzini, and Massimo Santarelli. “Low Temperature Fischer-Tropsch fuels from syngas: Kinetic modeling and process simulation of different plant configurations”. In: *Fuel* 186 (Dec. 2016), pp. 544–560. ISSN: 00162361. DOI: 10.1016/j.fuel.2016.08.093.

[73] Peter M. Maitlis and Arno de Klerk. *New Directions, Challenges, and Opportunities*. 2013, pp. 337–358. ISBN: 9783527329458. DOI: 10.1002/9783527656837.ch16.

[74] Branislav Todic et al. “Kinetic Model of Fischer Tropsch Synthesis in a Slurry Reactor on Co Re / Al 2 O 3 Catalyst”. In: (2013).

[75] Endar Puspawiningtiyas et al. “Sustainable Diesel from Pyrolysis of Unsaturated Fatty Acid Basic Soaps: The Effect of Temperature on Yield and Product Composition”. In: *Molecules* 27.3 (2022). ISSN: 14203049. DOI: 10.3390/molecules27030667.

[76] Carlo N. Hamelinck et al. “Production of FT transportation fuels from biomass; technical options, process analysis and optimisation, and development potential”. In: *Energy* 29.11 (2004), pp. 1743–1771. ISSN: 03605442. DOI: 10.1016/j.energy.2004.01.002.

[77] A. Al-Musa et al. “Hydrogen production by iso-octane steam reforming over Cu catalysts supported on rare earth oxides (REOs)”. In: *International Journal of Hydrogen Energy* 39.3 (2014), pp. 1350–1363. ISSN: 03603199. DOI: 10.1016/j.ijhydene.2013.11.013. URL: http://dx.doi.org/10.1016/j.ijhydene.2013.11.013.

[78] Benjamin T. Schädel, Matthias Duisberg, and Olaf Deutschmann. “Steam reforming of methane, ethane, propane, butane, and natural gas over a rhodium-based catalyst”. In: *Catalysis Today* 142.1-2 (2009), pp. 42–51. ISSN: 09205861. DOI: 10.1016/j.cattod.2009.01.008.

[79] José E.A. Graciano et al. *Production of Fuels from CO2-rich Natural Gas using Fischer-Tropsch Synthesis Coupled to Trireforming Process*. Vol. 40. Elsevier Masson SAS, 2017, pp. 2659–2664. ISBN: 9780444639653. DOI: 10.1016/B978-0-444-63965-3.50445-1. URL: https://doi.org/10.1016/B978-0-444-63965-3.50445-1.

[80] Szabina Tomasek et al. “Hydrocracking of Fischer-Tropsch Paraffin Mixtures over Strong Acid Bifunctional Catalysts to Engine Fuels”. In: *ACS Omega* 5.41 (2020), pp. 26413–26420. ISSN: 24701343. DOI: 10.1021/acsomega.0c02711.

[81] Anamaria P P Pires et al. “Alternative jet fuel properties”. In: *BioResources* 13.2 (2018), pp. 2632–2657.

[82] Ahmad Galadima and Oki Muraza. "Catalytic upgrading of vegetable oils into jet fuels range hydrocarbons using heterogeneous catalysts: A review". In: *Journal of Industrial and Engineering Chemistry* 29 (2015), pp. 12–23. ISSN: 22345957. DOI: 10.1016/j.jiec.2015.03.030. URL: http://dx.doi.org/10.1016/j.jiec.2015.03.030.

[83] Steven P. Pyl et al. "Biomass to olefins: Cracking of renewable naphtha". In: *Chemical Engineering Journal* 176-177 (2011), pp. 178–187. ISSN: 13858947. DOI: 10.1016/j.cej.2011.04.062.

[84] Thomas G. Smagala et al. "Hydrocarbon renewable and synthetic diesel fuel blendstocks: Composition and properties". In: *Energy and Fuels* 27.1 (2013), pp. 237–246. ISSN: 08870624. DOI: 10.1021/ef3012849.

[85] Alain Chauvel, Gilles Fournier, and Claude Raimbault. *Manual of Process Economic Evaluation - New, Revised and Expanded Edition*. URL: https://app.knovel.com/hotlink/toc/id:kpMPEENREC/manual-process-economic/manual-process-economic.

[86] Chirag Mevawala, Yuan Jiang, and Debangsu Bhattacharyya. "Techno-economic optimization of shale gas to dimethyl ether production processes via direct and indirect synthesis routes". In: *Applied Energy* 238.January (2019), pp. 119–134. ISSN: 03062619. DOI: 10.1016/j.apenergy.2019.01.044. URL: https://doi.org/10.1016/j.apenergy.2019.01.044.

[87] Oscar P.R. van Vliet, André P.C. Faaij, and Wim C. Turkenburg. "Fischer-Tropsch diesel production in a well-to-wheel perspective: A carbon, energy flow and cost analysis". In: *Energy Conversion and Management* 50.4 (2009), pp. 855–876. ISSN: 01968904. DOI: 10.1016/j.enconman.2009.01.008. URL: http://dx.doi.org/10.1016/j.enconman.2009.01.008.

[88] W. L. Becker et al. "Production of Fischer-Tropsch liquid fuels from high temperature solid oxide co-electrolysis units". In: *Energy* 47.1 (2012), pp. 99–115. ISSN: 03605442. DOI: 10.1016/j.energy.2012.08.047. URL: http://dx.doi.org/10.1016/j.energy.2012.08.047.

[89] Matches. *Fired Heater Cost Estimate*. 2014. URL: https://www.matche.com/equipcost/FiredHeater.html.

[90] International Energy Agency. "Outlook for biogas and biomethane. Prospects for organic growth. World Energy Outlook Special Report." In: (2020), p. 93. URL: https://www.iea.org/reports/outlook-for-biogas-and-biomethane-prospects-for-organic-growth.

[91] Yuanrong Zhou and Stephanie Searle. "Cost of Renewable Hydrogen Produced Onsite At Hydrogen Refueling Stations in Europe". In: February (2022). URL: www.theicct.orgcommunications@theicct.org.

[92] Gavin Towler and Ray Sinnott. "Chapter 3 - Utilities and Energy Efficient Design". In: ed. by Gavin Towler and Ray B T - Chemical Engineering Design (Second Edition) Sinnott. Boston: Butterworth-Heinemann, 2013, pp. 103–160. ISBN: 978-0-08-096659-5. DOI: https://doi.org/10.1016/B978-0-08-096659-5.00003-1. URL: https://www.sciencedirect.com/science/article/pii/B9780080966595000031.

[93] Yanqing Ma et al. "Comparative investigation of different CO2 capture technologies for coal to ethylene glycol process". In: *Processes* 9.2 (2021), pp. 1–19. ISSN: 22279717. DOI: 10.3390/pr9020207.

[94] Trading Economics. *EU Natural Gas*. 2022. URL: https://tradingeconomics.com/commodity/eu-natural-gas.

[95] Statista. *Prices of electricity for industry in Sweden from 2008 to 2021*. 2022. URL: https://www.statista.com/statistics/596262/electricity-industry-price-sweden/.

[96] Gavin Towler and Ray Sinnott. "Chapter 8 - Estimating Revenues and Production Costs". In: ed. by Gavin Towler and Ray B T - Chemical Engineering Design (Second Edition) Sinnott. Boston: Butterworth-Heinemann, 2013, pp. 355–387. ISBN: 978-0-08-096659-5. DOI: https://doi.org/10.1016/B978-0-08-096659-5.00008-0. URL: https://www.sciencedirect.com/science/article/pii/B9780080966595000080.

[97] Evridiki Dimitriadou. "Europe's nascent bionaphtha market gearing up to serve demand for cleaner fuels and petchems". In: *S&P Global Commodity Insights* (2021). URL: https://www.spglobal.com/commodityinsights/en/market-insights/blogs/oil/060921-bionaphtha-market-biofuels-gasoline-petchems-plastics-clean-energy.

[98] Jennifer A. Hayward et al. "The economics of producing sustainable aviation fuel: A regional case study in Queensland, Australia". In: *GCB Bioenergy* 7.3 (2015), pp. 497–511. ISSN: 17571707. DOI: 10.1111/gcbb.12159.

[99] International Energy Agency. "Renewable Energy Market Update". In: *Renewable Energy Market Update* (2020). DOI: 10.1787/afbc8c1d-en.

[100] Bitumen World. "Comparative prices for bitumen grade 70/100". In: (). URL: https://bitumen.world/.

A Component list

Component ID	Type	Component name	Alias	Component ID	Type	Component name	Alias
CH4	Conventional	METHANE	CH4	C30H60	Conventional	1-TRIACONTENE	C30H60
CO2	Conventional	CARBON-DIOXIDE	CO2	C2H6	Conventional	ETHANE	C2H6
CO	Conventional	CARBON-MONOXIDE	CO	C3H8	Conventional	PROPANE	C3H8
H2	Conventional	HYDROGEN	H2	C4H10	Conventional	N-BUTANE	C4H10-1
H2O	Conventional	WATER	H2O	C5H12	Conventional	2-METHYL-BUTANE	C5H12-2
C2H4	Conventional	ETHYLENE	C2H4	C6H14	Conventional	N-HEXANE	C6H14-1
C3H6	Conventional	PROPYLENE	C3H6-2	C7H16	Conventional	(+)-3-METHYLHEXANE	C7H16
C4H8	Conventional	2-BUTENE	C4H8	C8H18	Conventional	2,2,3,3-TETRAMETHYLBUTANE	C8H18
C5H10	Conventional	2-PENTENE,-(CIS+TRANS)	C5H10	C9H20	Conventional	2,3,4-TRIMETHYLHEXANE	C9H20
C6H12	Conventional	2-HEXENE,-(CIS+TRANS)	C6H12	C10H22	Conventional	2,5,5-TRIMETHYLHEPTANE	C10H22
C7H14	Conventional	2-HEPTENE	C7H14	C11H24	Conventional	N-UNDECANE	C11H24
C8H16	Conventional	2-OCTENE	C8H16	C12H26	Conventional	N-DODECANE	C12H26
C9H18	Conventional	1-TRANS-3,5-TRIMETHYLCYCLOHEXANE	C9H18	C13H28	Conventional	N-TRIDECANE	C13H28
C10H20	Conventional	P-MENTHANE	C10H20	C14H30	Conventional	N-TETRADECANE	C14H30
C11H22	Conventional	CYCLOUNDECANE	C11H22	C15H32	Conventional	N-PENTADECANE	C15H32
C12H24	Conventional	2,2,4,6,6-PENTAMETHYL-3-HEPTENE	C12H24	C16H34	Conventional	N-HEXADECANE	C16H34
C13H26	Conventional	CYCLOTRIDECANE	C13H26	C17H36	Conventional	N-HEPTADECANE	C17H36
C14H28	Conventional	CYCLOTETRADECANE	C14H28	C18H38	Conventional	N-OCTADECANE	C18H38
C15H30	Conventional	CYCLOPENTADECANE	C15H30	C19H40	Conventional	N-NONADECANE	C19H40
C16H32	Conventional	CYCLOHEXADECANE	C16H32	C20H42	Conventional	N-EICOSANE	C20H42
C17H34	Conventional	N-DODECYLCYCLOPENTANE	C17H34	C21H44	Conventional	N-HENEICOSANE	C21H44
C18H36	Conventional	1-OCTADECENE	C18H36-1	C22H46	Conventional	N-DOCOSANE	C22H46
C19H38	Conventional	N-TETRADECYLCYCLOPENTANE	C19H38	C23H48	Conventional	N-TRICOSANE	C23H48
C20H40	Conventional	N-PENTADECYLCYCLOPENTANE	C20H40	C24H50	Conventional	N-TETRACOSANE	C24H50
C21H42	Conventional	N-HEXADECYLCYCLOPENTANE	C21H42	C25H52	Conventional	N-PENTACOSANE	C25H52
C22H44	Conventional	CYCLODOCOSANE	C22H44	C26H54	Conventional	N-HEXACOSANE	C26H54
C23H46	Conventional	CYCLOTRICOSANE	C23H46	C27H56	Conventional	N-HEPTACOSANE	C27H56
C24H48	Conventional	CYCLOTETRACOSANE	C24H48	C28H58	Conventional	N-OCTACOSANE	C28H58
C25H50	Conventional	HEPTADECANE,-9-(3-CYCLOPENTYLPROPYL)-	C25H50	C29H60	Conventional	N-NONACOSANE	C29H60
C26H52	Conventional	CYCLOHEXAEICOSANE	C26H52	C30H62	Conventional	N-TRIACONTANE	C30H62
C27H54	Conventional	CYCLOHEPTACOSANE	C27H54	O2	Conventional	OXYGEN	O2
C28H56	Conventional	1-OCTACOSENE	C28H56-N2	N2	Conventional	NITROGEN	N2

B FTS reactions and conversions from CO

Carbon number	Conversion from CO	Paraffin conversion from CO	Olefin conversion from CO
1	0.009	0.009	0
2	0.0162	0.01458	0.00162
3	0.02187	0.019683	0.002187
4	0.026244	0.0236196	0.0026244
5	0.0295245	0.02657205	0.00295245
6	0.03188646	0.028697814	0.003188646
7	0.033480783	0.030132705	0.003348078
8	0.034437377	0.030993639	0.003443738
9	0.034867844	0.03138106	0.003486784
10	0.034867844	0.03138106	0.003486784
11	0.034519166	0.031067249	0.003451917
12	0.033891544	0.03050239	0.003389154
13	0.033044256	0.02973983	0.003304426
14	0.032027509	0.028824758	0.003202751
15	0.03088367	0.027795303	0.003088367
16	0.029648323	0.026683491	0.002964832
17	0.028351209	0.025516088	0.002835121
18	0.027017034	0.024315331	0.002701703
19	0.025666183	0.023099564	0.002566618
20	0.352572298	0.317315068	0.03525723
21			
22			
23			
24			
25			
26			
27			
28			
29			
30			

C Process block diagram

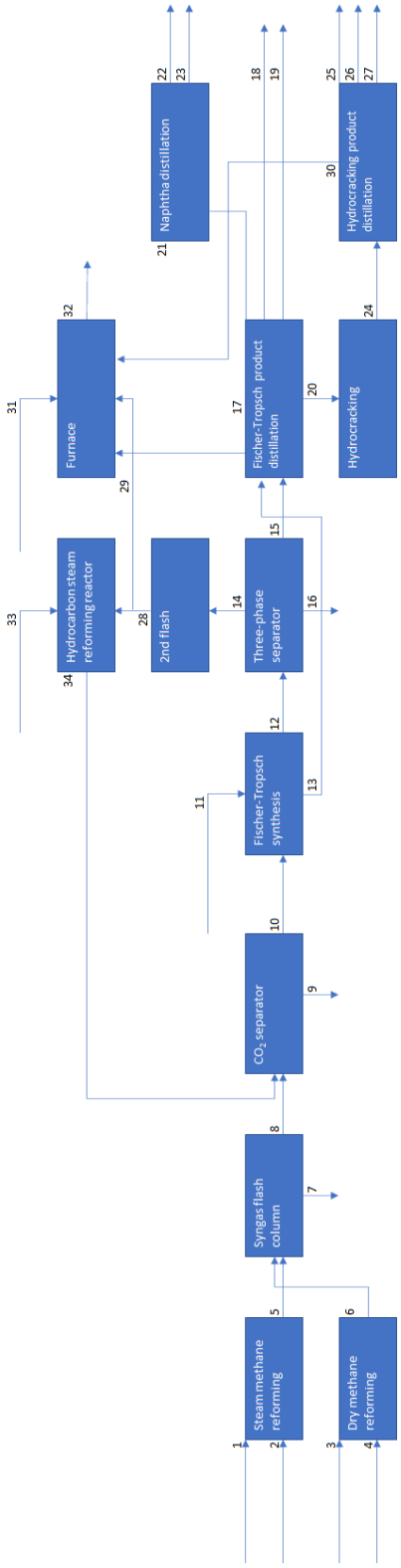

D Process mass balance

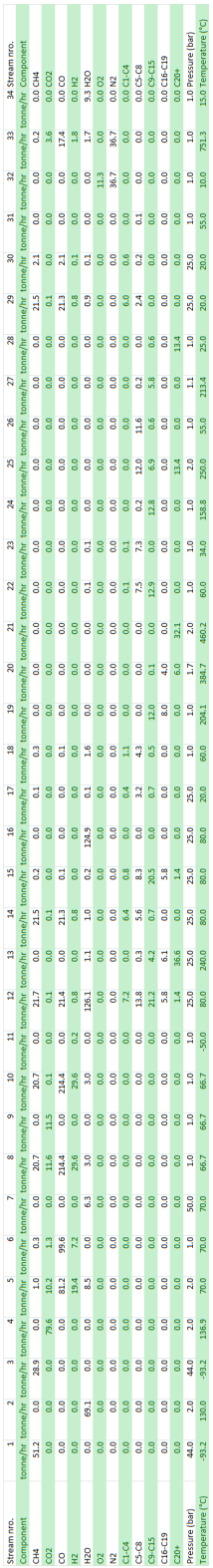

Stream nro.	1	2	3	4	5	6	7	8	9	10	11	12	13	14	15	16	17	18	19	20	21	22	23	24	25	26	27	28	29	30	31	32	33	34 Stream nro.
Component	tonne/hr	tonne/hr	tonne/hr	tonne/hr	tonne/hr	tonne/hr	tonne/hr	tonne/hr	tonne/hr	tonne/hr	tonne/hr	tonne/hr	tonne/hr	tonne/hr	tonne/hr	tonne/hr	tonne/hr	tonne/hr	tonne/hr	tonne/hr	tonne/hr	tonne/hr	tonne/hr	tonne/hr	tonne/hr	tonne/hr	tonne/hr	tonne/hr	tonne/hr	tonne/hr	tonne/hr	tonne/hr	tonne/hr	Component
CH4	51.2	0.0	28.9	0.0	1.0	0.3	0.0	20.7	0.0	20.7	0.0	21.7	0.0	21.5	0.2	0.0	0.1	0.3	0.0	0.0	0.0	0.0	0.0	0.0	0.0	0.0	0.0	0.0	21.5	2.1	0.0	0.0	0.2	0.0 CH4
CO2	0.0	0.0	0.0	79.6	16.2	1.3	0.0	11.6	11.5	0.1	0.0	0.1	0.0	0.1	0.0	0.0	0.0	0.0	0.0	0.0	0.0	0.0	0.0	0.0	0.0	0.0	0.0	0.0	0.1	0.0	0.0	0.0	3.6	0.0 CO2
CO	0.0	0.0	0.0	0.0	81.2	99.6	0.0	214.4	0.0	214.4	0.0	21.4	0.0	21.3	0.1	0.0	0.0	0.1	0.0	0.0	0.0	0.0	0.0	0.0	0.0	0.0	0.0	0.0	21.3	2.1	0.0	0.0	17.4	0.0 CO
H2	0.0	0.0	0.0	0.0	19.4	7.2	0.0	29.6	0.0	29.6	0.2	0.8	0.0	0.8	0.0	0.0	0.0	0.0	0.0	0.0	0.0	0.0	0.0	0.0	0.0	0.0	0.0	0.0	0.8	0.1	0.0	0.0	1.8	0.0 H2
H2O	0.0	69.1	0.0	0.0	8.5	0.8	6.3	3.0	0.0	3.0	0.0	126.1	1.1	1.0	0.2	124.9	0.1	1.6	0.0	0.0	0.0	0.1	0.1	0.0	0.0	0.0	0.0	0.0	0.9	0.1	0.0	11.3	1.7	9.3 H2O
CO2	0.0	0.0	0.0	0.0	0.0	0.0	0.0	0.0	0.0	0.0	0.0	0.0	0.0	0.0	0.0	0.0	0.0	0.0	0.0	0.0	0.0	0.0	0.0	0.0	0.0	0.0	0.0	0.0	0.0	0.0	0.0	0.0	0.0	0.0 CO2
N2	0.0	0.0	0.0	0.0	0.0	0.0	0.0	0.0	0.0	0.0	0.0	0.0	0.0	0.0	0.0	0.0	0.0	0.0	0.0	0.0	0.0	0.0	0.0	0.0	0.0	0.0	0.0	0.0	0.0	0.0	0.0	36.7	36.7	0.0 N2
C1-C4	0.0	0.0	0.0	0.0	0.0	0.0	0.0	0.0	0.0	0.0	0.0	7.2	0.0	6.4	0.8	0.0	0.4	1.1	0.0	0.0	0.0	0.1	0.1	0.0	0.0	0.0	0.0	0.0	6.0	0.6	0.0	0.0	0.0	0.0 C1-C4
C5-C8	0.0	0.0	0.0	0.0	0.0	0.0	0.0	0.0	0.0	0.0	0.0	13.8	0.3	5.6	8.3	0.0	3.2	4.3	0.0	0.0	0.0	7.5	7.3	0.2	12.0	11.6	0.2	0.0	2.4	0.2	0.1	0.0	0.0	0.0 C5-C8
C9-C15	0.0	0.0	0.0	0.0	0.0	0.0	0.0	0.0	0.0	0.0	0.0	21.2	4.2	0.7	20.5	0.0	0.7	0.5	12.0	0.1	0.0	12.9	0.0	12.8	6.9	0.6	5.8	0.6	0.0	0.0	0.0	0.0	0.0	0.0 C9-C15
C16-C19	0.0	0.0	0.0	0.0	0.0	0.0	0.0	0.0	0.0	0.0	0.0	5.8	6.1	0.0	5.8	0.0	0.0	0.0	8.0	4.0	0.0	0.0	0.0	0.0	0.0	0.0	0.0	0.0	0.0	0.0	0.0	0.0	0.0	0.0 C16-C19
C20+	0.0	0.0	0.0	0.0	0.0	0.0	0.0	0.0	0.0	0.0	0.0	1.4	36.6	0.0	1.4	0.0	0.0	0.0	0.0	6.0	32.1	0.0	0.0	0.0	13.4	0.0	0.0	13.4	0.0	0.0	0.0	0.0	0.0	0.0 C20+
Pressure (bar)	44.0	2.0	44.0	2.0	2.0	1.0	50.0	1.0	1.0	1.0	-50.0	25.0	25.0	25.0	25.0	25.0	25.0	1.0	1.0	1.7	2.0	1.0	1.0	1.0	2.0	1.0	1.1	1.0	25.0	25.0	1.0	1.0	1.0	1.0 Pressure (bar)
Temperature (°C)	-93.2	130.0	-93.2	136.9	70.0	70.0	70.0	66.7	66.7	66.7	-50.0	80.0	240.0	80.0	80.0	80.0	20.0	60.0	204.1	384.7	460.2	60.0	34.0	158.8	250.0	55.0	213.4	25.0	20.0	20.0	55.0	10.0	791.3	15.0 Temperature (°C)

E Aspen flowsheet for synthesis gas generation

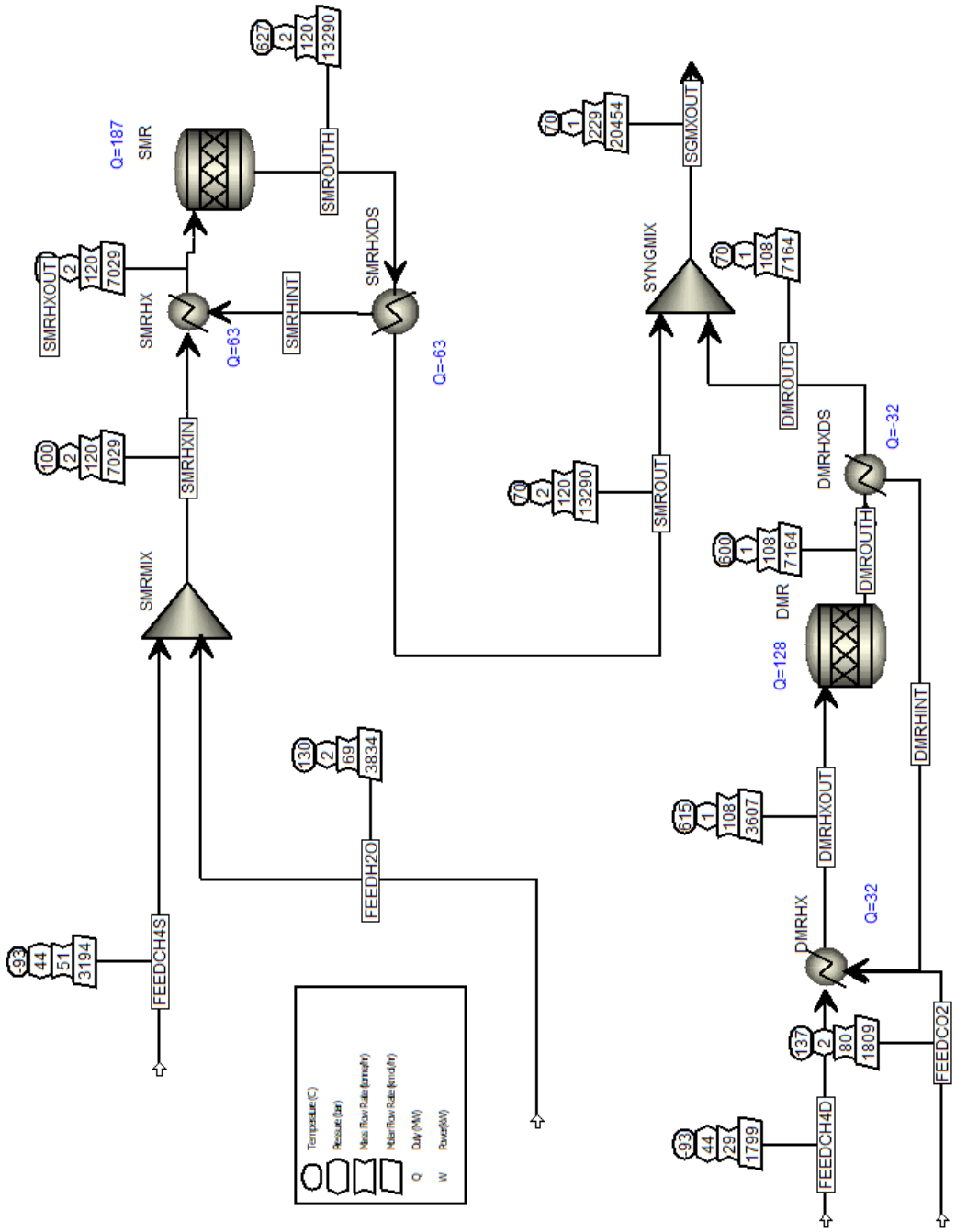

F Aspen flowsheet for Fischer-Tropsch synthesis and recycling

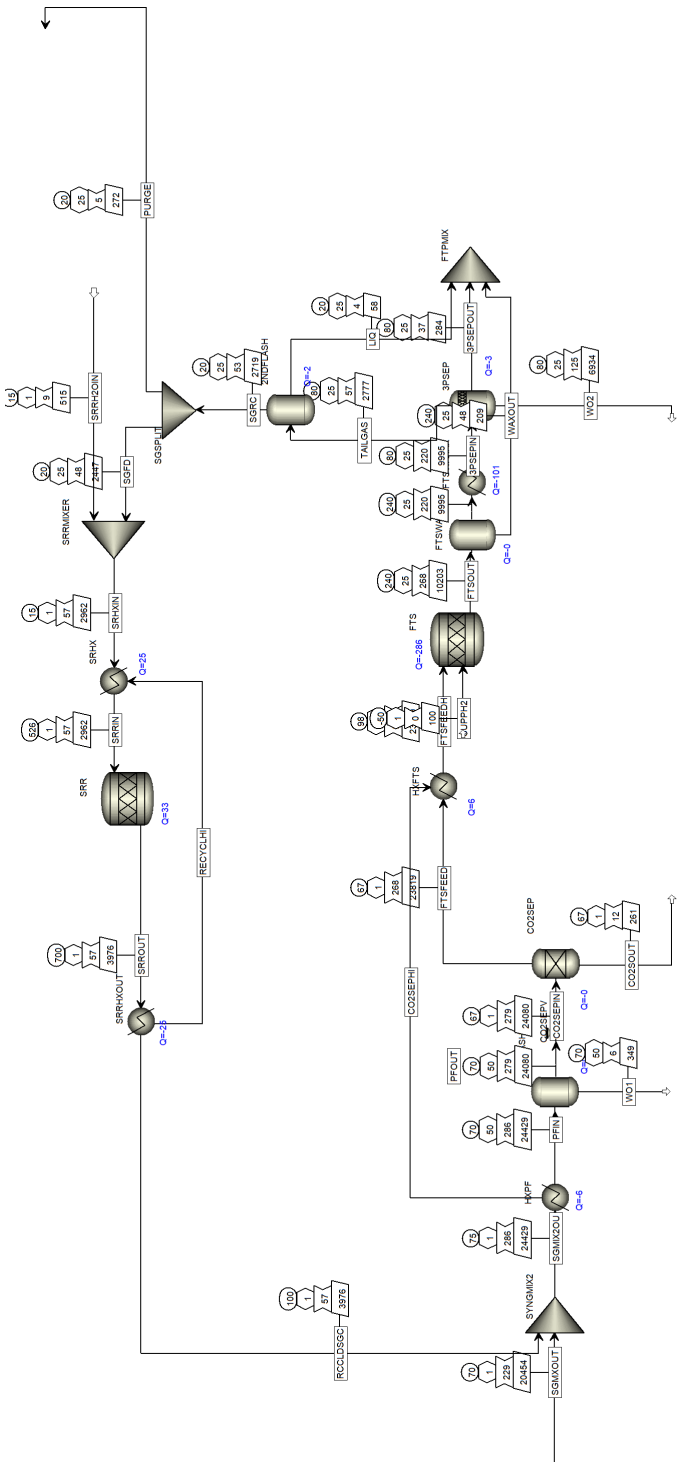

G Aspen flowsheet for downstream processing and off-gas utilization

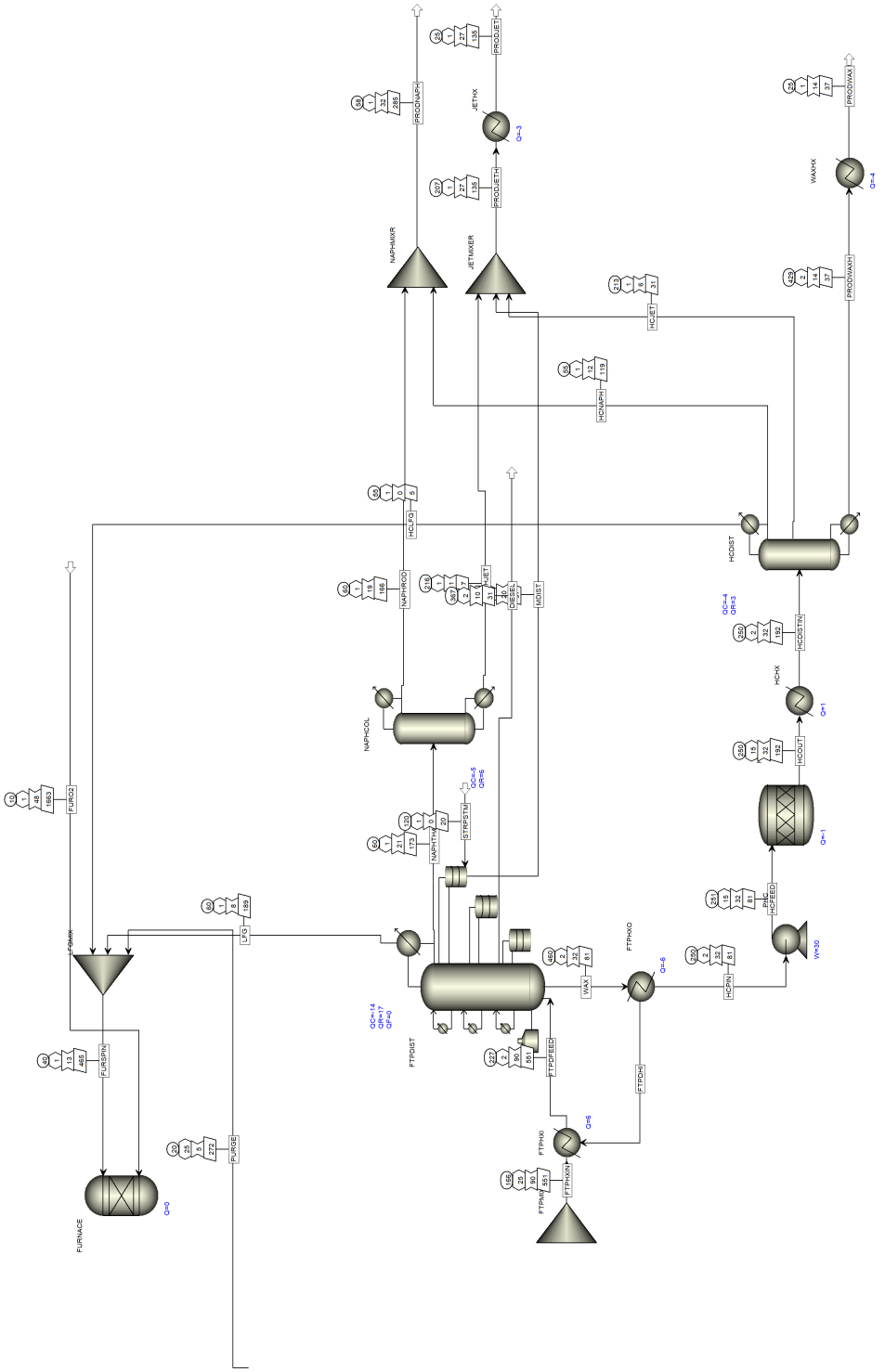

H Equipment list from Aspen Plus

Equipment name	Notes	Equipment name	Notes
2NDFLASH-flash vessel	Flash drum	HCHX	Hydrocracking product heat exchanger
3PSEP-flash vessel	Three-phase separator	HCR	Hydrocracking reactor
CO2SEP	Rectisol	HXFTS	FT reactor heat exchanger
CO2SEPV	Inlet valve	HXPF	Pre-flash heat exchanger
DMR	DMR reactor	JETHX	Jet product heat exchanger
DMRHX	DMR inlet heat exchanger	JETMIXER	Jet product mixer
DMRHXDS	DMR outlet heat exchanger	LFGMIX	Light fuel gas mixer
FTPDIST - MAIN COLUMN-bottoms split	FTP distillation column	NAPHCOL-bottoms split	Naphtha distillation
FTPDIST - MAIN COLUMN-cond		NAPHCOL-cond	
FTPDIST - MAIN COLUMN-cond acc		NAPHCOL-cond acc	
FTPDIST - MAIN COLUMN-overhead split		NAPHCOL-overhead split	
FTPDIST - MAIN COLUMN-reb		NAPHCOL-reb	
FTPDIST - MAIN COLUMN-reflux pump		NAPHCOL-reflux pump	
FTPDIST - MAIN COLUMN-tower		NAPHCOL-tower	
FTPDIST - MDIST-tower		NAPHMIXR	Naphtha product mixer
FTPHXI	FTP distillation column inlet heat exchanger	PHC	Hydrocracker pump
FTPHXO	FTP distillation column outlet heat exchanger	PREFLASH-flash vessel	Syngas flash vessel
FTPMIX	FTP distillation column mixer	SGSPLIT	Syngas recycling stream splitter
FTS	FT reactor	SMR	SMR reactor
FTSWAXO-flash vessel	FT reactor wax outlet	SMRHX	SMR reactor inlet heat exchanger
FURNACE	Furnace	SMRHXDS	SMR reactor outlet heat exchanger
HCDIST-bottoms split	Hydrocracking product distillation	SMRMIX	SMR inlet mixer
HCDIST-cond		SRHX	SR inlet heat exchanger
HCDIST-cond acc		SRR	SR reactor
HCDIST-overhead split		SRRHXOUT	SR outlet heat exchanger
HCDIST-reb		SRRMIXER	SR inlet mixer
HCDIST-reflux pump		SYNGMIX	Syngas mixer
HCDIST-tower		SYNGMIX2	Recycled syngas mixer
		WAXHX	Wax product heat exchanger